# CONTROL OF BIOAEROSOLS AND VOLATILE ORGANIC COMPOUNDS WITH MICROWAVE AND INFRARED RADIATION-BASED TECHNOLOGIES

By

BRIAN DAMIT

A DISSERTATION PRESENTED TO THE GRADUATE SCHOOL
OF THE UNIVERSITY OF FLORIDA IN PARTIAL FULFILLMENT
OF THE REQUIREMENTS FOR THE DEGREE OF
DOCTOR OF PHILOSOPHY

UNIVERSITY OF FLORIDA

2013

For my loving family - my mom, dad, and brother

ACKNOWLEDGMENTS

I first would like to thank my advisor, Professor Chang-Yu Wu. Without his guidance during my study, this PhD would not have been possible. With his genuine concern and compassion for his students, his patience, and his diligence, he is an inspiration to everyone who interacts with him. Dr. Wu is a role model for what all of his students aspire to be.

I would also like to thank my committee members: Drs. Ben Koopman, Jennifer Curtis, Robert Moore, and Meng-Dawn Cheng. They have been very helpful with improving the quality of my work and giving me advice throughout my PhD study. I want to especially thank Dr. Cheng for mentoring me during my time at Oak Ridge National Laboratory (ORNL); he really has been a second advisor to me.

My research could not have been accomplished without my lab mates who helped me with training, technical questions, and everyday tasks. I would like to thank all my lab mates at the University of Florida past and present, but especially: Dr. Myung-Heui Woo, Christiana Garst, Qi Zhang, Nima Afshar-Mohajer, Jun Wang, Dr. Hsing-Wang Li, and Dr. Hailong Li. I would also like to thank all the folks at ORNL and my colleagues at Peking University in Beijing, especially Professor Maosheng Yao.

I am very grateful to the National Science Foundation for funding me for five years. I am also truly fortunate for the support of Dr. Laurence Alexander and UF's Office of Graduate Minority Programs (OGMP). Finally, I want to thank my mom (Becky), my dad (Ed), my brother Michael, and my family in the U.S. and in the Philippines for their love and support during these past five years.

TABLE OF CONTENTS

page

LIST OF TABLES

LIST OF FIGURES

## LIST OF ABBREVIATIONS

| | |
|---|---|
| ACC | Activated Carbon Cloth |
| APS | Aerodynamic Particle Sizer |
| ATCC | American Type Culture Collection |
| CFU | Colony-Forming Unit |
| CI | Confidence Interval |
| CPC | Condensation Particle Counter |
| CV | Coefficient of Variation |
| DBD | Dielectric Barrier Discharge |
| DI | Deionized |
| EPA | Environmental Protection Agency |
| GAC | Granular Activated Carbon |
| GC | Gas Chromatography |
| HCoV | Human Coronavirus |
| HEPA | High Efficiency Particulate Air |
| IR | Infrared |
| LED | Light-Emitting Diode |
| LUB | Length of Unused Bed |
| MEK | Methyl Ethyl Ketone |
| MPPS | Most Penetrating Particle Size |
| NIOSH | National Institute for Occupational Safety and Health |
| OPC | Optical Particle Counter |
| ORNL | Oak Ridge National Laboratory |
| PBS | Phosphate Buffered Saline |
| PCF | Pair Correlation Function |

| | |
|---|---|
| PCO | Photocatalytic Oxidation |
| PERC | Tetrachloroethylene |
| PFU | Plaque-Forming Unit |
| PRE | Physical Removal Efficiency |
| PSD | Particle Size Distribution |
| SARS | Severe Acute Respiratory Syndrome |
| SEM | Scanning Electron Microscopy |
| SF | Survival Fraction |
| SMPS | Scanning Mobility Particle Sizer |
| SNR | Signal-to-Noise Ratio |
| TPR | Throughput Ratio |
| UHT | Ultrahigh Temperature |
| UV | Ultraviolet |
| UVGI | Ultraviolet Germicidal Irradiation |
| VOC | Volatile Organic Compound |
| VRE | Viable Removal Efficiency |
| VZV | Varicella Zoster Virus |

Abstract of Dissertation Presented to the Graduate School
of the University of Florida in Partial Fulfillment of the
Requirements for the Degree of Doctor of Philosophy

# CONTROL OF BIOAEROSOLS AND VOLATILE ORGANIC COMPOUNDS WITH MICROWAVE AND INFRARED RADIATION-BASED TECHNOLOGIES

By

Brian Damit

August 2013

Chair: Chang-Yu Wu
Major: Environmental Engineering Sciences

Bioaerosols and volatile organic compounds (VOCs) are two common air pollutants which cause adverse human health effects: bioaerosols can transmit diseases while VOCs are associated with a range of respiratory symptoms. To address limitations of current pollutant control technologies, novel radiation-based devices were developed in this dissertation to (1) inactivate bioaerosols using high temperatures and short exposure times and (2) regenerate activated carbon cloth (ACC) after VOC adsorption.

For bioaerosol control, microwave and infrared (IR) radiations were used to kill microbes collected on air filters and also microbes suspended in the air. Microwaves showed some disinfection of *B. subtilis* spores collected on the filter. To improve disinfection, an ultrahigh temperature (UHT) treatment process generated by IR was adopted, which disinfected filters loaded with *E. coli*, MS2 viruses, and *B. subtilis* spores within seconds. Filter temperatures greater than the traditional 125 °C were required. The IR-UHT concept was also incorporated into an on-line system to treat microbes suspended in air. Testing demonstrated that the system produced high and more

uniform airflow temperatures and inactivated both laboratory-generated and environmental microbes.

Because a high temperature disinfection process can degrade traditional filters, a metallic granular bed filter was also tested. The filter showed high efficiency against MS2 and *B. subtilis* spores but its pressure drop caused low filter quality. Due to the filter's high efficiency and consequent challenge in obtaining an accurate concentration measurement, a complementary study was undertaken to examine the validity of the Poisson process in aerosol sampling. Experiments with indoor air revealed that the Poisson process adequately described nanometer-sized aerosol sampling possibly because of Brownian motion.

In ACC regeneration experiments, ACC was first saturated with toluene vapor and then regenerated with IR heating. IR regeneration for 1 h restored the adsorption capacity of saturated ACC using an incident surface IR power density of 9.10 $W/cm^2$. The adsorption performance of ACC after one and two regenerations was found to be similar to fresh.

In summary, IR and microwave-based technologies were successfully developed to control bioaerosol and VOC air pollutants. The technologies offer advantages over existing technologies and can improve control strategies.

# CHAPTER 1
# INTRODUCTION

## Bioaerosols and Pathogen Transmission

Air pollutants include airborne micrometer and submicrometer particles, inorganic vapors, ozone, volatile organic compounds (VOCs), and bioaerosols. Bioaerosols are defined as aerosols - a liquid or solid suspended in a gaseous medium - of biological origin (Hirst 1995). Common examples of bioaerosols include airborne bacteria cells, viruses, pollen, and fungal spores but the formal definition also extends to particles like fragments of insects, endotoxin from bacteria, and skin cells that have been aerosolized and are suspended in air (Cox and Wathes 1995). Because bioaerosols can be different types of biological material, their size range spans four orders of magnitude: on the order of 10 nm for viruses to 100 μm for pollen or fungi (Hinds 1999). Bioaerosols can be generated from a variety of different sources including occupational and agricultural processes, waste processing, and bioterrorism (intentional dissemination of pathogens) (Douwes et al. 2003; Kummer and Thiel 2008; Haas et al. 2010). In indoor environments, humans and pets are common sources but bioaerosols like pollen can also infiltrate residential and commercial structures through ventilation (Stock and Morandi 1988; Jo and Kang 2006).

The prevalence of these particles depends on the emission source, air flow patterns, the size and species of the microbe, as well as other factors. To give the reader prospective of the approximate concentration of bioaerosols in indoor air, the National Institute for Occupational Safety and Health (NIOSH) recommends that a healthy environment should contain no more than 1,000 colony-forming units (CFU)/$m^3$ of culturable bacteria and fungi (Kalogerakis et al. 2005). This number is lower than the

total number of bioaerosols because it only includes culturable microbes (the percentage of unculturable microbes is much higher) that can be sampled and it does not include viruses or other types of bioaerosols (Stewart 2012). Bioaerosol motion is governed by the same physics as non-biological aerosols; however, there is the additional dimension of biological properties (e.g. viability) that must be considered when sampling, analyzing, and developing control technologies for bioaerosols (Griffiths and Decosemo 1994).

Although some bioaerosols are harmless to humans, pathogenic bioaerosols are responsible for transmitting a variety of bacterial, viral, and fungal infections (Tang et al. 2006). A single sneeze by a human can generate up to 40,000 droplets that can be propelled several meters and have sizes between 0.5-12 μm (Cox 1987). Other emission events include coughing and talking which generate 3,000 droplets/cough and 600 droplets/min respectively (Des Prez and Heim 1990). Provided that the person producing the droplets is infectious, these droplets can consist of infectious microbes surrounded by saliva, mucus, or other protecting fluid and can cause infection through inhalation or direct contact (Tyrrell 1967). Thus, these microbes pose a threat for transmission unless they are removed by ventilation, filtration, etc. or lose their infectivity due to adverse environmental conditions. Besides aerosol transmission, bioaerosols can deposit on objects and thus be a fomite threat - an inanimate object capable of transmitting disease (Morawska 2006).

Many diseases can be transmitted by the airborne (aerosol or droplet) route: anthrax, aspergillosis, chickenpox, common cold, influenza, whooping cough, tuberculosis, measles, and varicella zoster virus (VZV) (Tang et al. 2006). Of these, only

the latter three are considered to be truly airborne (Sehulster and Chinn 2003). For these diseases, the acquisition, replication, and subsequent dispersal of infectious microbes occur in the respiratory tract. For infection exclusively by the aerosol route, there are several requirements that must be met.

First, after emission from a source, the microbes must stay suspended in air so they can be inhaled. Like non-biological aerosols, bioaerosol motion is influenced by air flow forcing, diffusion, electrical forces, thermophoresis, and gravity. When influenced by gravity, bioaerosols obtain a terminal settling velocity when the gravitational force is equal to and opposed by the drag force. This velocity increases with particle size so that the suspension time for a 1,000-μm particle is 5 orders of magnitude less than for a 1-μm particle (0.3 s compared to 30,000 s) dropped from a height of 1 m (Wells 1934). If the relative humidity is sufficiently low to permit the encasing fluid to evaporate so that the final particle size is around 1 μm, the microbe (often referred to as droplet nuclei in literature) can remain suspended in the air almost indefinitely given air currents (Knight 1973; 1980). Thus, smaller bioaerosols like viruses have greater potential to remain airborne and become inhaled compared to larger bioaerosols like fungi which settle more quickly.

Once in the air, microbes must stay infectious during suspension to cause infection in a host. Environmental conditions like adverse ambient temperature and relative humidity cause inactivation of bioaerosols. Viruses without a lipid envelope are inactivated more readily at a relative humidity lower than 50% while lipid-enveloped virus are inactivated more readily at a higher relative humidity (Tang et al. 2006). Like lipid-enveloped viruses, Gram-negative bacteria tend to prefer lower relative humidity

although this observation is not consistent among all species (Theunissen et al. 1993). With regards to ambient temperature, a temperature of around 10 °C is believed to be optimal for survival (Ehrlich et al. 1970; Cox 1998). Other stresses like ultraviolet (UV) light, reactive oxygen species, and ions can also contribute to bioaerosol inactivation (Cox 1995). Although pathogenic bioaerosols are susceptible to death outside a host, being outside a host is a stage of the microorganism life cycle (dispersal), and studies have shown, for example, that human coronavirus (HCoV-229E) has a survival half-life of 67 hours at moderate relative humidity (Ijaz et al. 1985).

Another requirement is that the inhaled bioaerosols must be at the correct size for deposition in the appropriate location of the human respiratory system. *Mycobacterium tuberculosis* aerosols, for example, must be sufficiently small to deposit in the lungs to cause tuberculosis infection (Smith et al. 1966; Smith and Wiegeshaus 1989; Gonzalez-Juarrero et al. 2001). The bioaerosol particle size distribution (PSD) dictates the degree of penetration within the respiratory system and consequently the potential for infection.

To cause infection, a sufficient number of infectious microbes must deposit. If the number of microbes is too low, the host's immune system will be able to resist infection. The infectious dose varies considerably among pathogens but can be quite low: 10 microorganisms for rotavirus infection, 10-50 for tularemia, 10-100 for smallpox, and just one for tuberculosis (Des Prez and Heim 1990; Franz et al. 1997). In addition to causing infection, exposure to both viable and nonviable bioaerosols can trigger allergic reactions, irritation, and other adverse respiratory effects (Karol 1991; Lacey and Dutkiewicz 1994; Robbins et al. 2000).

Besides the airborne transmission route, direct contact with an infectious agent can also cause infection. The relative contribution of the airborne or contact routes in the transmission of a particular disease is poorly understood; however, the consensus in literature is that indoor air quality control measures such as building design, ventilation, and filtration, reduce the spread of infection (Morawska 2006; Tang et al. 2006). An example of the role of air quality control measures in airborne disease transmission is the well-documented Severe Acute Respiratory Syndrome (SARS) incident at Amoy Gardens in Hong Kong in 2003 (Yu et al. 2004). Research conducted retrospectively determined that feces from a single individual infected with the virus were inadvertently aerosolized from a bathroom exhaust fan. Due to airflow patterns in the complex, the virus was dispersed throughout 15 blocks containing over 150 apartments and resulted in 321 infections (Chu et al. 2005). The spread of the virus was blamed on the natural ventilation within the building which, although dilutes the concentration of bioaerosols, is able to transport bioaerosols between apartments (Morawska 2006). Besides suppression of the viral source, the Amoy Gardens incident may have been avoided with proper airflow design within the building as well as increased ventilation or other control measures (Li et al. 2005).

In indoor environments, increased ventilation and recirculation have been shown to reduce the spread of bioaerosols (Mendell et al. 2002). Infection by the aerosol route can be further reduced by employing control technologies to disinfect recirculated air (Morawska 2006). Although ventilation, recirculation, and disinfection technologies are critical in preventing aerosol infection, there is insufficient data to specify the exact requirements for these control measures (Li et al. 2007). Regardless, developing

disinfection technologies to reduce the concentration of bioaerosols has been an active area of research as current technologies have limitations.

## Current Bioaerosol Control Technologies

### Physical Removal of Bioaerosols via Filtration

Technologies which address the threat of bioaerosols fall into two categories: (1) capture or physical removal of bioaerosols from an air stream and (2) on-line or airborne inactivation. Technologies which compose the former category usually have not been developed specifically for bioaerosols but rather for aerosol control in general. In the latter category, technologies apply external stress like heat or ultraviolet light to render airborne microbes non-infectious and exclusively target bioaerosols.

Because bioaerosols physically behave identically to non-biological particles of the same aerodynamic size and composition, common aerosol control devices (air filters, electrostatic precipitators, etc.) which physically remove particles from an airstream can be applied to bioaerosol control (Lia and Wena 2003; Burton et al. 2007). Filtration is one of the most efficient methods for the removal of particles, viable and nonviable alike (Hinds 1999). High efficiency particulate air (HEPA) filters, for example, by definition have 99.97% removal efficiency of 0.3-µm sized particles.

Filters mechanically remove particles by a combination of four basic filtration mechanisms: inertial impaction, gravitational settling, diffusion and interception (Hinds 1999). Impaction occurs for larger aerosols which, due to their inertia, cannot adapt to changes in a flow streamline caused by a collector (fiber, granule, etc.). Gravity can also cause larger particles to contact a collector, especially when the flow velocity is low. For particles in the submicrometer range, diffusion and interception are the two dominant mechanical collection mechanisms. Aerosols are collected by diffusion when they

deviate from a flow streamline by Brownian motion and subsequently deposit on a collector. In interception, aerosols following a streamline and contact a collector when the streamline distance from a collector is equal to the particle radius. When the combined influence of the individual collection mechanisms is minimal, filters exhibit a most penetrating particle size (MPPS) near 300 nm (Lee and Mukand 2001). Electrostatic effects due to charges on the aerosol and collector also contribute to collection.

Standard air filters are effective in capturing bioaerosols, but do not inhibit the viability of microorganisms collected on the filter. For instance, bacterial endospores are able to survive for weeks on filters under unfavorable conditions (Wang 1999). Collected fungal spores can also remain viable and grow abundantly at high relative humidity (Kemp et al. 2001; Maus et al. 2001). Even sensitive Gram-positive and Gram-negative bacterial vegetative cells can survive for days on filters under ideal conditions (Maus et al. 1997; Reponen et al. 1999; Wang 1999).

The sustained viability of microorganisms collected on the filter is a concern to human health for two reasons: fomite transmission and bioaerosol reaerosolization. Fomite transmission is particularly hazardous for workers who handle filter disposal and replacement. For respirator wearers, contaminated masks can act as a fomite, transferring collected microorganisms to the hands during mask removal. Researchers have observed a 1-2 log transfer of test MS2 virus to the hands when a human subject removed contaminated mask and goggles (Casanova et al. 2008).

In addition to fomite transmission, sustained viability on the filter allows for reaerosolization of infectious bioaerosols from the filter fibers. Reentrainment rates of

collected bioaerosols can be up to 12% during high flow accelerations (Jankowska et al. 2000). In general, reaerosolization is usually less than a percent and may not seem significant. However, considering the infectious dose of some pathogens is quite low (as mentioned in the section above), reentrainment can pose a danger to those intended for protection. Microorganism reaerosolization can also occur from respirators during violent coughing or sneezing especially for larger particles like microorganism aggregates (Qian et al. 1997; Willeke and Qian 1998; Wang 1999).

**Air Filter Disinfection**

Because of the risks associated with sustained viability of bioaerosols collected on the filter, many technologies have been developed to disinfect filter media. Table 1-1 lists the current approaches, microbe tested in disinfection experiments, magnitude of inactivation, and time required for disinfection. The list includes photocatalytic oxidation (PCO), UV light, anti-microbial filters, as well as other technologies. Below is a brief description of several notable filter disinfection technologies:

- PCO: PCO functions by the creation of electron-hole pairs due to irradiation of a semiconductor (e.g. $TiO_2$) with UV light. If the energy of the UV light is greater than the band gap energy of the semiconductor, an electron will be promoted to the conduction band from the valence band. This electron-hole pair can generate radicals like hydroxyl radicals and superoxide ions which then disrupt the cell membrane to inactivate captured bioaerosols (Chuaybamroong et al. 2010).

- UV light: Irradiation of bioaerosols with UV light (without the presence of a photocatalyst) can cause inactivation through breaking of DNA bonds. Referred to as ultraviolet germicidal irradiation (UVGI), this technique produces thymine dimmers in DNA and inhibits the targeted microbe from replicating (Kujundzic et al. 2006).

- Anti-microbial filters: Air filters which have been treated with biocidal chemicals like iodine have also been tested against bioaerosols. For iodine-treated filters, inactivation is hypothesized to occur by the penetration of iodine molecules through the microbe cell wall and subsequent damage to the capsid protein. In addition to killing microbes collected on the filter, it is speculated that iodine species can inactivate microbes passing through the filter, resulting in a decrease

in penetrating viable bioaerosols. An advantage of anti-microbial filters is that they do not need external equipment (e.g. UV light) and thus can be readily incorporated into respirators (Lee et al. 2008; Ratnesar-Shumate et al. 2008; Lee et al. 2009).

Although these technologies have demonstrated inactivation against tested surrogates - as seen in Table 1-1 - each technology has their own disadvantages: PCO technologies can require hours for disinfection, UVGI creates ozone, and iodine-treated filters can release iodine vapor which is an upper and lower respiratory system irritant. Furthermore, for all the technologies, inactivation is dependent on environmental conditions and microbe species with highly-resistant Gram-positive bacterial endospores proving to be extremely challenging to kill (Nicholson et al. 2000).

**Airborne-Inactivation Technologies**

Besides the physical removal of bioaerosols from an airstream via filtration, air can be disinfected with airborne-inactivation technologies. Table 1-2 lists airborne-inactivation technologies, tested microbes, and magnitude of inactivation. The technologies can be installed in an on-line system (e.g. heating ventilation and cooling system) to process contaminated air. Below are descriptions of several airborne-inactivation technologies:

- UVGI: UVGI lamps can be positioned before or after an air filter to reduce the number of penetrating infectious bioaerosols by direct irradiation of the suspended microbes. Implementation of UVGI is relatively complex as engineering design must take into account many factors: airflow patterns, microbe residence time (dose), relative humidity, differing resistance among bioaerosols to UV light, ray-tracing optics, power consumption, dust on the lamps, shielding effect of material surrounding the bioaerosol, and generation of ozone from the UV lamps (Lin and Li 2002; Kujundzic et al. 2006).
- Microwave irradiation: Bioaerosols can be inactivated by direct irradiation with microwaves. Wu and Yao (2011) demonstrated reduction in the concentration of laboratory-generated and ambient bioaerosols using microwave radiation with a 2.45-GHz frequency. Electron microscopy of irradiated cells indicated that structural damage may be responsible for cell death (Wu and Yao 2010).

- Cold plasma: Plasma inactivation has been used in surface disinfection and sterilization but it has recently been applied to on-line bioaerosol inactivation. Plasma for disinfection purposes can be generated by dielectric barrier discharge (DBD) - a non-thermal technique which uses the electrical discharge between electrodes separated by a dielectric material. Microbe death occurs possibly by damage to DNA and cell membrane (Yang et al. 2011; Liang et al. 2012).

- Toxic vapors: Chemicals like chlorine dioxide ($ClO_2$) have been shown to effectively reduce the concentration of culturable airborne bacteria and fungi and thus decontaminate buildings. $ClO_2$ is an oxidizing agent which is speculated to cause microbe death by membrane damage or disrupting protein synthesis. Unlike the technologies discussed above, toxic vapors cannot be implemented in an on-line system and cannot be used with human occupants due to the vapor's toxicity (Burton et al. 2008).

- Ultrahigh temperature (UHT) treatment: UHT processes (applying temperatures of > 125 °C for several seconds) have traditionally been devoted to the sterilization or disinfection of liquids (e.g. milk) to kill resistant bacterial spores (Martin et al. 1966). Recent studies, however, have demonstrated their success against bioaerosols. In UHT bioaerosol studies, airflow has been heated to temperatures of greater than 1,000 °C for less than a second for inactivation (Lee and Lee 2006; Grinshpun et al. 2010a). In addition to causing high inactivation (> 3-log), UHT destroys Gram-negative bacteria endotoxin and fungi (1→3)-β-D-glucan, both of which can cause adverse respiratory effects (Jung et al. 2009a; Jung et al. 2009b).

Like with filter disinfection technologies, these airborne-inactivation technologies can successfully inactivate bioaerosols but they have disadvantages as well, briefly: UVGI design is complicated, microwave radiation is relatively ineffective, cold plasma can create harmful ozone during electrical discharge, toxic vapors are not suitable for on-line disinfection, and UHT treatment is limited by the difficulty in obtaining uniform airflow temperatures. Because of these drawbacks, further research is needed to either address the limitations of existing technologies or develop new technologies (Lee 2011).

## Infrared and Microwave Disinfection

With all the recent developments in bioaerosol control technologies, infrared (IR) and microwaves have been given relatively little attention. Although microwaves have been tested in air disinfection - through direct irradiation of suspended microbes - their

use in killing microbes captured on air filters has been investigated only minimally (Woo et al. 2012b). IR is radiation with wavelength between about 0.7 μm to 1,000 μm or frequency of 428 THz to 300 GHz (Siegel and Howell 2002). This type of radiation can be generated from a variety of sources: incandescent IR heat lamps, light emitting diode (LED), lasers, etc. Incandescent lamps produce IR by passing an electric current through a filament to heat the filament to thousands of degrees Kelvin by resistive heating. As the filament temperature increases, it emits IR photons (as well as visible light and other radiation) with a spectral distribution, $e_{\lambda b}$, described by Planck's Law, assuming the filament acts as a blackbody radiator (Siegel and Howell 2002):

$$e_{\lambda b}(\lambda_0, T) = \frac{2\pi h c_0^2}{\lambda_0^5 \left( e^{\frac{hc_0}{k\lambda_0 T}} - 1 \right)} \tag{1-1}$$

where $c_0$ is the speed of light in a vacuum, $h$ is Planck's constant, $\lambda_0$ is the emission wavelength, $k$ is the Boltzmann constant, and $T$ is the filament temperature. For a given filament temperature, the wavelength of maximum emission, $\lambda_{max}$, can be estimated by Wien's displacement law:

$$\lambda_{max} = \frac{C}{T} \tag{1-2}$$

where the value of $C$ is defined as 2,897.8 μm K. As shown in Eq. 1-2, as the temperature of the filament increases, the emitted wavelengths become shorter and the photons become more energetic.

IR is generated by LEDs when a voltage is applied to the LED semiconductor and electrons move to fill holes created in a P-type layer (Mishra and Singh 2008). Lasers produce light with a narrower emission spectrum than incandescent or LED sources and are used primarily for spectroscopy in scientific applications. IR

femtosecond laser pulses, however, have shown application in the selective inactivation of microbes suspended in liquids (Tsen et al. 2007).

Microwaves are radiation with wavelength of 1 mm to 1 m (Hashisho et al. 2005). Many devices exist which create microwaves, but a ubiquitous device found in the household microwave oven is the magnetron. A magnetron consists of a cathode surrounded by vacuum resonant cavities which is enveloped in a magnetic field. Electrons that are emitted from the cathode follow a curved path rather than a straight path due to the magnetic force, and microwaves are generated from the motion of the bunched electrons (Love 1995). Residential microwave ovens have magnetrons that are continuous wave as opposed to pulsed wave and output radiation at frequencies of 2.45 GHz or 0.915 GHz. After generation by the magnetron, radiation can be directed with a waveguide to a conducting chamber to impinge on and subsequently heat a target through dielectric heating.

Microwaves and more energetic IR rely on fundamentally different interactions with targeted molecules to cause heating: IR heating is mainly from bond vibrations while microwave heating is caused by molecular rotations. A material will absorb IR when the energy of the source photon matches the energy of a vibrational mode associated with the target material. The presence of vibrational modes in a material is dependent on the material's chemical bonding; for example, liquid water has an absorption band at 1.94 μm due to the O-H stretching and bending modes (Workman and Weyer 2008). Microwaves, on the other hand, are less energetic and heating is caused by rotations of molecules. Targeted molecules with a permanent dipole rotate in response to the time variation in electric field but are unable to adjust adequately.

Friction with other molecules and dissipation of energy results in heating of the material. Microwave heating is only achievable for polar molecules which have a dipole moment and consequently high loss factor (Hashisho et al. 2005). For both IR and microwaves, if the source radiation has a spectrum that does not correspond to any absorption wavelengths in the target material, the radiation will not be absorbed. Although the mechanisms that cause heating are different, IR and microwaves are governed by the processes of absorption, reflection, scattering, and refraction described by Maxwell's equations and quantum theory.

Due to their ability to heat materials, IR and microwaves have been used successfully in the disinfection of solid surfaces and liquids where the motivation has generally been food disinfection or decontamination of medical equipment (Heddleson and Doores 1994; Hamanaka et al. 2003; Gangneux et al. 2004; Neppelenbroek et al. 2008; Basso et al. 2010).

A study investigating IR disinfection of *B. subtilis* spores on a glass surface found D-values (time required for 1-log inactivation at constant temperature) of 26 min, 66 s, and 3.2 s at 120 °C, 150 °C, and 180 °C, respectively (Molin and Östlund 1976). Hamanaka et al. (2003) irradiated wheat and soybean with IR and found a reduction of 99% in the number of microbes within a few seconds of treatment. In that study, inactivation was achieved at moderate temperatures (50 °C) thus suggesting that death was caused by direct heating of the microbes rather than heat conduction from the cereal surface. Catalytic IR heating has also been used to effectively decontaminate raw almond kernels containing *Salmonella enterica* (Brandl et al. 2008). A 1.51-log reduction in the number of bacteria was observed when the almond kernels were

irradiated to a temperature of 113 °C for irradiation time of 45 s followed by immediate cool down. The authors found that by holding an elevated temperature after initial IR treatment instead of the cool down period, 7.5-log inactivation was achieved after 1 h.

Microwaves have been used to disinfect materials which contain polar molecules (e.g. water). Cañumir et al. (2002) examined microwave pasteurization of apple juice by first inoculating the juice with *E. coli*. Using power levels of 270-900 W, the authors obtained an *E. coli* reduction of 2-4 log after 60-90 s of irradiation (Cañumir et al. 2002). In another study, complete microwave decontamination was observed for herbal tea, liquid reconstituted dried food, and an *A. fumigatus* spore suspension (Gangneux et al. 2004). Besides food and beverages, microwaves have successfully disinfected non-food items like dentures and contact lens cases (Hiti et al. 2001; Dovigo et al. 2009). Dovigo et al. (2009) irradiated dentures inoculated with *S. aureus*, *P. aeruginosa*, and *B. subtilis* at 650 W and afterward cultured the microbes extracted from the dentures. Although sterilization was not achieved for *B. subtilis*, 3 min of irradiation completely inactivated *S. aureus* and *P. aeruginosa*. In all of these studies, the temperatures were not reported likely due to the difficulty in measuring temperature inside a microwave oven.

For both IR and microwaves, inactivation may not be exclusively attributed to heating as literature suggests that non-thermal effects may contribute to death. Hamanaka et al. (2006) irradiated stainless steel Petri dishes inoculated with *B. subtilis* spores using three IR heaters with different emission spectra (peak wavelengths of 0.950 μm, 1.10 μm and 1.15 μm). For each heater, the temperature was 100 °C at 2 min of irradiation. Even with the same temperature, higher inactivation was found for the

0.950-µm heater, with the shorter wavelengths producing the highest inactivation when the spore's water activity increased (Hamanaka et al. 2006). In a different study, Sawai et al. (2003) fabricated an IR irradiation chamber to investigate *E. coli* death as well as lipase and α-amylase enzyme inactivation. The authors found that the death rate constants were higher for IR heating than for conductive heating at the same temperature thus also indicating a possible non-thermal IR effect (Sawai et al. 2003).

Even though microwaves have a longer wavelength than IR and so are less energetic, a non-thermal contribution to inactivation has been proposed by several studies (Shamis et al. 2008). George et al. (2008) examined protein unfolding from microwave irradiation using surface plasmon resonance sensing. Compared to conventional heating of the test protein (citrate synthase) to the same maximum temperature, microwaves induced significantly greater protein unfolding, suggesting an additional effect from interaction with an electromagnetic wave (George et al. 2008). A study on the microwave inactivation of *B. atrophaeus* spores in medical waste found that activation energy decreased as the power per mass of waste increased and concluded that this was due to the inherent nature of microwave irradiation (Oliveira et al. 2010). Not all studies have observed this non-thermal microwave effect, however (Heddleson and Doores 1994). While investigating the death kinetics of *E. coli* suspended in phosphate buffer, Fujikawa et al. (1992) noted no considerable difference between the survival curves for microwave heating and conventional heating under the same temperature conditions. Regardless of the exact inactivation mechanism, both IR and microwaves offer unique advantages that make them an attractive option in practical disinfection processes.

First, radiational heating delivers energy directly to a target rather than relying on a medium to transfer energy. Because of this, it can be more energy efficient than conventional heating by convection and diffusion. Second, the devices that generate the radiation are ubiquitous and inexpensive; residential microwave ovens and incandescent IR heat lamps can be purchased for less than $100 and $10 respectively at common retail stores. Third, unlike chemical treatments or UV light which may be hazardous to human health (respiratory effects, DNA damage, etc.), IR and microwaves are safer and more environmentally friendly (Robinette et al. 1980; Inoué and Kabaya 1989; Schieke et al. 2003). Finally, IR and microwaves can generate high temperatures in a target material very quickly. An important consequence of this rapid heating is that radiational heating can be potentially employed in UHT treatment which is able to inactivate highly resistant bacterial endospores. With these four advantages - especially the latter advantage - IR and microwave technologies can address limitations of current bioaerosol disinfection technologies.

## IR and Microwave Heat Disinfection of Bioaerosols

### IR and Microwave Filter Disinfection

IR and microwaves can be applied to inactivate both microbes collected on air filters and microbes suspended in air. To inactivate microbes captured on filters, the filters need to be irradiated by a source, absorb incident radiation, and heat to a sufficiently high temperature. Although indiscriminate heating may be effective, to specifically achieve UHT, the filters must be heated for several seconds at a temperature of greater than 125 °C - the required temperature reported in literature. With this UHT treatment, previous studies have achieved 7-log reduction of bacterial spores in milk and water for 2-4 s of heating at around 130 °C (Williams et al. 1957;

Franklin et al. 1958). Due to the successes of these studies, it is hypothesized that applying an UHT process to a filter loaded with bioaerosols can achieve a similar result. UHT has not been tested for the disinfection of a substrate like an air filter, but temperatures greater than 125 °C are likely required because dry heat will be applied. Although simply using a microwave oven or IR lamp alone may be effective, filter disinfection can be optimized by incorporating reflectors and IR/microwave-absorbing materials to obtain higher filter temperatures more rapidly.

**On-Line UHT Bioaerosol Disinfection Using Radiation**

In addition to filter disinfection, radiation can be adopted in an UHT on-line bioaerosol disinfection process as well. UHT treatment of microbes suspended in air has demonstrated high inactivation in previous works: Jung and coauthors achieved greater than 2-log inactivation for *A. versicolor* and *C. cladosporioides* and greater than 3-log for *E. coli* and *B. subtilis* vegetative cells while Grinsphun and coauthors found greater than 5-log and 4-log inactivation of *B. subtilis* spore and MS2 virus, respectively (Jung et al. 2009a; Jung et al. 2009b; Grinshpun et al. 2010a; Grinshpun et al. 2010b). Although UHT treatment of these suspended microbes has been successful, the previous studies have noted the difficulty in obtaining a uniform air flow temperature to ensure predictable and efficient air disinfection. Radiational heating may be able to address this challenge.

Jung and coauthors designed an UHT system (Figure 1-1 A) which consisted of a quartz tube surrounded by electric heating coils to expose fungal and bacterial bioaerosols to temperatures from 50-700 °C. Because heat was applied to the air from the walls of the cylindrical tube, axial and radial temperature gradients were present in the heated flow. The authors discussed the temperature gradients and the complexity in

relating temperature to inactivation for continuous-flow systems. Grinshpun et al. (2010a; 2010b) developed a similar UHT system but positioned the electric heating element along the axis of a cylindrical test chamber instead as shown in Figure 1-1 B. Again, the spatial non-uniformity in temperature was discussed and thus a correction factor was used to relate a single temperature to an inactivation value.

In all previous studies, heat sources were parallel to the direction of airflow resulting in high temperature gradients within the heating chamber. Consequently, bioaerosols were exposed to vastly different temperatures in the heating chamber so the inactivation process could not be accurately characterized. An alternative to axial heating to possibly reduce temperature gradients is to heat a porous material positioned perpendicularly to the flow. In this manner, flow is heated by conduction when passing through the porous material. A novel way to realize this design is to use IR to irradiate porous IR-absorbing cloths as shown in Figure 1-1 C. IR radiation is well suited (compared to microwaves) for the heating because it offers very stable and uniform heating for flat and thin surfaces.

To heat the flow uniformly, the porous heating element must be itself at a uniform temperature and also must have a pore size that is conducive for rapid heat conduction within a pore. If heat is unable to fully transport in the air traveling through a pore within the flow residence time, then temperature gradients will exist. Temperature uniformity of a flow leaving a pore space can be estimated by calculating the Fourier number, *Fo* (Kreith et al. 2011):

$$Fo = \frac{\alpha\, t}{R^2} \tag{1-3}$$

where $\alpha$ is air's thermal diffusivity, $t$ is the residence time of the air in the heated pore space, and $R$ is the pore size. The Fourier number is the ratio of the rates of conductive heat transfer to energy storage and is used in heat conduction problems to determine whether steady-state has been achieved. A Fourier number greater than 1 indicates that the flow within a pore has been uniformly heated to the temperature of the heating element. Carbon cloths are an appropriate candidate for the porous material because they have pore sizes of a few hundred micrometers and have high IR absorption (Friedel and Hofer 1970). Although nichrome wire-based heating tapes could be employed for heating, their large pore sizes result in low Fourier numbers (especially with the $R^2$ relationship) and thus greater thickness is required.

### Heat Resistant Air Filters

Because a bioaerosol heat disinfection process can damage air filters, it is beneficial to explore appropriate types of filters. A possible alternative to traditional fibrous filters are heat-resistant metallic granular bed filters. Granular bed filters are filters composed of spherical collectors (granules) opposed to cylindrical fibers for fibrous filters. Though traditional granular bed filters have millimeter-sized granules, advances in material science have led to the development of granular bed filters with micrometer and submicrometer-sized granules to improve filtration efficiency.

Relatively recently, experimental and theoretical studies have been conducted on the aerosol filtration of these filters. Heikkinen and Harley (2000), Ruiz et al. (2000), and Endo et al. (2002) experimentally tested the performance of filters with micrometer and submicrometer-sized granules as a function of face velocity and pore/granule sizes. These filters were fabricated from either ceramic or steel and had a sintered structure. In theoretical studies, Jung and Lee (2004) and Marre et al. (2004) developed analytical

expressions for the efficiency by diffusion in unconsolidated media and diffusion and interception in sintered media, respectively. Overall, these works have demonstrated that the filters are effective in filtering aerosols but have high pressure drop.

Although metallic/ceramic granular bed filters with small collectors have been characterized, their potential application in bioaerosol filtration has not been examined. Thus, the filtration performance of these heat-resistant filters against bioaerosols should be tested. Filters with small granules have high efficiency and so they may be useful for airborne pathogen control, especially for filtering microbes with a low infectious dose. Like a membrane filter, these filters can be fabricated with a specific pore size (< 1 μm) to prohibit larger bioaerosols like bacteria or fungi from penetrating. All previous studies have tested non-biological particles but the results do not accurately reflect filtration of bioaerosols; non-biological particles yield different penetration values than biological particles of identical size (Eninger et al. 2009; Miaskiewicz-Peska and Lebkowsk 2012). This has been attributed to differing shape and chemical composition between biological particles and their surrogates. To obtain an accurate assessment of the filtration performance of these filters against bioaerosols, bioaerosols themselves should be tested directly.

**Sampling Behavior of Nanometer-Sized Aerosols**

Granular bed filters with small collectors tend to have high filtration efficiency: Endo et al. (2002) found penetration of less than $10^{-8}$ for 0.02 μm-sized aerosols with their tested filter. When counting penetrating aerosols downstream of a very efficient filter, only a low number of aerosols will be detected. Because aerosols are stochastically distributed in space so the count will vary from sample to sample, the accuracy of a measurement is believed to be lower with fewer detected aerosols

(Larsen et al. 2003). Consequently, obtaining a representative measurement of aerosol counts (or concentration) downstream of a highly efficient filter is very challenging. It is thus useful to explore the nature of aerosol sampling.

Traditionally, it is widely accepted that the number of aerosols sampled or detected is probabilistic and follows a Poisson process (Hinds 1999; McMurry 2000). The probability, $P(k|\mu)$, of detecting $k$ number of aerosols in a single sample volume with population mean count, $\mu$, is given by the Poisson distribution displayed in Eq. 1-4 (Ramachandran and Cooper 2011).

$$P(k|\mu) = \frac{\mu^k e^{-\mu}}{k!} \tag{1-4}$$

In aerosol sampling, the Poisson distribution is the expected probability distribution of counts obtained from using an aerosol counting instrument (e.g. optical particle counter (OPC)) over many samples. Two identifying characteristics of a Poisson process are that the mean and variance calculated over all the volumes will be equal and the waiting times between particle detections are distributed exponentially (Larsen et al. 2003). It is useful to assume that aerosol sampling behaves according to a Poisson process for several reasons.

First, uncertainty in the concentration can then be described as inversely proportional to the square root of the measured count (Ramachandran and Cooper 2011). Second, using Bayes' theorem, the probability distribution and the maximum likelihood value of the population mean count can be found from the measured count. The application of Bayes' theorem here is especially powerful because the probability the measured concentration represents the actual concentration can be calculated from

one measurement. When sampling with short time periods so that a low number of aerosols are detected, knowledge of the Poisson distribution is helpful.

Due to Brownian motion or other phenomena, the inherent randomness associated with aerosol sampling is expected. However, the Poisson assumption is a strict embodiment of stochastic behavior that requires a perfectly random process. A Poisson process would only be realized when the probability of detecting a particle is not influenced (i.e. enhanced or inhibited) due to particle detections before it; particle detections must be completely independent of each other (Shaw et al. 2002). Any change in the probability of detecting a particle due to a preceding particle detection indicates that chance described by the Poisson process is not responsible for variability in the measured aerosol concentration. Non-Poissonian behavior of detected aerosols thus makes the relationship between measured concentration and actual concentration unclear.

Although a Poisson process is a convenient model to describe the sampling of aerosols, its validity has not been verified experimentally for nanometer-sized aerosols. Previous works which have investigated the Poisson assumption have been related to cloud physics or rainfall events (Shaw et al. 2002). The primary goal of these works was to investigate if cloud droplets/rain were distributed perfectly randomly in space. Additional studies also investigated whether a Poisson process describes the spatial distribution of aerosols but inadvertently examined the sampling nature of micrometer-sized aerosols (Larsen et al. 2003; Larsen 2007). Although the consensus was that the spatial distribution of aerosols did not exactly follow a Poisson process, the effect of this in the realm of aerosol sampling was not discussed. Furthermore, only aerosols with

sizes greater than 300 nm were considered and they were grouped into relatively coarse size bins by an OPC. These studies did, however, develop the framework for assessing Poissonian behavior so that its context in aerosol sampling can be fully examined.

There are several ways to quantitatively determine whether a process is Poissonian but a powerful and routinely-used tool is the pair correlation function (PCF). The PCF can be described in the following manner (Shaw et al. 2002; Larsen et al. 2003). First, consider two differential sampling time periods, $dt_1$ and $dt_2$, which are separated by time *t* and defined to be sufficiently small as to contain only one or zero aerosols. For a Poisson process, the probability that a differential time period contains a particle is then $\frac{N}{T}\, dT = \bar{N} dT$, where *T* is the total sampling time, *N* is the total count of aerosols in *T*. As particle detections are independent of each other, the probability, *P(1,2)*, of detecting a particle in both time periods is the product of the probabilities of detecting a particle in each time period.

$$P(1,2) = \bar{N}^2 dt_1 dt_2 \tag{1-5}$$

If, however, the process is not Poissonian, then the probability will be enhanced or inhibited by modifying Eq. 1-5 into Eq. 1-6 (Green 1969).

$$P(1,2) = \bar{N}^2 dt_1 dt_2 (1 + \eta(t)) \tag{1-6}$$

The term $\eta(t)$ is the PCF which indicates how a time series of particle detections deviates from a Poisson process. A value of $\eta(t)$ greater than zero means that there is enhancement (positive correlation) of particle detection when time periods are separated by *t*. For $-1 \leq \eta(t) < 0$, a particle detection at $dt_1$ decreases the chance a particle will be detected *t* away at $dt_2$ (negative correlation). For the process to be

considered Poissonian, the PCF must be zero for all *t*. A more thorough background of the PCF is discussed in literature and will not be repeated here (Shaw et al. 2002; Larsen et al. 2003).

When calculating the PCF with an experimental time series, the differential time periods $dt_1$ and $dt_2$ cannot be rigorously achieved. Practically, the PCF can be calculated via the operational PCF formula displayed in Eq. 1-7 using particle counts within the smallest sampling period available for the instrument (Kostinski and Jameson 2000).

$$\eta(t) = \frac{\overline{N(t)N(0)}}{(\bar{N})^2} - 1 \tag{1-7}$$

To use Eq. 1-7 with time series data, the total sampling time can be divided into small time periods determined by the instrument resolution. Then, the number of particles in a small time period, *N(0)*, can be multiplied by the number of particles in the period that is time *t* away, *N(t)*. This process is repeated in *T* for each pair of *N(0)* and *N(t)* and the average for all multiplied pairs is calculated. This average is divided by $(\bar{N})^2$ and subtracted by unity to yield the PCF. Since differential time periods as defined above cannot be used in the most precise sense, the time series must satisfy dilute criteria (to be discussed in Chapter 6) for the PCF to be meaningful. In general, using non-differential sampling periods causes the exact detection time of a particle to be ambiguous so the calculated PCF is simply an estimation.

The PCF shows how the probability of a particle detection differs from the Poissonian case when two sampling periods are separated by some time *t*; and it is the most rigorous test for the Poisson assumption. However, a more practical metric in the field of aerosol sampling is the time-averaged PCF, $\bar{\eta}(s)$. The time-averaged PCF

indicates how aerosol detection deviates from a Poisson process over sampling period with length *s*. The operational formula of $\bar{\eta}(s)$ is displayed in Eq. 1-8 (Kostinski and Jameson 2000):

$$\bar{\eta}(s) = \frac{\overline{(\delta N)}_s^2 - \bar{N}_s}{(\bar{N}_s)^2} \tag{1-8}$$

where $\bar{N}_s$ and $\overline{(\delta N)}_s^2$ are the mean and variance, respectively, in a sampling period of length *s*. For the Poisson case, the mean and variance are equal so that $\bar{\eta}(s)$ will be zero. The presence of correlations as shown by *η(t)* within sampling period *s* will affect the value of $\bar{\eta}(s)$. However, if these correlations are equal and opposite, the net sampling behavior will appear to be Poissonian. When this occurs, aerosol detection is considered to be “Poisson distributed” but not considered a Poisson process because *η(t)* is not zero for all times (Larsen et al. 2003). The characterization of “Poisson distributed” is adequate for aerosol sampling because concentration measurements are taken over a time period.

No studies in literature have confirmed the validity of the Poisson assumption for nanometer-sized aerosol sampling and thus its validity should be examined. Because of their size, nanometer-sized aerosols are influenced by physical mechanisms (e.g. Brownian motion, air turbulence, electrostatic forces, etc.) differently than micrometer-sized aerosols so their sampling behavior may be very different. Furthermore, in filtration testing, the MPPS tends to be in the range of hundreds of nanometers. To test this hypothesis, a scanning mobility particle sizer (SMPS) can be employed to create a time series of particle detections for aerosols of a specific size. The time series can then be analyzed with the PCF and time-averaged PCF to gain insight into the validity of the Poisson assumption.

### Application of IR Irradiation in Volatile Organic Compound Desorption

Besides the use of IR heating in disinfecting filters and air, IR can possibly be used to regenerate adsorbents which are saturated with VOCs. VOCs like benzene and toluene are dangerous to humans due to their positive association with adverse health effects like asthma, fatigue, and chronic respiratory symptoms (Otto et al. 1992; Ware et al. 1993; Kostiainen 1995; Pappas et al. 2000). Furthermore, VOCs are linked to an increased cancer risk for people in indoor environments (Guo et al. 2004). These compounds are released from construction adhesives, paints, furniture polishes, etc. and tend to have a much higher concentration indoors than outdoors (Guo 2000; Guo and Murray 2000; 2001; Jia et al. 2008). Considering that humans spend about 90% of their time indoors, the prevalence of these pollutants in the indoor environment is a concern (U.S. EPA 1989). Besides effects on indoor air quality, anthropogenic VOCs can also serve as precursors in the creation of photochemical smog and other harmful byproducts in the outdoor environment (Volkamer et al. 2006).

Activated carbon has been widely employed to remove VOCs through the process of adsorption. Granular activated carbon (GAC) has traditionally been used, but activated carbon cloths (ACC) are an attractive alternative due to their mass and heat transfer properties and high specific surface area (Cal et al. 1994; Hashisho et al. 2005). Once ACC is saturated from adsorption, ACC can be regenerated to restore the ACC to its initial capacity. Regeneration can be accomplished by heating the ACC to thermally desorb the adsorbate molecules; the molecules can then be captured and reused in the case of industrial applications or vented outdoors for residential applications (Sidheswaran et al. 2012). Numerous studies have proposed ways to regenerate ACC including steam, electrothermal (Joule) heating, and electromagnetic

induction heating (Brasquet and Le Cloirec 1997; Sullivan et al. 2001; Subrenat and Le Cloirec 2004; Sullivan et al. 2004; Luo et al. 2006; Johnsen et al. 2011). Recently, microwave heat regeneration of ACC has been proposed by Hashisho et al. (2005) to be advantageous to previous methods due to its theoretical ability to selectively desorb captured pollutants. This is because microwaves only heat compounds that have a dipole moment so that polar pollutants rather than nonpolar pollutants will be heated when irradiated with microwaves. In practice, however, the study showed that microwaves heated the activated carbon adsorbent so both captured polar and nonpolar adsorbates were desorbed and thus selective desorption was not realized (Hashisho et al. 2005). If achieved, selective desorption has the potential to reduce energy consumption because regeneration power is directed completely to a targeted adsorbate and is not lost in heating absorbent mass.

Although the concept is novel, microwaves have the disadvantages of non-uniform heating for targets which results in both cool spots and thermal runaway (Vadivambal and Jayas 2010). Designing a microwave oven to reduce these non-uniformities is not trivial because the electric field inside the oven is also dependent on interaction with a dielectric target. In addition, a microwave oven and magnetron must be specially constructed to incorporate an entire adsorption/desorption system (Hashisho et al. 2005). A possible alternative to the current desorption methods is IR heating. IR has several advantages in heating processes described in the sections above, namely: (1) rapid generation of high temperatures in a thin, IR-absorbing material like ACC (Wade 1987), (2) spatially uniform heating to ensure complete and predictable regeneration, (3) ease of constructing a regeneration system using simple

reflective surfaces (e.g. foil), and (4) inexpensiveness of the heating source (IR bulb). There is also the potential of using focused sunlight instead of a light bulb in an effective and green regeneration process. Finally, because a molecule will only absorb radiation with a specific frequency, multi-component adsorbates can be separated by tuning an IR source to a particular wavelength. Although selective desorption is an intriguing possibility, an initial study should focus on the use of untuned (broadband) light to gain fundamental understanding into an IR regeneration process.

## Research Objectives

In this dissertation, microwave and IR-based control devices were designed and tested for bioaerosols and VOCs to address the limitations of current technologies. The use of radiation offers significant advantages and can help improve strategies to reduce the effects of these air pollutants. Microwave/IR devices were developed for bioaerosol inactivation and an IR device was developed for regeneration of ACC saturated with a test VOC. Two additional studies were undertaken to test the effectiveness of a heat-resistant granular bed filter against bioaerosols and to examine the nature of aerosol sampling. Overall, six objectives were completed to fully study the use of radiation-based technologies in air pollutant control:

1. Microwave disinfection of air filters: Bacterial spores were loaded onto a filter, the filters were irradiated with microwaves, and afterward the microbes were extracted from the filter to assess the reduction in viable bacteria due to irradiation. Spores were selected because they are among the hardiest microbes and have not been tested previously.
2. IR-UHT disinfection of air filters: An IR filter disinfection setup was developed to achieve UHT and inactivate collected bioaerosols. Similar to the first objective, filters were loaded with bioaerosols, irradiated, and underwent an extraction procedure to remove the microbes. The effectiveness of a UHT process when applied to air filter disinfection was assessed.

3. IR-UHT disinfection of air: The proposed on-line IR-UHT disinfection system (Figure 1-1 C) was tested for its ability to obtain uniform temperatures and inactivate test bioaerosols. The mechanism causing death of airborne bacteria from UHT was also examined. Besides testing in the lab setting, the system was also tested against environmental bacterial and fungal bioaerosols.

4. Filtration of bioaerosols using a metallic granular bed filter: The filtration performance of a filter composed of micrometer-sized granules against bacterial and viral bioaerosols was determined. A metallic filter fabricated by Oak Ridge National Laboratory (ORNL) and previously used in the filtration of liquid-borne bacteria (Phelps et al. 2008) was investigated.

5. Validity of the Poisson assumption: The validity of the Poisson process was determined in nanometer-sized aerosol sampling. The PCFs and other metrics (e.g. coefficient of variation of the concentration) were calculated from both the experimental time series and a computer-generated Poissonian time series to examine how experimentally-measured values differed from a true Poisson process.

6. IR regeneration of ACC: The effectiveness of IR in heating ACC to desorb a captured VOC (toluene) was investigated. ACC were first loaded to saturation and then irradiated with IR to regenerate the adsorbent. The restoration of the ACC's performance by IR regeneration was determined.

Table 1-1. List of filter disinfection technologies.

| Disinfection Technology | Microorganism Species | Maximum Log Inactivation* | Time Required | Notes |
|---|---|---|---|---|
| Ultraviolet irradiation (Kujundzic et al. 2006) | *M. parafortuitum* | 1.5 | 1 hour | The disinfection process was not optimized |
| | *A. versicolor* | 0.60 | | |
| Microwave irradiation (Woo et al. 2012b) | MS2 virus | > 4 | 10 min/cycle | 750 W power |
| Iodine treatment (Lee et al. 2008) | *B. subtilis* spore | ≈ 0.50 | n/a | Dependent on relatively humidity |
| Iodine treatment (Lee et al. 2009) | MS2 virus | ≈ 0.20 | n/a | Dependent on temperature and relative humidity |
| Silver copper based treatment †, ‡ (Rengasamy et al. 2010) | MS2 virus | ≈ 2 | 4 hours | 37 ºC and 80% RH |
| EnvizO3-Shield technology †, ‡ (Rengasamy et al. 2010) | MS2 virus | ≈ 2 | 4 hours | 37 ºC and 80% RH |
| Iodinated Resin †,‡ (Rengasamy et al. 2010) | MS2 virus | 3.7 | 4 hours | 37 ºC and 80% RH |
| Photocatalytic Oxidation -$TiO_2$ †, ‡ (Rengasamy et al. 2010) | MS2 virus | < 1 | 8 hours | - |
| Silver nanoparticles (Lee et al. 2010) | *E. coli* | 2 | 1 min | Dependent on RH and nanoparticle PSD |
| | *S. epidermidis* | > 2 | 9 min | |
| | *B. subtilis* | ≈ 0.4 | 9 min | |
| Photocatalytic Oxidation † (Chuaybamroong et al. 2010) | *A. niger* | 0.64 | 10 hours | Dependent on loading conditions |
| | *P. citrinum* | 0.77 | | |
| | *S. epidermidis* | > 2 | | |
| | *B. subtilis* | 0.70 | | |
| Photocatalytic Oxidation (Vohra et al. 2005) | *B. cereus* spore | Total | 10 min | Observed inactivation likely due to extraction method and low control CFU/plaque-forming units |
| | *S. aureus* | Total | 5 min | |
| | *E. coli* | Total | 5 min | |
| | *A. niger* | Total | 45 min | |
| | MS2 virus | Total | < 2 min | |
| Positive ions (Park et al. 2009) | *E. coli* | 0.60 | 10 min | Required $1.3 \times 10^7$ ions/$cm^3$ |

* This is the maximum quantifiable inactivation that was described. Percent values have been converted to log inactivation for comparison between studies.

† Results were not compared directly against a control so that the effect of the treatment is confounded with the natural decrease in viability over time.

‡ The authors noted that the observed inactivation was not statistically significant when compared to the inactivation found on an untreated filter under identical conditions.

Table 1-2. List of airborne bioaerosol disinfection technologies.

| Disinfection Technology | Microorganism Species | Maximum Log Inactivation or Removal* | Operating Condition | Notes |
|---|---|---|---|---|
| UVGI (Lin and Li 2002) | *E. coli* | 2.5 | 1,000 μWs/cm$^2$ | Microbes generally more susceptible at 50% RH than at 80% RH |
| | *B. subtilis* spores | 2.5 | 14,000 μWs/cm$^2$ | |
| | *Candida famata var. flareri* | 1.8 | 8,000 μWs/cm$^2$ | |
| | *P. citrinum* | 0.92 | 14,000 μWs/cm$^2$ | |
| Microwave Irradiation (Wu and Yao 2010) | *B. subtilis* spores | 0.46 | 119 W | Irradiation for 1.5 min, power level not statistically significant for spore |
| | *P. fluorescens* | 1.2 | 700 W | |
| | *A. versicolor* | 0.96 | 700 W | |
| Carbon nanotube plasma (Yang et al. 2011) | *E. coli* | 1.2 | -7.5 kV | Inactivation decreased with increasing flow rate |
| | *B. subtilis* | 0.92 | 6 kV | |
| | λ virus | 0.72 | | |
| Nonthermal plasma (Liang et al. 2012) | *B. subtilis* | 1.8 | 14 kV, 10 kHz | Exposure to plasma of 1.2 s |
| | *P. fluorescens* | 7 | | |
| Toxic vapors (Burton et al. 2008) | Culturable bacteria | 0.8219 | 10,351 ppm hr | Experiment conducted inside a contaminated house |
| | Culturable fungi | 1.585 | | |
| UHT setup by Jung and coauthors (2009a; 2009b) | *A. versicolor* | >2 | 350 °C | Exposure times of 0.17 - 0.29 s, heated wall of test chamber heated air |
| | *C. cladosporioides* | >2 | 400 °C | |
| | *E. coli* | >3 | >160 °C | |
| | *B. subtilis* | >3 | >400 °C | |
| UHT setup by Grinsphun and coauthors (2010a; 2010b) | *B. subtilis* spore | >5 | 375-400 °C | Flow rates of 18 LPM and 36 LPM, heating element within test chamber heated air |
| | MS2 virus | >4.4 | 170-250 °C | |
| Negative air ions (Yu et al. 2008) | λ virus | 0.210 | Ion concentration of 9.8 ×10$^5$ ions/cm$^3$ | Dependent on RH |
| | *E. coli* | 0.123 | | |
| | *C. famata* | 0.155 | | |
| PCO, UV - $TiO_2$ filter (Goswami et al. 1997) | *S. marcescens* | Total | 100 W/m$^2$ UV light intensity, required > 700 min | Highly dependent on RH |
| PCO, UV - $TiO_2$ filter (Pal et al. 2005) | *E. coli* | Total | 2.28 mW/cm$^2$ light intensity, required 3.57 min | Challenging number of *E. coli* not reported |

* This is the maximum quantifiable inactivation that was described. Percent values or survival fractions have been converted to log inactivation for comparison between studies.

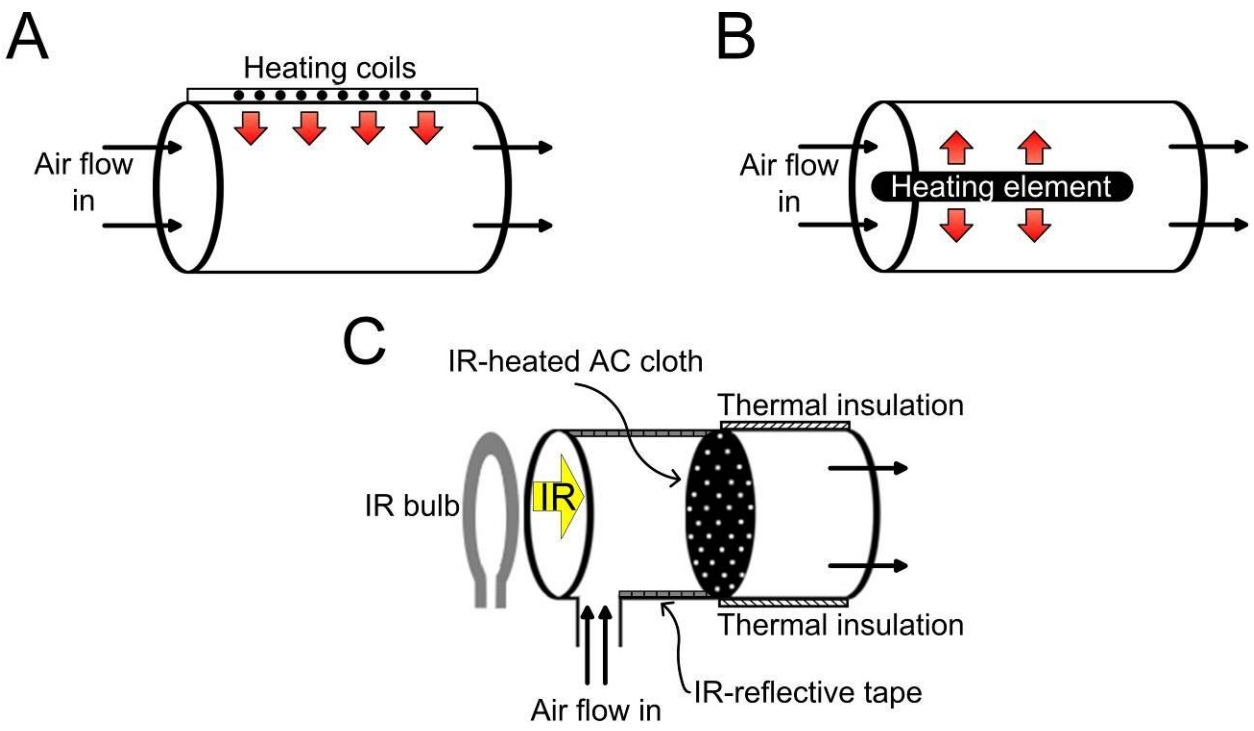


Figure 1-1. Simplified schematics of the systems used for the UHT treatment of bioaerosols. A) This system was tested by Jung et al., 2009a, 2009b, 2010, B) Grinshpun et al. 2010a, 2010b, and Johansson et al., 2011, tested this system. C) A design which incorporates IR heating.

# CHAPTER 2
# MICROWAVE ASSISTED NANOFIBROUS AIR FILTRATION FOR DISINFECTION OF BACTERIAL SPORES*

## Objective

The objective of the study in this chapter was to evaluate the effectiveness of microwaves in inactivating bacterial spores collected on an air filter. Two separate experiments were conducted: static filter disinfection and on-line filter disinfection. In static tests, filters were removed from the bioaerosol loading system prior to irradiation while in on-line tests filters were irradiated during filtration.

## Materials and Methods

### Test Air Filter

Nanofiber filters were used as the test air filter. Nanofiber filters are composed of cylindrical collectors (fibers) with a nanometer-sized diameter as opposed to the conventional micrometer-sized diameter. The smaller fiber diameter and larger surface area yields higher collection efficiency than conventional filters. Furthermore, gas slip at the nanofiber surface reduces the fiber's air resistance and the filter's pressure drop. Test polyacrylonitrile (PAN) nanofiber filters were fabricated by University of Florida Department of Material Science and Engineering using electrospinning as described by Zhang et al. (2009). To improve the resistance of the filters during microwave heating, the filters were heat treated for 1 h at 250 °C to ensure crosslinking of the PAN molecules. Scanning electron microscopy (SEM) and analysis with ImageJ ver. 1.40 g indicated that the completed filters had fiber diameter and coefficient of variation of 195 nm and 0.166, respectively. Filters between 40-46 mm in diameter were used for testing.

* Reprinted with permission from Zhang, Q., Damit, B., Welch, J., Park, H., Wu, C.Y. and Sigmund, W. (2010a) Microwave assisted nanofibrous air filtration for disinfection of bioaerosols. *J Aerosol Sci* **41**, 880-888.

**Preparation of Test *B. subtilis* Endospore Bioaerosol**

A spore-forming Gram-positive bacterium, *Bacillus subtilis* is an appropriate surrogate for bacterial endospores in thermal resistance studies (Montville et al. 2005). *B. subtilis* spores are ellipsoid shaped and have an aerodynamic diameter of approximately 0.9 μm (Aizenberg et al. 2000). *B. subtilis* vegetative cells, obtained from the University of Florida Department of Microbiology and Cell Sciences, were subjected to a sporulation process to produce endospores (Lee et al. 2008). Sporulation was induced by culturing the vegetative cells in a growth medium consisting of 200 mL African violet soil extract, 800 mL deionized (DI) water, 1 g yeast extract (Fisher Scientific, Cat. No.:BP1422), and 15 g Difco Nutrient Agar. After inoculation on an agar slant, the cultures were incubated at 37 °C for one week. A 2-mL DI water suspension of *B*. *subtilis* was obtained by washing the slant. The suspension was then heated in an 80-°C water bath for 30 minutes to kill vegetative cells. Vegetative cell debris was removed by centrifuging the suspension at 3,500 RPM for 10 minutes. Immediately after the purification process, the spore suspension was diluted to about $10^6$ colony-forming units (CFU) $mL^{-1}$ and aerosolized.

**Disinfection Experiments**

In static disinfection, filters were loaded with spores, removed from the test system entirely, and placed in an empty microwave oven to be irradiated. In on-line disinfection, spore-laden airflow was directed toward a test filter held by a quartz chamber inside the oven. The filters were then irradiated during spore filtration. Thus, static testing provided basic understanding of the power and exposure time needed for disinfection while the on-line experiments were more relevant in investigating the feasibility of microwave disinfection in air filtration systems.

**Static filter disinfection**

The system used to load the filter in static tests is shown in Figure 2-1 and is represented by the red colors. A 6-jet Collison nebulizer (Model CN25; BGI Inc., Waltham, MA) aerosolized the spore suspension at a flow rate of 5.5 LPM. An air cylinder supplied particle-free compressed air to the nebulizer and to a dilution dryer (11 LPM) to evaporate the water surrounding the nebulized bacteria. A flow rate of 4.1 LPM was directed to the filter for spore loading while the remaining 12.4-LPM flow left the system as excess. All of the flow rates were controlled with calibrated rotameters (OMEGA Engineering Inc., Stamford, CT).

After loading for 30 min, the filter was removed from the system and cut into quadrants. One of the quadrants was directly placed in 50 mL of Ringer's solution to serve as the control. The Ringer's solution was vortexed to extract spores from the fibers and then 1 mL of the extracted solution was serially diluted for culturing. Petri dishes inoculated with dilutions of the extracted solution were incubated for 1 day before counting the number of CFU. In counting, only Petri dishes containing 30-300 CFU were considered. The remaining three filter quadrants were sandwiched between silicon carbide (SiC) disks and then placed into the microwave oven for heating. Surrounding the filters with these disks during irradiation improves heating because SiC has a high absorption of microwave radiation unlike PAN. Power levels of 250 W and 750 W and exposure times of 30 s, 45 s, 60 s, and 90 s were tested using a Panasonic model NN-T945SF microwave oven. After irradiation, the quadrants were removed and subjected to the identical extraction and culturing procedure outlined above with the control quadrant. The survival fraction, *SF*, of the spores after heating was then calculated by Eq. 2-1:

$$SF = \frac{N_i}{N_n} \quad (2\text{-}1)$$

where $N_i$ and $N_n$ are the number of microbes extracted and cultured from the irradiated and non-irradiated filters respectively. Calculating the survival fraction in this manner allows for a direct assessment of the effect of microwave heating by eliminating the natural loss of viability due to retention on the filter.

To achieve different heating settings, many residential microwave ovens output one power and reduce the time the magnetron generates microwaves. For example, a 1,000-W oven operating at “500 W” could have a 10-s cycle where the magnetron would output 1,000 W for the first 5 s and then be switched off for the last 5 s yielding an average output power of 500 W. The oven model used is this study, however, irradiated a target continuously at the actual reduced power. Therefore, all the powers shown in this study represent stable powers received by the filter. Obtaining a filter temperature measurement is critical in determining the relationship between temperature, microwave power, and bioaerosol inactivation or identifying whether UHT has been achieved. However, measuring the temperature of a target inside a microwave oven during irradiation is not trivial and was not conducted here (Hashisho et al. 2005).

**On-line filter disinfection**

A diagram of the system used in on-line experiments is shown in Figure 2-1 and is represented by both the black and red colors but excludes the excess line. Again, the spores were first aerosolized with a Collison nebulizer and sent to a dilution dryer. After leaving the dilution dryer, the flow was then divided into three flows which were directed toward a BioSampler (SKC, Eighty-Four, PA) to sample the airborne bacteria concentration, a filter that was not microwaved (control), and a filter inside the

microwave oven that was microwaved. The experimental microwave oven was modified by cutting 2.54-cm holes for the inlet and outlet air flow. Bioaerosol-laden airflow was directed through the inlet hole and entered a microwave-transparent quartz chamber which held a filter in the oven during filtration and irradiation. The PAN filters were surrounded by SiC mats during initial experiments but were later replaced by SiC disks. After passing through the filter, the airflow left the oven through the outlet hole and then left the test system. Experiments were run for a total of 30 min which was divided into three 10-min cycles. During filtration, the filter was irradiated constantly (10 min/cycle), 5 min at the beginning of a cycle (5 min/cycle), and 1.25 min at the beginning of a cycle (1.25 min/cycle). The 5 min/cycle and 1.25 min/cycle applications were to examine whether periodic microwave applications could save energy and still adequately disinfect the filter via residual heat when the oven was turned off. Microwave powers of 250 W, 500 W, and 750 W were tested in on-line experiments.

After the 30 min experiment, the filters were removed from the system and a whole filter underwent an identical extraction and culturing procedure as the filter quadrants in the static experiments. Log inactivation was calculated from Eq. 2-2.

$$Log\ inactivation = -\log(SF) \quad (2\text{-}2)$$

Log inactivation indicates the order of magnitude in the reduction of an initial microbe population with 1-log inactivation corresponding to 90% inactivation, 2-log inactivation corresponding to 99%, etc.

To verify that similar numbers of bioaerosols entered the experimental and control paths, separate experiments were conducted using BioSamplers attached

downstream of each path. A difference in CFU of less than 5% between paths was found indicating that the filters were challenged with a similar number of spores.

## Results and Discussions

The results of the static experiments are displayed in Table 2-1. In general, spore survival was lower at the higher 750-W power and with increased application time. After irradiation at 750 W for 90 s, only 0.20% survival was observed. Less powerful microwave power applications proved less effective. For 250 W, 45 s of application time was required to achieve any disinfection at all. Compared with *E. coli* disinfection found in a companion microwave study (Zhang et al. 2010a), *B. subtilis* spores were much more difficult to destroy, requiring a higher microwave power for the same level of disinfection. This apparent difficulty in destroying the spores would also be observed during on-line testing.

In on-line testing using SiC mats as the microwave absorber, disinfection of only 1 log was observed for the spore at 500-W continuous irradiation. At the lowest setting of 125 W and 1.25 min/cycle application, no disinfection was found. Because of the inadequate spore disinfection, the SiC mats were replaced by SiC disks, and the maximum tested power was increased from 500 W to 750 W. Results with these changes, displayed in Figure 2-2, showed considerable increase in spore disinfection. Like in the static tests, an increase in power and application time resulted in higher disinfection. With continuous microwaving at 750 W, about 2.8-log disinfection was observed. Compared to the *E. coli* results, spore disinfection was still less effective and this is likely attributed to the heat resistivity of the spore due to its coat (Nicholson et al. 2000). Although complete disinfection could potentially be achieved by increasing the microwave power further, the durability of the filter in such conditions was a concern.

After irradiation at 750 W for a continuous 30 min period, slight discoloration and burning of the filter was noticed.

It was observed that the static tests had greater inactivation than the on-line experiments under similar conditions. Because of this, it was hypothesized that heat loss from the filter to the flow caused decreased inactivation during the on-line experiments. Hence, experiments were conducted with a lower face velocity during irradiation (at the same microwave power level) to verify the hypothesis. For the 750 W and 1.25 min/cycle condition, decreasing the face velocity 50% during irradiation resulted in an increase of 0.636-log inactivation of spores. This result provides evidence that heat conduction to the flow decreases the filter temperature and the inactivation on the filter. It also provides some evidence that thermal effects, rather than non-thermal effects, may be the dominant factor in spore inactivation.

ANOVA statistical analysis with Minitab 15 statistical software indicated that microwave power, rather than application time, was the most significant factor in the reduction of viable *B. subtilis* spores on the filter ($p\text{-value}<0.05$). Therefore, to maximize the effects of disinfection on PAN nanofiber filters, microwave power should be the most important consideration in on-line disinfection. In optimizing this disinfection process, the highest microwave power should be selected (without possible damage to the filter) with a short application time.

This series of spore experiments reflect the first attempts to inactivate collected *B. subtilis* endospore aerosols with microwave irradiation. Celandroni et al. (2004) observed complete disinfection of *B. subtilis* spores in a 0.25-mL saline solution under 100-W microwave power for 20 min where boiling occurred within 45±5 s. Because a

different heating medium and setup were used, it is not appropriate to compare their results directly to the present study. In that previous study, spores were suspended in a solution during irradiation while in this study spore aerosols were collected on microwave transparent PAN fibers which required SiC disks for heating (Celandroni et al. 2004). Although fiber heating occurred by conduction from the SiC disks rather than direct heating by radiation, the SiC disks were able to reach a much higher temperature than boiling water near 100 °C. Therefore, the method developed in this study may have greater potential for faster spore disinfection provided that a high relative humidity can be introduced in the system. Overall, while encouraging spore disinfection was achieved (2.8 log), *B. subtilis* spores were considerably more challenging to inactivate than *E. coli* (Zhang et al. 2010a).

The relative difficulty in inactivating spores on the filter provides motivation for the more systematic UHT approach. Used in filter disinfection, microwaves have some limitations. First, microwaves may not be able to practically achieve higher inactivation as a high power (750 W) produced less than 3-log inactivation with a relatively long 90-s application. Second, in implementing UHT treatment, filter temperature must be measured and measuring the temperature of an object inside a microwave oven is difficult; thermocouple probes or conventional thermometers cannot be simply placed in the oven during irradiation because they distort the electromagnetic field and can be heated by the microwaves themselves. IR is better suited for the disinfection of a substrate like an air filter because it can be emitted to heat a flat target uniformly and because it can be absorbed in a thin surface layer. The filter temperature can also be

measured more easily during IR heating. Therefore, in the next chapter, IR will be used in an UHT filter disinfection process.

Table 2-1. Survival fraction of *B. subtilis* spores for the static tests.

| Power | | Microwave irradiation time | | | |
|---|---|---|---|---|---|
| | | **30 s** | **45 s** | **60 s** | **90 s** |
| **250 W** | Mean (%) | 100 | 93.3 | 30.2 | 2.19 |
| | SD (%) | 0.013 | 1.04 | 1.43 | 0.75 |
| **750 W** | Mean (%) | 74.0 | 6.00 | 1.26 | 0.20 |
| | SD (%) | 7.42 | 2.04 | 0.87 | 0.15 |

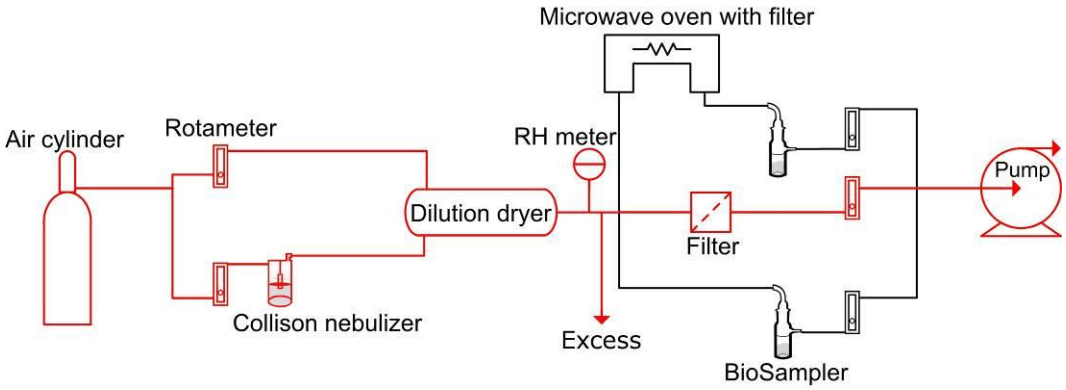


Figure 2-1. Testing system for the static and on-line experiments. The system for loading filters in static testing is highlighted in red. The on-line system consists of both colors but excludes the excess line.

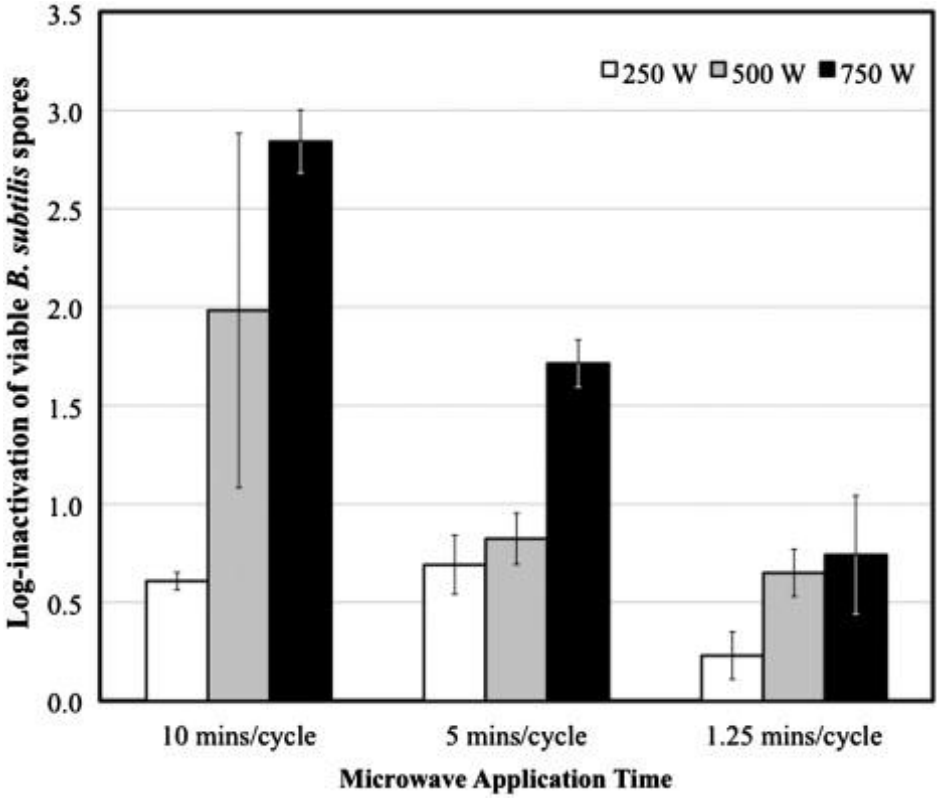


Figure 2-2. On-line filter disinfection as a function of microwave power and application time.

# CHAPTER 3
# UHT FLASH INFRARED RADIATION DISINFECTION OF FIBROUS FILTERS CONTAMINATED WITH BIOAEROSOLS*

## Objective

In this chapter, an IR radiation disinfection device for filters loaded with bioaerosols was designed and constructed. The device was tested for its ability to achieve UHT filter temperatures within a short period of time as well as its ability to flash inactivate challenging *E. coli*, MS2 virus, and *B. subtilis* spores captured on the filter. Finally, the fate of *E. coli* after heating and filter damage were examined with SEM.

## Materials and Methods

### IR Lamp, Disinfection Device, and Temperature Measurement

Commercially available IR lamps (BR40, Sylvania, MA) were used in this study because they are inexpensive, ubiquitous, as well as practical. For these lamps, IR radiation is emitted from a tungsten filament at a temperature of about 3,000 K. Given this temperature, the wavelength of maximum energy output is in the near IR band (~1 μm) by Wien's displacement law. These bulbs included a parabolic reflector that surrounded the filament to direct emitted radiation normal to the bulb face.

It was confirmed in exploratory heating tests that most glass fiber filters do not have strong absorption of near IR, resulting in slow and inefficient heating. To rapidly achieve the necessary UHT, near IR-absorbing activated carbon cloths (ACC) were placed in contact with the filter. The cloths would then transfer energy to the filter by conduction. The ACCs would not serve for bioaerosol collection, but rather were used exclusively for IR absorption as carbon is a strong IR absorber. Low-pressure-drop

* Reprinted with permission from Damit, B., Lee, C. and Wu, C.Y. (2011) Flash infrared radiation disinfection of fibrous filters contaminated with bioaerosols. *J Appl Microbiol* **110**, 1074-1084.

ACCs (Model ACC-5092-20, American Kynol, NY) with pore size of 250 µm, were placed on both sides of the filter, forming a sandwich as displayed in Figure 3-1 A. The 1-mm thick ACCs were cut into 46-mm circles to fully cover the test filters during irradiation. The ACC placed under the filter ensured that any transmitted radiation was absorbed. Although an IR-absorbing filter could have simply been employed, the ACC sandwich offers adaptability allowing different filters to be readily tested or substituted.

The filament of the bulb was positioned 20 cm from the ACC surface. To direct radiation toward the filter, a cylindrical aluminum foil (Reynolds Wrap, Reynolds, VA) waveguide was fitted around the lamp. Aluminum foil is reflective to near IR although some foil heating was observed during experiments. By adding this waveguide, a higher ACC temperature was achieved compared to heating without the waveguide. Aluminum foil was also placed beneath the filter sandwich. This again ensured that transmitted or scattered radiation was directed back toward the sandwich. With the waveguide and foil placed beneath the filter sandwich, the setup behaved as an IR-reflective enclosure, maximizing the radiation incident on the sandwich.

To investigate the dependence of microorganism inactivation on filter temperature, two bulbs of different powers, 250 W and 125 W, were tested. These are the powers consumed by the lamp, rather than emitted by the filament. IR heat lamps are about 80-95% efficient; hence, the power consumed by the lamp is similar to the emitted power. Assuming an average efficiency of 87.5% and given that the diameter of each reflector bulb was 12 cm, the power density emitted from the bulb face was $2.0\times10^{4}$ W $m^{-2}$ and $1.0\times10^{4}$ W $m^{-2}$ for the 250-W and 125-W bulbs, respectively.

The temperature of the ACC was measured with an IR pyrometer (OS533E, Omega, CT). A pyrometer has a short response time and is able to more accurately measure the rapid heating of the ACC than even a wire thermocouple. The pyrometer estimates temperature by detecting the irradiance from a 2.5-cm diameter circle on the ACC's surface. Thus, the measured temperature is the averaged temperature over the surface. The pyrometer was calibrated before the temperature measurements per the manufacturer's instructions. A special setup displayed Figure 3-1 B was constructed to obtain real-time temperature measurements during heating. The 46-mm diameter circular filter/ACC was carefully placed over a 37-mm diameter hole on a stand with an aluminum foil top. Under the stand, the pyrometer detector was directed toward the hole covered by the filter/ACC. The detector was placed 22 cm from the hole so that the detector field of view (25-mm spot at 22 cm) consisted entirely of the filter/ACC. To prevent radiation directly emitted from the bulb from entering the detector, the pyrometer was positioned at a 40º angle to the filter/ACC surface normal. By measuring the temperature in this manner, only IR radiation emitted from the filter/ACC entered the detector thus providing accurate temperature readings. To make the best estimation of the actual filter temperature, two sets of temperature measurements were taken. In the first set, the temperature of a single ACC was measured. Because the pyrometer detected the temperature at the bottom of the ACC, the recorded temperature estimated the temperature at the top of the filter when placed in the sandwich. In the second set, an identical measurement setup was employed but now the temperature of a half-sandwich (an ACC top and filter bottom) was measured so that the filter was in the field of view of the pyrometer. The corresponding temperature represented the temperature

at the bottom of the filter. The temperatures from the two sets were then averaged at each time. This averaged temperature is the estimated temperature that the average microorganism experiences assuming bioaerosol collection is uniform through the filter.

The filter temperature profiles were recorded for both bulbs. A scientific timer (Model 451, GraLab, OH) with accuracy of ±0.1% at 1 s was attached to the IR lamp ensuring consistent irradiation applications. Temperature measurements were taken five times for each bulb power. Comparison of these temperature data with the inactivation data will provide insight into the temperature required for desirable microbe inactivation. It will also determine whether conventional UHT protocol can be applied to filter disinfection.

**HEPA Filter Selection and Test Bioaerosols**

Selecting an appropriate HEPA filter was crucial in this study. The filter must be able to withstand intermittent heating to UHT without decrease in filtration efficiency. Glass microfiber LydAir®MG (HEPA grade 4450HS, Lydall, NH) filters were chosen for their high-temperature resistance. These filters have a collection efficiency of 99.985% for a particle size of 0.3 µm and maintain their efficiency for a continuous operating temperature up to 480 ºC. Filter sheets were cut into 46-mm circles to fit into filter holders during bioaerosol loading.

Three non-pathogenic microorganisms, *Escherichia coli*, MS2 bacteriophage and *B. subtilis* endospore were tested. As the test microorganisms physically and biologically resemble diverse bioaerosols, they provide an estimation of the IR inactivation capacity for a range of airborne pathogens. *B. subtilis* was prepared according to the procedure described in the previous chapter.

*E. coli* is a bacterium commonly used in bioaerosol literature as a representative of vegetative cells (Ratnesar-Shumate et al. 2008; Jung et al. 2009a; Park et al. 2009; Lee et al. 2010; Zhang et al. 2010a). A Gram-negative bacterium, *E. coli* is rod-shaped with an aerodynamic diameter of about 0.8 μm (Li et al. 1999). *E. coli* strain ATCC 15597 was obtained from the American Type Culture Collection (ATCC; Manassas, VA) and grown in Difco Nutrient Agar (Becton, Dickinson and Company, MD). An *E. coli* suspension was prepared by inoculating a Difco nutrient agar slant with a single colony from stock. After incubation at 37 ºC for 24 hours, 2 mL of Ringer's solution (Fisher, Cat. No. S77939, NY) was added to the slant to wash the *E. coli* from the slant surface. This 2-mL *E. coli* suspension was further diluted in Ringer's solution to about $10^6$-$10^9$ colony-forming units (CFU) $mL^{-1}$ before nebulization.

MS2 bacteriophage has similarities to human enterovirus due to its resistance against stress and because it lacks a lipid envelope around its nucleocapsid (Aranha-Creado and Brandwein 1999). Therefore, it is commonly used in bioaerosol studies (Tseng and Li 2005; Vohra et al. 2005; Lee et al. 2009; Grinshpun et al. 2010b; Rengasamy et al. 2010). MS2 is an icosahedral virus that is approximately 27.5 nm in diameter and replicates in male *E. coli* (Golmohammadi et al. 1993). Freeze-dried viruses (MS2; ATCC® 15597-B1) were suspended in deionized (DI) water and stored at 3 °C. An aliquot of this suspension was diluted to about $10^7$-$10^9$ plaque-forming units (PFU) $mL^{-1}$ and aerosolized. For enumeration, the viruses were propagated in a log-phase culture of *E. coli* and incubated at 37 °C for 24 hours before counting.

**Filter Loading and IR Flash Disinfection**

Filters were loaded with test microorganisms to simulate the collection of bioaerosols by a fibrous filter. In this manner, the bioaerosols were collected throughout the filter matrix. The bioaerosol loading system is displayed in Figure 3-2.

Before loading, the system was flushed with 70% isopropyl alcohol to prevent contamination. Afterward, a 6-jet Collison nebulizer (CN25; BGI Inc., Waltham, MA) operating at 5 LPM and filled with 40 mL of test microorganism suspension was used to aerosolize the test microbes with particle-free compressed air. The flow was directed to the dilution dryer where water content evaporated yielding the microorganism aerosol. Then the flow was split into three parallel flows toward three filters. The three filters were loaded simultaneously to obtain triplicate data. Microscopic analysis of the filter fibers after 30 minutes of *E. coli* bioaerosol loading found that the fibers were evenly covered by the microorganism. It must be noted that the viability of microorganisms collected on an air filter can decrease depending on relative humidity, loading time, and microbial species (Wang et al. 2001). However, each experimental filter would be compared to a control filter that was subjected to identical conditions during loading. Furthermore, although exposure to the flow conditions may make collected microorganisms more susceptible to a disinfection process, 30 min was required to obtain sufficient loading.

Once removed from the filter holder, a loaded filter was cut into equal quadrants like in the previous chapter. One quadrant, the control, was directly suspended in 20 mL of Ringer's solution (*E. coli)* or 20 mL of DI water (MS2 and *B. subtilis*) and vortexed at the highest setting for 2 min to extract the test microorganisms from the filter fibers (Wang et al. 2001). Although filter extraction and culture based techniques are not

recommended for virus (Farnsworth et al. 2006), both control and experimental quadrants underwent an identical vortexing procedure. Assuming that extraction from the filter is consistent, the low virus recovery will be the same for control and experimental quadrants allowing an accurate assessment of inactivation.

This vortexed suspension was serially diluted to a titer between 30 and 300 CFU/PFU $mL^{-1}$, plated with required growth medium, and incubated at 37 ºC. The remaining three quadrants were irradiated with the IR disinfection device for time applications from 1 to 15 s. After irradiation, the filter sandwich was left to cool to room temperature before it was removed from the irradiation device. At least triplicates were conducted for each time application. Samples from the irradiated filter quadrants were cultured by an identical process described with the control filter quadrant. After incubation for 24 hours, the number of CFU for *E. coli* and *B. subtilis* spores and PFU for MS2 were counted on the control and experimental plates. After counting, log inactivation was calculated from Eq. 2-2. To investigate whether the quadrants collected similar amounts of bioaerosols during the loading process, a set of tests where all quadrants were not irradiated was conducted. A coefficient of variation of about 20-50% was found between the quadrants.

## Results

### Temperature Measurement of the ACC and Filter

The temperature profiles of the filter are displayed in Figure 3-3. For a given time, the point represents the averaged temperature of the filter while the top and bottom bars indicate the temperatures at the top and bottom of the filter respectively. The 250-W bulb and 125-W bulb achieved the UHT of about 125 ºC from room temperature within 2 and 4 s, respectively. The 250-W bulb and 125-W bulb also heated the filter to

maximum steady state temperatures of about 360 ºC and 200 ºC, respectively. These temperatures were reached with emitted power densities of $2.0\times10^{4}$ W $m^{-2}$ from the 250-W bulb and $1.0\times10^{4}$ W $m^{-2}$ from the 125-W bulb. The actual energy flux absorbed by the filter is lower due to energy dissipation by the waveguide, and the surface porosity and spectral properties of the filter and ACC. From a design standpoint, however, the emitted power density values describe the powers required to achieve the temperatures shown in Figure 3-3.

Besides energy dissipation to the reflective enclosure, only the filament and filter/ACC participated in the radiation exchange. Following the laws of thermodynamics, heat is transferred from the hotter filament to the cooler filter and a thermodynamic steady state is reached. The steady state filter temperatures are dependent on enclosure geometry and spectral properties of the filter/ACC and waveguide, but most importantly on the filament temperature. A higher filament temperature produced a higher filter temperature due to a greater temperature difference present in the enclosure. Furthermore, the hotter filament provided greater power density by Planck's law, heating the filter faster. This can be observed by comparing the slopes of the 250-W and 125-W temperature curves during the first 4 s of irradiation. In general, the rapid heating of the filter can be explained by the shallow penetration of IR. For absorbing materials with sufficient thickness, incident IR energy is absorbed within a thin surface layer and converted to internal energy (Siegel and Howell 2002). The ACC sandwich also has a large surface-area-to-mass ratio, causing it to readily receive incident radiation and heat quickly.

**IR Disinfection of Bioaerosols Collected on the Filter**

The inactivation data as a function of time for both bulbs are presented in Figure 3-4. Microorganism inactivation of less than 1 log to greater than 5 log can be seen. Recalling that the coefficient of variation for a set of non-irradiated quadrants was 20-50%, it is apparent that the inherent variation between quadrants cannot be neglected. In the most extreme case, assuming that the control quadrant had the highest initial loading of the four quadrants, false inactivation could be 0.60 log. The variation is relatively minor for points where the inactivation is almost an order of magnitude greater than the variation. However, for data points where the inactivation was less than 0.60 log, the observed inactivation cannot be definitively attributed to heating or to variation between filter quadrants.

To address this issue, all data points were tested with a t-test. The tests compared the replicates of each heating condition to the false inactivation values for the run with a coefficient of variation of 50%. Data points where statistical difference was found are denoted with an asterisk in Figure 3-4 to indicate that the inactivation was likely due to heating. The t-tests demonstrated that the majority of the points at the 250-W power were a result of heating applications. However, for most of the points at the 125-W power, the observed inactivation may be due to the inherent variation between quadrants. The inactivation that did occur from heating for these points was sufficiently low that it could not be detected.

In general, significant microorganism inactivation was achieved by the 250-W bulb with short time applications. An IR application of 5 s resulted in 4.38- and 5.32-log inactivation of *E. coli* and MS2, respectively. The more heat resistant *B. subtilis* spore, however, required at least 5 s of irradiation for greater than 3-log inactivation. The

higher thermal resistance of the spores is due to the spore coating and the presence of dipicolinic acid and calcium in the cell protecting inner proteins against denaturation (McDonnell 2007).

Microorganism inactivation with the 125-W bulb was not as effective as 250-W bulb applications. Low spore inactivation was observed for 1 s and 3 s at 125 W; hence, 10 s and 15 s applications were conducted as well. Only two data points, MS2 at 5 s and *B. subtilis* at 15 s, could be attributed to the IR heating. These inactivation values were still low compared the values obtained with the 250-W bulb. Consequently, the inactivation values with the 125-W bulb are much less than expected for an UHT treatment. This indicated that although the 125-°C temperature was reached with the 125-W bulb, the temperatures were not high enough for a flash disinfection process and that a greater power density would be needed.

Scanning Electron Microscopy (SEM) was used to examine the fate of the collected *E. coli* after heating and the possible heat damage sustained by the filter. Figure 3-5 displays two images at 1,900 X magnification comparing two *E. coli*-loaded filters: one unheated (A) and the other heated for 15 s with the 250-W bulb thereby reaching a temperature of 360 ºC (B). The bioaerosols collected on the fiber surfaces appear to be *E. coli* aggregates rather than individual cells. A decrease in the size of the *E. coli* aggregates on the heated filter can be observed. From the images, it is estimated that the diameter of the aggregates shrank by greater than 50% due to a loss in moisture content during heating. The overall morphology of aggregates, however, did not appear to be altered.

Figure 3-6 displays a clear comparison between an unheated filter and a heated filter to examine fiber damage. Melting or change in shape of the fibers, which usually occurs during thermal degradation of polymer fibers, was not seen, although cross-sectional breaking of the fibers was observed. The heated filter reached a temperature about 120 ºC less than the threshold for decreasing efficiency specified by the manufacturer. From single-fiber efficiency theory, cross-sectional breaking of the fibers does not affect the total efficiency of the filter (Hinds 1999). Measurement of the filter's pressure drop with a Magnehelic differential pressure gauge before and after heating also found no change in pressure drop, supporting that the observed breaking would not decrease the efficiency of the filter.

## Discussions

### Flattening in the 250-W Log Inactivation Curve with Longer Applications

Although the 250-W bulb data displayed in Figure 3-4 displays significant microorganism inactivation, the *E. coli* and MS2 inactivation values approach a limit at increasing times. It was expected that the slope of the curve would actually increase due to higher temperatures from heating. The observed curve flattening may be explained by relatively low number of CFU/PFU extracted from the control filter. Control CFU/PFU values were less than $10^5$ $mL^{-1}$ in the vortexed sample, providing the ability to detect a maximum of 5-log inactivation. This concentration, however, is similar to that extracted in other filter disinfection studies (Rengasamy et al. 2010). If the filters were loaded to a higher concentration or if filter extraction were more efficient, greater log inactivation might have been observed. However, it was found that increasing the loading time to 45 minutes increased the control CFU/PFU by less than an order of magnitude.

Another explanation for flattening in the inactivation curve is that the device is effective enough to completely disinfect *E. coli* and MS2 within 3 s as nearly identical inactivation values were seen with increasing time applications. Given a control filter number of CFU/PFU, if zero CFU/PFU are observed on both experimental 3- and 5-s plates, the log inactivation will be almost identical and cause flattening of the curve with increasing time. For plates with zero experimental CFU/PFU, a value of 0.5 was used. Therefore, the inactivation values at these time applications were then conservative estimates of the actual inactivation. Furthermore, inactivation values where the control sample had less than $10^4$ CFU/PFU $mL^{-1}$ were included in the calculation of mean inactivation. This results in lower mean inactivation than if the control CFU/PFU were higher. Because the exact reason for the flattening in the curve is not known, calculation of the death kinetic parameters was not appropriate. It is interesting to note that the observed flattening behavior has been reported in other bioaerosol disinfection studies (Xu et al. 2002).

**The Applicability of Conventional UHT Protocol and Threshold Temperature**

The 125-W temperature data in Figure 3-3 display that the UHT of about 135 ºC was reached in 4 s but there was negligible inactivation for heat-sensitive *E. coli* and MS2. As the holding time of 1 s at the UHT was sufficient, there should have been complete disinfection according to UHT protocol. There are two possible explanations for the observed discrepancy: (1) decreased water content during heating and (2) non-uniform heating in the fibrous filter matrix.

Because the IR heating was performed at unsaturated humidity conditions, the process was dry heat disinfection. Dry heat is less effective than moist heat disinfection and requires more intense heating applications (Pflug et al. 2001). The protocol for dry

heat sterilization recommends holding temperatures of greater than 160 ˚C for minutes to hours, but in general, this applies to thick objects, for which deep heat penetration is required (McDonnell 2007). There is no protocol for dry heat sterilization of thin porous materials like fibrous filters. The other possible reason for the discrepancy is that conventional UHT protocol assumes a uniform temperature distribution so that all microorganisms experience identical heat treatment. Uniform temperatures may not have been achieved in the filter due to non-uniform conductive or convective heating between the ACC and filter or between the randomly oriented fibers in the filter matrix. Microorganism aggregates collected on the fibers may have also contributed to temperature non-uniformity. Because a single microorganism is relatively thin and its aggregate has a similar order of magnitude in size, however, thermal protection offered by aggregation is minor.

Overall, the results of the 125-W bulb tests demonstrate that heat disinfection of fibrous filters cannot be described by conventional UHT protocol for liquids. The results suggest that the process behaves more like dry heat disinfection and that flash filter heating requires temperatures greater than about 200 ºC. However, because filter disinfection is essentially a surface disinfection process, it most likely requires less intense heating applications than dry heat protocol recommends.

By combining the 250-W and 125-W data, it was found that filter disinfection can be characterized by a threshold temperature. This value is the minimum temperature that must be reached for successful flash heating disinfection (3 log or greater) without regard to total heating time. The threshold temperature can be estimated by Figure 3-7, which is a graph displaying inactivation as a function of the temperature reached after

an irradiation application. For both *E. coli* and MS2, inactivation remains unsatisfactory until about 250 ºC, at which it jumps to 4-log or greater. If the filter reaches 250 ºC, effective disinfection of vegetative cells and viruses can be assumed. For *B. subtilis* spore, there is no sharp increase in the inactivation curve suggesting that the threshold temperature may be greater than about 300 ºC. The inexplicit dependence on time in Figure 3-7 also shows the unimportance of total heating time. For example, although the filter heated to 200 °C was heated for 12 s longer than the filter heated to 240 °C, 1 log greater spore inactivation was still achieved in the latter case.

**Device Effectiveness and Comparison to Other Studies**

There is no consensus in scientific literature on the magnitude of inactivation that can be obtained from IR irradiation under dry conditions. In general, the D-value for spore inactivation during dry heat processes can vary considerably depending on the spore species and the test methods (McDonnell 2007). A dry heat IR inactivation study with *B. subtilis* spore by Molin and Östlund (1975) found a D-value of 3.2 s at 180 °C. In contrast, a dry heat study by Hamanaka et al. (2006) found *B. subtilis* spore D-values of minutes although temperature was not carefully monitored but greater than 100 °C.

It is difficult to compare the present study with other IR studies which used different test microorganisms, substrates, and lamps. This is because there are two distinct mechanisms for heating: where IR is absorbed primarily by the substrate the microbes reside on and where IR is absorbed by the microbes directly. Water-containing microorganisms are able to absorb IR radiation due to the symmetric stretching, asymmetric stretching and deformation modes of the O-H bond in water. If the emitted IR frequency matches the vibrational frequency of a particular mode in water, increased inactivation can be observed (Hamanaka et al. 2006). Therefore, if IR

absorption is high for the target microorganisms but low for the substrate then substrate temperature is not a good indicator of inactivation. However, if the opposite is true, substrate temperature is a good indicator due to conduction heating from the substrate to the microorganisms.

In this study, a higher filter temperature corresponded to higher microorganism inactivation, which suggests that heat conduction from the fibers was the primary mechanism. Direct absorption by microbes, due to the pores of the overlaying ACC, may be responsible for some inactivation but the lamps were not specifically tuned to match the absorption peaks of the microorganisms. Furthermore, the ACC did absorb a significant amount of incident radiation. Inactivation was then most likely caused by heat conduction from the fibers to collected microorganisms rather than direct absorption. The effect of water vapor within the aluminum foil chamber during irradiation was not investigated but would have likely affected disinfection. In a previous study regarding microwave disinfection of air filters, higher relative humidity resulted in higher inactivation of MS2 viruses on the filter (Woo et al. 2012b). Increasing the relative humidity here and thus simulating a more effective moist heat disinfection process could have had the same effect.

Compared to other filter disinfection technologies (see Table 1-1), the device was extremely effective, inactivating up to 5 log of test microorganisms within seconds. A study investigating filter disinfection by UV irradiation achieved less than 2-log inactivation of both bacterial vegetative cells and fungal spores after irradiation for 1 h (Kujundzic et al. 2006). As demonstrated in the previous chapter, microwave irradiation required minutes for greater than 2-log inactivation of endospores. The IR disinfection

device also outperformed biocidal filters impregnated or coated with antimicrobials like iodine, silver-copper, and titanium dioxide (Rengasamy et al. 2010). Iodine treatment, for example, showed less than 1-log inactivation of endospores collected on the filter (Lee et al. 2008). Another antimicrobial, silver nanoparticles, deposited on filter media inactivated 0-2 log of bacterial vegetative cells depending on exposure time, humidity conditions, and the PSD of the nanoparticles (Lee et al. 2010). Similarly, other filter disinfection technologies, e.g., PCO and positive ions, have achieved less success than the IR device.

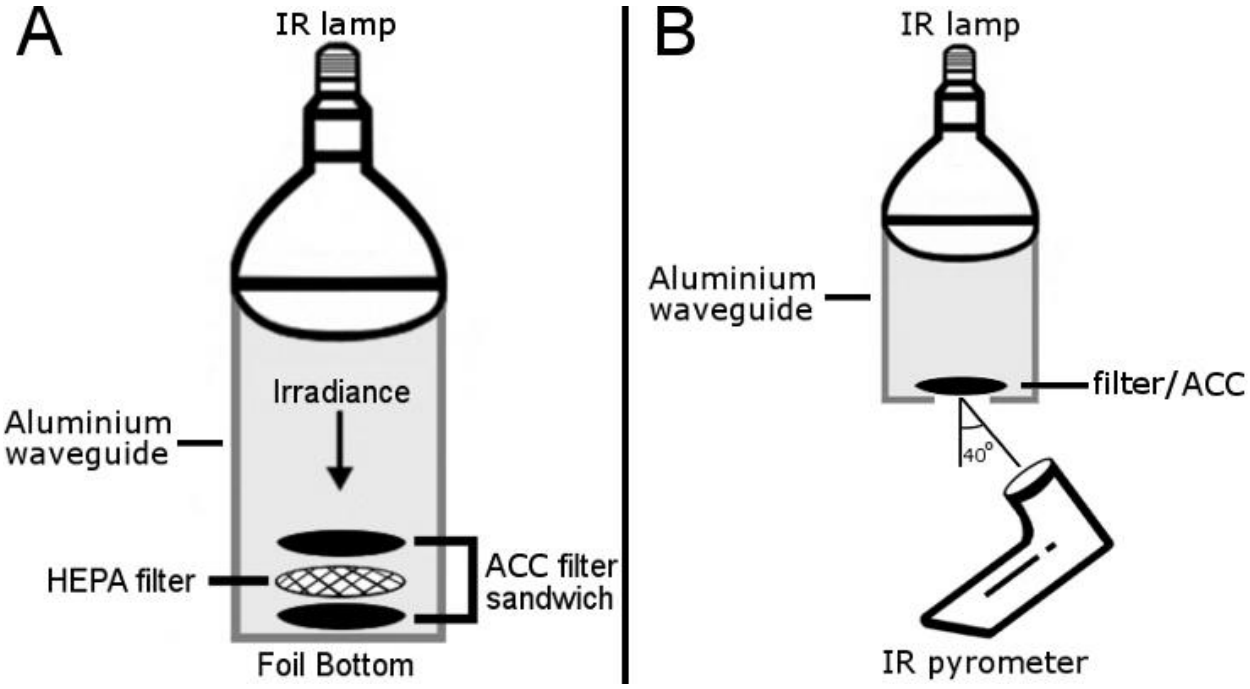


Figure 3-1. Diagrams of the device during disinfection and temperature measurement. A) Schematic of the IR disinfection device. The components of the filter sandwich were placed in contact during heating. B) Temperature measurement setup.

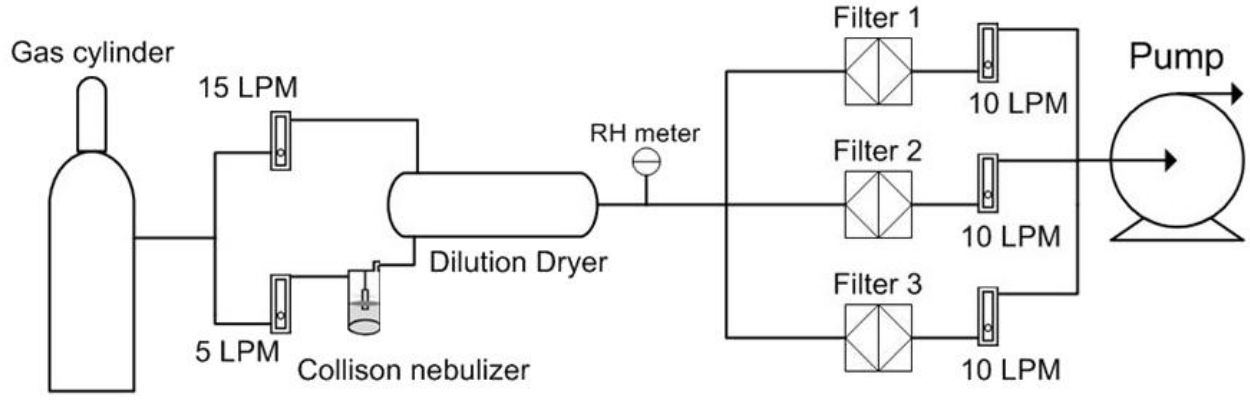


Figure 3-2. Diagram of the bioaerosol loading system.

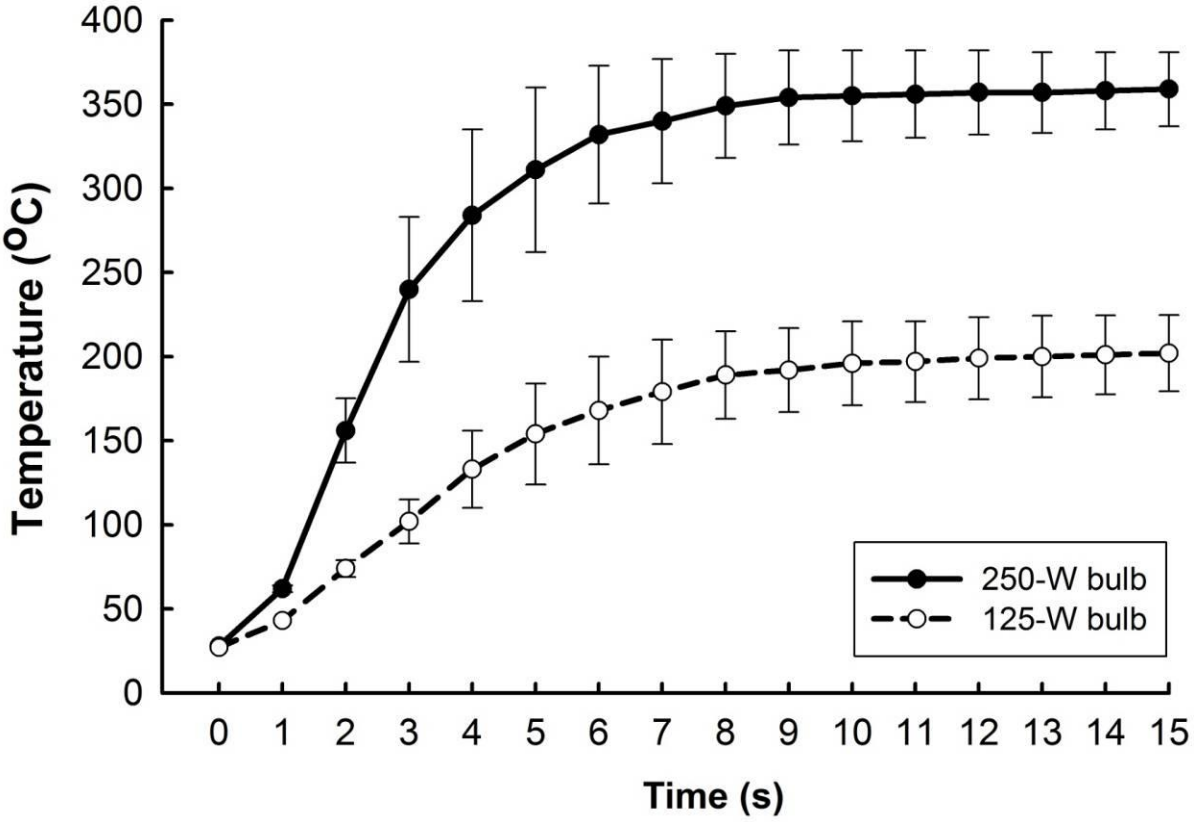


Figure 3-3. Temperature of the filter as a function of IR irradiation time. Points represent the averaged filter temperature at a given time while the bars indicate the temperatures at the top and bottom of the filter.

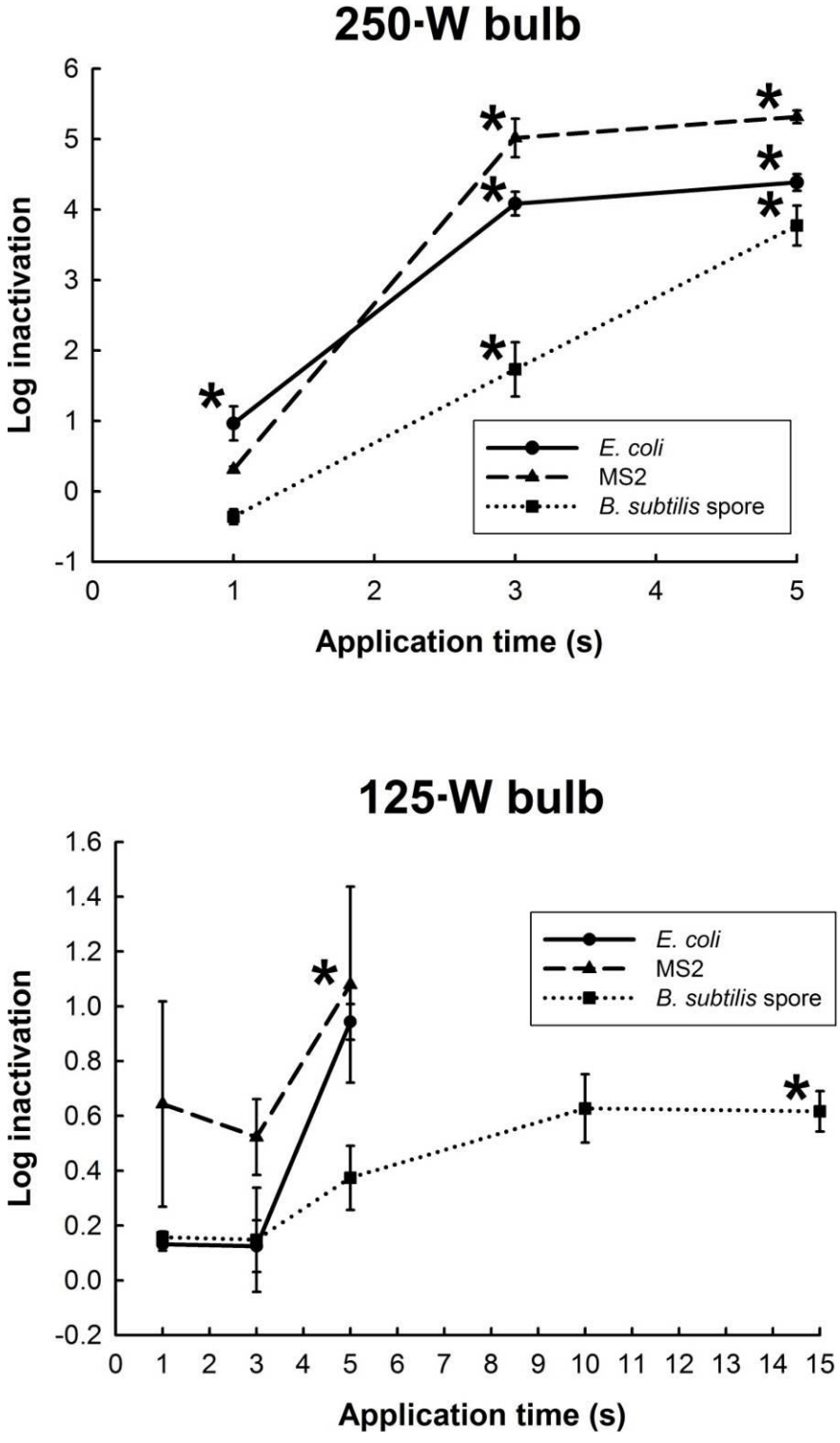


Figure 3-4. Log inactivation of test microorganisms with the 250-W and 125-W bulbs. The error bars represent one standard error. Asterisks indicate that the observed inactivation is due to IR heating.

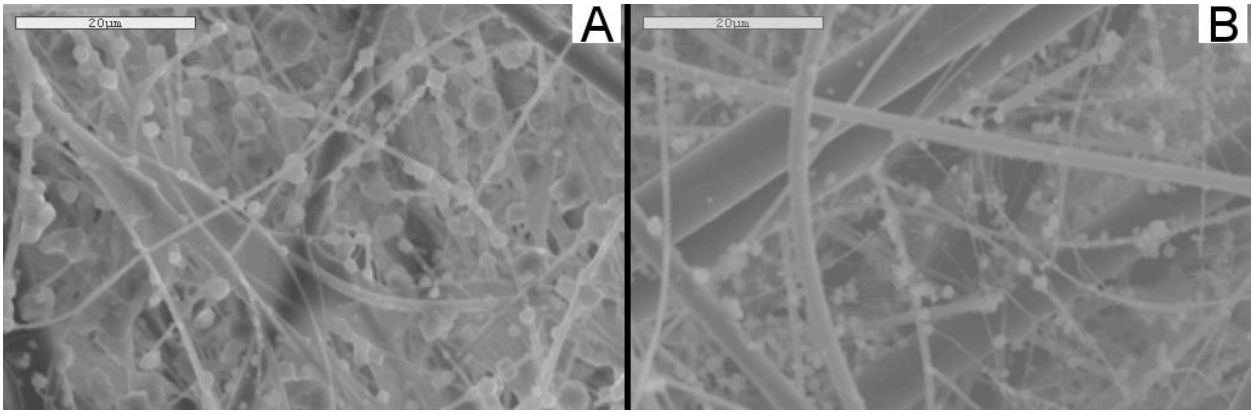


Figure 3-5. SEM images of the *E. coli*-loaded filter with and without heating. A) Unheated filter. B) Filter heated to about 360 ºC.

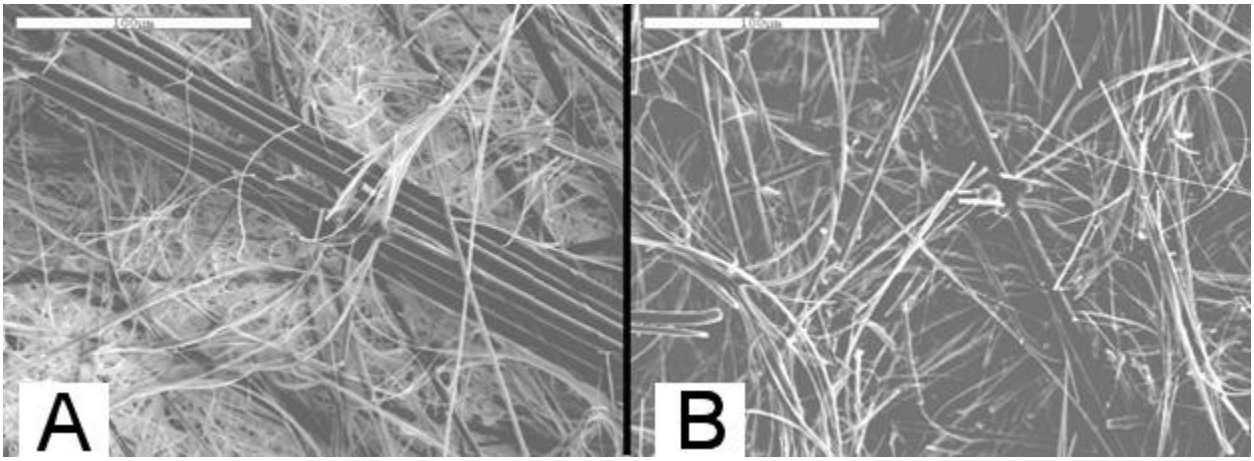


Figure 3-6. SEM images examining damage to the filter due to heating. A) Unheated filter. B) Filter heated to about 360 °C.

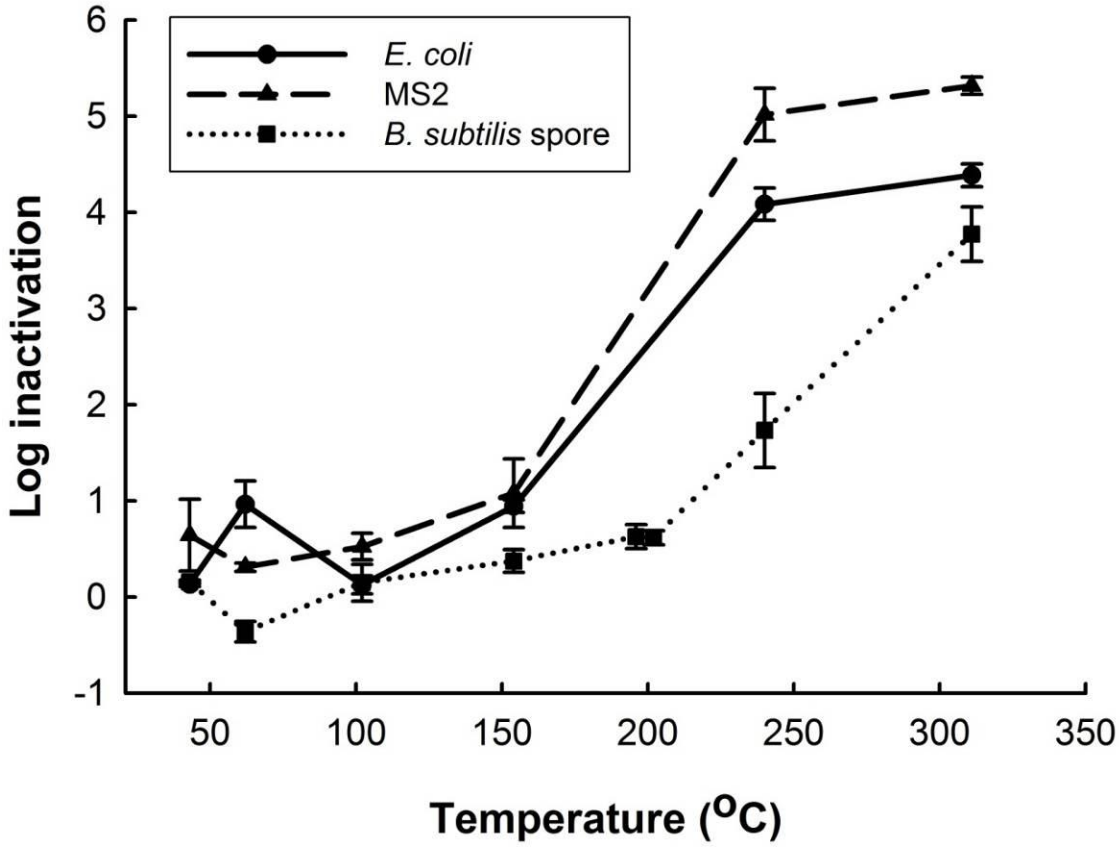


Figure 3-7. Inactivation as a function of the maximum temperature reached during irradiation.

# CHAPTER 4
# UHT INFRARED DISINFECTION OF BIOAEROSOLS*

## Objective

The objective of this study was to develop and test an IR-UHT system capable of generating high and uniform airflow temperatures to disinfect air. The IR-UHT system consisted of a heating chamber which held an IR-heated ACC perpendicular to the airflow. The cloth and airflow temperatures were measured and inactivation was determined for both laboratory-generated (*E. coli* and MS2 virus) and environmental bioaerosols. The inactivation mechanism of *E. coli* bioaerosols subjected to UHT was also investigated.

## Materials and Methods

### IR-UHT Heating Chamber, Temperature Measurements, and Lab Testing System

A custom quartz heating chamber was fabricated to hold the cloth perpendicularly to incoming bioaerosol-laden airflow as shown in Figure 1-1 C. On the surface of the chamber, a flat optical window was created so the IR bulb could be positioned outside the chamber to irradiate the cloth. The chamber was approximately cylindrical and had a length of 15 cm and outer diameter of 4 cm. The section downstream of the cloth was about 4 cm long. The cloth that was used was a commercial piece of 0.5-mm activated carbon cloth (ACC-507-15; American Kynol, Pleasantville, NY) that was similar to the ACC used in Chapter 3. An image which shows the pore size of the cloth is displayed in Figure 4-1 A. Once the ACC was inserted in the chamber, airflow passed through a cross-sectional cloth area of 12 $cm^2$.

* Reprinted with permission Damit, B., Wu, C.Y. and Yao, M. (2013) Ultra-high temperature infrared disinfection of bioaerosols and relevant mechanisms. Accepted in *J Aerosol Sci*.

The IR bulb was a specialty bulb purchased from Heraeus Noblelight LLC (Product # 80008213; Buford, GA) and produced near IR radiation. Operating at 115 V and 250 W, the ring-shaped bulb had a gold reflector and was essentially a straight filament bent into a circular shape. The diameter of the filament circle, 39 mm, closely matched the 37 mm diameter of cloth in the quartz chamber. During lab testing, the 250-W power was used for all experiments.

The spatial uniformity of heating by the bulb was determined using a thermal-imaging camera (i50; FLIR, Wilsonville, OR). The bulb was positioned 5 cm from a sheet of aluminum foil (the same distance of the bulb to the cloth in the heating chamber) with a black coating on both sides, and a thermal-imaging camera was placed behind the foil. When the bulb was turned on, the camera captured an image of the heating distribution which is shown in Figure 4-1 B. It can be seen that the bulb provided a spatially uniform irradiation pattern ensuring uniform heating of the cloth. Heat-resistant IR-reflective tape was applied to the sides of the quartz chamber upstream of the cloth so that radiation would be directed onto the cloth. Downstream of the cloth, the quartz chamber was wrapped with two layers of 0.32 cm-thick thermal insulation tape (G65P752-04; Amatex Corporation, Laconia, NH). This ensured that air exiting the cloth would maintain its temperature profile in the axial direction within the heating chamber.

For each experimental condition, the temperatures of both the cloth and the air downstream of the cloth were measured. The cloth temperature can potentially be used to conveniently estimate the flow temperature because the flow passes through the small pores of the cloth. To measure the cloth temperature, an infrared pyrometer

(OS533E; Omega, Stamford, CT) was positioned 5 cm downstream of the cloth so that the pyrometer's entire field of view (2.5-cm diameter spot) consisted of the cloth.

Airflow temperatures were measured with a thermocouple (HH806AU; Omega, Stamford, CT) at multiple locations within the cylindrical chamber to assess temperature uniformity and to elucidate the relationship between the cloth temperature and flow temperature. The bulb was turned on for 20 min before measurement to allow the cloth to reach a steady-state temperature. Air temperature was measured with the thermocouple at three cross-sections within the chamber: at the cloth surface, and 2 cm and 4 cm downstream of the cloth. At each cross-section, the temperature was measured at eight positions denoted in polar coordinates (r, θ): (5 mm, 45°), (5 mm, 135°), (5 mm, 225°), (5 mm, 315°), (15 mm, 45°), (15 mm, 135°), (15 mm, 225°), (15 mm, 315°). After all 24 measurements were taken, the data were plotted using OriginPro's Contour function which employed an interpolation and extrapolation algorithm. Displaying temperature contours aided in the visualization of flow temperature within the chamber.

The schematic of the lab testing system is shown in Figure 4-2 A. Particle-free compressed air, supplied by an air cylinder, was sent to a 6-jet Collison nebulizer (CN25; BGI Inc., Waltham, MA) at a flow rate of 5 LPM to generate bioaerosols. To evaporate water from the bioaerosols, the microbes were directed into a dilution dryer and then entered either a control or experimental path. For the control path, microbes were directly collected with a BioSampler (Model No: 225-9595; SKC Inc., Eighty Four, PA) and for the experimental path the bioaerosols were first subjected to UHT treatment before collection. Both BioSamplers contained 20 mL of 1X phosphate buffered saline

(PBS) and after sampling, 1 mL was extracted for culturing. A BioSampler flow rate of 12.5 LPM was used for *E. coli* while 3.8 LPM was used for MS2 virus. The 3.8-LPM flow rate for MS2 allowed for the same collection efficiency for nanometer-sized MS2 while preventing reaerosolization (Hogan et al. 2005; Riemenschneider et al. 2010). The sampling period was 30 min to obtain a high number of control bioaerosols and accurately assess the magnitude of inactivation. During the 30 min, there was some evaporation of the PBS which reduced the BioSampler's collection efficiency and may have caused loss of already collected particles. However, the liquid loss was found to be nearly the same for both the control and experimental Biosamplers. Hence, the effect of reduced BioSampler efficiency cancels when inactivation was calculated. To allow a flow rate higher than 12.5 LPM to be tested through the heating chamber, an excess line was placed before the experimental BioSampler.

Two flow rates were tested through the heating chamber: 19.2 LPM and 3.8 LPM, which corresponded to face velocities of 27 and 5.3 cm/s, respectively. With these face velocities and given the cloth's thickness, pore size, and porosity, Fourier numbers of greater than one could be achieved. During testing, the cloth was irradiated constantly and also periodically to test the possibility of using residual cloth heat to inactivate bioaerosols (thus saving power). Two types of periodic application were tested: 3-min periodic and 1-min periodic. For the 3-min applications, the bulb was turned on for 3 min at the beginning of every 6 min of testing in the 30 min period. Similarly, for the 1-min applications the bulb was turned on for 1 min at the beginning of every 3 min of testing. These periodic irradiation cycles are illustrated in Figure 4-3 where the gray areas correspond to the time the bulb was turned on. To accurately time

the irradiation applications, the bulb was attached to a scientific timer (Model 451; GraLab, Centerville, OH) which had accuracy of ±0.1% at 1 s. Three trials were run for each condition.

Two microorganism species, *E. coli* and MS2 virus, were tested to serve as representatives of Gram-negative bacteria and virus bioaerosols, respectively. After collection with the BioSampler, both microbes were enumerated by culturing the collection liquid and counting the CFUs/PFUs present after incubation. Culturing and enumeration of these microbes was outlined in Chapter 3. As with filter disinfection, log inactivation was used to relay the effectiveness of the UHT treatment.

Besides inactivation experiments, tests were conducted to measure the physical removal of bioaerosols by the cloth itself. An aerodynamic particle sizer (APS; TSI, Shoreview, MN) and a scanning mobility particle sizer (SMPS; TSI) were attached to the heating chamber for *E. coli* and MS2 respectively, and bioaerosols were directed toward the cloth in separate tests. The concentration of bioaerosols was measured upstream and downstream of the unheated cloth. Removal efficiency by the cloth was calculated by $1 - \frac{C_{bo}}{Cb_i}$ where $C_{bo}$ is the outlet bioaerosol concentration and $C_{bi}$ is the inlet bioaerosol concentration. The experiment was replicated four times. For *E. coli*, the cloth had a removal efficiency of about 14% and 20% for the low and high flow rates, respectively. For MS2, the removal efficiency was 36% and 32% for the low and high flow rates, respectively. When included in log inactivation, these values give an understanding of the bioaerosols inactivated by heat rather than simply filtered by the cloth.

### *E. coli* Inactivation Mechanism

Two possible causes of bacteria death include (1) structural damage to the cell membrane resulting in cellular content leakage and (2) DNA degradation or damage. To investigate the *E. coli* inactivation mechanism, UHT-treated *E. coli* and untreated *E. coli* were collected with a BioSampler and examined with SEM to assess structural damage and with gel electrophoresis to assess DNA damage. These tests were conducted at the 5.3 cm/s face velocity and an electrical transformer was used to subject the *E. coli* aerosols to three heating conditions with cloth temperatures of 150 °C, 310 °C, and 470 °C. Again, the BioSampler contained 20 mL of 1X PBS for these experiments. Because the sampling liquid from the BioSampler can be at concentrations of $10^5$ cells/mL or lower after aerosol collection, the entire sampling liquid was centrifuged after collection and the supernatant was removed to make a 250-µL concentrated suspension. This suspension was then used in both SEM analysis and gel electrophoresis.

For SEM analysis, cells were first fixed with 2.5% glutaraldehyde solution, chilled overnight at 4 °C, centrifuged for 1 min at 10,000 RPM, and then the supernatant was removed. Afterward, the samples were treated with an alcohol dehydration series consisting of 30%, 50%, 90% and 100% ethanol solutions. Dried overnight at 50 °C, the samples were then heated at 70 °C for 15 min before SEM imaging. A toothpick was used to remove the sample from the inside of the micro-centrifuge tubes and the samples were coated with gold (Pan et al. 2013).

In examining DNA degradation, the entire *E. coli* DNA (genomic DNA) was extracted from the 250-µL concentrated suspension and then underwent gel electrophoresis. As the genomic DNA will be subjected to electrophoresis, a single, clear band will be observed for undamaged DNA while damaged DNA may display

smearing or blurring of the band. No difference between the untreated and treated samples demonstrates that another process (like cell structure damage) may be responsible for inactivation. *E. coli* DNA was first extracted from each of the samples treated with the three heating conditions and a control using a bacteria DNA extraction kit (Tiangen Co., Beijing, China). During extraction, RNAse A was added to remove RNA so that RNA would not be confused with DNA fragments. The extracted DNA for each heating condition was then loaded into a gel containing an agarose concentration of 3% and then electrophoresis was performed at 120 V for 30 min. A Bio-Rad DCode mutation-detection system (Bio-Rad, Hercules, CA) was used to view the banding pattern. The gel electrophoresis procedure described here is typically used in microbiology and molecular biology labs to determine the quantity of DNA before a more complex analysis procedure.

**The Effectiveness of UHT against Ambient Bacteria and Fungi Aerosols**

The sampling system used to determine the effectiveness of the UHT treatment against ambient bacterial and fungal bioaerosols is displayed in Figure 4-2 B. A procedure similar to that used by Wu and Yao (2011) was followed. Ambient microbes were first drawn into the heating chamber at a flow rate of 28.3 LPM, were then cooled, and finally were collected with a six-stage Andersen impactor (Thermo Scientific, Franklin, MA) so that culturable concentration as a function of aerodynamic size could be calculated. Two temperatures, 60 °C and 210 °C, were tested using an electrical transformer set to 40 and 115 V (83 and 250 W) respectively. The estimated bioaerosol residence times for these temperatures were 0.15 s for 60 °C and 0.1 s for 210 °C. In the bacteria testing, trypticase soy agar (Becton, Dickson and Company, Sparks, MD) plates were placed in the impactor and after collection were incubated for 2 days at 26

°C. Malt extract agar (Becton, Dickson and Company, Sparks, MD) was used for fungi and the plates were incubated for 3 days also at 26 °C after collection. The sampling system was placed outside the entrance of the laboratory in Beijing, China. Sampling was conducted for at least 10 min for each test. The inlet concentration may not be exactly equal for every test; however, sampling for each condition was conducted in random order over a three-week period and three trials were run for the three conditions (no heating, 60 °C, and 210 °C). To determine whether temperature and/or particle size influenced inactivation, the data was analyzed with a two-way ANOVA test using Minitab software.

## Results and Discussions

### Temperature Measurements of the Cloth and Airflow

The temperatures of the cloth for each condition in the lab testing are displayed in Figure 4-3. Again, for each condition in the lab testing the bulb power was kept at 250 W. For the constant irradiation applications, the cloth reached steady-state temperatures of 450 °C and 250 °C for the 5.3 cm/s and 27 cm/s face velocities, respectively. The higher temperature at the lower face velocity is because less airflow mass must be heated with the same supplied power. Heating was relatively rapid as 90% of the maximum temperature was achieved within several minutes and afterward the system generally provided stable temperatures. For the 3-min and 1-min periodic applications, the cloth not only heated quickly but also dissipated energy to the flow quickly so that residual-heat inactivation would be reduced. This sharp rise and fall in cloth temperature is due to the low specific heat capacity and low mass of the cloth. Using a ceramic material as the heating element would maximize residual-heat inactivation but it would necessitate higher application powers or longer start-up heating

times. The maximum temperatures for the periodic applications were only slightly lower than those reached during constant application (e.g. 225 °C for 1 min periodic vs. 250 °C for constant application).

Figure 4-4 displays the temperatures of the cloth and airflow within the chamber via measurement by the thermocouple. Each circle on the figure represents the temperature at a cross-section at the cloth or downstream of the cloth. The 0° location corresponds to the top of the cloth as shown in Figure 1-1 C. At the 27 cm/s face velocity (Figure 4-4 A), the thermocouple-measured cloth temperature ranged from 186-271 °C and varied in both the radial and azimuthal directions. Lower temperatures were measured at the center and bottom left of the cloth while the highest temperatures were found near the top right of the cloth. Air at the position 2 cm downstream of the cloth had a temperature profile with similar radial and azimuthal inhomogeneities and only a slight decrease in temperature (average difference of < 15 °C) from the cloth temperature. Similarly, the difference in temperature between the 2-cm and 4-cm cross sections for any of the (r, θ) positions was small with a maximum of 15 °C and with most positions having a difference less than 10 °C. These data indicated that although the radial/azimuthal temperature gradients were present, the axial temperature remained relatively constant. Cloth temperatures measured with the thermocouple were generally close to those obtained with the pyrometer. As the pyrometer reports the average temperature of a 2.5-cm diameter spot on the cloth, a measured pyrometer temperature of 250 °C is reasonable given the cloth temperature profile shown in Figure 4-4 A.

The airflow temperatures for the 5.3 cm/s face velocity are shown Figure 4-4 B. At the cloth surface, the temperature ranged from 402-499 °C with the lowest

temperatures again occurring near the center and bottom of the cloth. Like 27 cm/s, airflow temperatures became progressively lower downstream of the cloth with the lowest (r,θ) temperatures measured at the bottom left of the chamber. There were also greater temperature gradients in the radial/azimuthal direction than axially. The 5.3-cm/s temperatures, however, were not as constant in axial direction compared to 27 cm/s. For 5.3 cm/s, the maximum difference between the cloth surface and the 2-cm cross section for any (r,θ) position was 100 °C although many of the positions had a difference of less than 30 °C. The maximum difference was 71 °C between the 2-cm and 4-cm cross sections. A greater difference was present for the 5.3 cm/s face velocity due to the overall higher temperatures and consequently greater heat transfer to the ambient through the thermal insulation on the chamber walls. Additionally, the higher residence time of the air at 5.3 cm/s allowed for more time for heat loss to the walls. Uniformity of the temperatures in the axial direction can be further improved by adding thicker thermal insulation to the chamber's outside walls. The cloth temperature measured with the pyrometer (450 °C) was again close to the cloth temperatures measured with the thermocouple.

For both face velocities, the lower temperatures found at the bottom half of the cloth (see Figure 1-1 C) were likely due to the velocity profile arriving at the cloth surface. Laminar flow that was initially fully developed entered the chamber through the 90° bend as shown in Figure 1-1 C. Because of the bend, the fully-developed flow was disturbed by inertia so the maximum velocity occurred near the wall opposite the entrance and at the cloth bottom. The fully-developed flow will be recovered if the

entrance length (distance before a flow is fully developed), $L_e$, calculated by Eq. 4-1 is shorter than the distance to the cloth (Bird et al. 2007):

$$L_e = 0.035\ Re\ D \tag{4-1}$$

where *Re* is the Reynolds number and *D* is the chamber diameter. For the calculated *Re* of 120 and 600 (for the two test velocities), the entrance length was found to be about 15 cm and 76 cm respectively - much larger than the 4.5 cm distance from the chamber entrance to cloth surface. Therefore, the flow remained distorted; the velocities remained higher near the bottom half of the chamber, resulting in lower temperatures at the bottom of the cloth. Temperature uniformity can be improved by placing a flow straightener a distance less than the entrance length before the cloth. The flow straightener eliminates fully-developed laminar flow so the velocity remains uniform across the chamber's cross section (i.e. plug flow) (Jaques et al. 2011). A flow straightener will also ensure that each bioaerosol entering the heating chamber will have nearly the same residence time. The shift of the minimum temperature area to the bottom left might be due to inconsistent emission from the bulb filament. After repeated use, visual inspection of the bulb indicated that the circular filament did not glow uniformly across its circumference and had less visible light emanating from the left side. Overall, the results of the airflow temperature measurements here show that the velocity at the cloth surface and irradiation must be uniform for uniform radial/azimuthal air temperatures.

The temperatures reported in this study were similar to the UHT studies mentioned in the introduction and this demonstrates that the IR system is able to realize UHT treatment. The temperature can be increased further by decreasing the flow rate or

increasing the IR bulb power to greater than 250 W. Analysis in a previous study showed that bioaerosols with a particle size of about 0.73 μm or less adjust to the flow temperature within a millisecond, so the temperatures here can be representative of the microbe exposure temperatures (Grinshpun et al. 2010a). Overall, the IR system was able to produce high air temperatures that were relatively uniform axially (especially at 27 cm/s) but less so in the radial/azimuthal direction. The axial uniformity here is an improvement to previous studies which reported a temperature range of about 20-350 °C in the axial direction for a given (r,θ) position (Grinshpun et al. 2010a).

**Inactivation of *E. coli* and MS2 Bioaerosols**

Displayed in Figure 4-5 are the inactivations of *E. coli* and MS2 for the two flow rates and three IR applications cycles. Inactivation of greater than 4.7 log was observed for both test bioaerosols at constant IR application and the lower face velocity. For this experimental condition, zero CFU/PFU were observed downstream of the heated cloth and so the conventional value of 0.5 CFU/PFU was used in the calculation of log inactivation (Heinrich et al. 2003). Finding no culturable bioaerosols has been commonly experienced in UHT studies as it is difficult to obtain a sufficiently high number of challenging microbes in the aerosol phase and because UHT tends to be very effective (Grinshpun et al. 2010b). As expected, the lower flow temperatures shown in the previous section resulted in lower inactivation at 27 cm/s.

Irradiating the cloth periodically to reduce power consumption showed some inactivation in Figure 4-5. However, the inactivation values presented were obtained for the integrated 30 min sampling with the BioSampler. During the time the bulb was turned off, the cloth temperature was reduced, and the device did not offer considerable protection against incoming bioaerosols. For the periodic applications, the peak

temperatures reached during irradiation were only slightly less than the constant-application temperature but the temperature was held for half (3-min periodic) or one-third (1-min periodic) of the time. Provided that the viable bioaerosol concentration entering the heating chamber was constant, the total inactivation should be about that fraction (half or one-third) of the constant-application inactivation. The periodic inactivation fractions were less than their corresponding IR application time fraction possibly indicating that extra increase in temperature contributes considerably to inactivation. This was found by Grinshpun et al. (2010b) who observed that bioaerosol inactivation was exponentially dependent on temperature.

The log inactivation versus the time-averaged cloth temperature and bioaerosol residence time (assuming gas expansion due to heating) is plotted as a 3-D graph in Figure 4-6. *E. coli* inactivation increased with increasing temperature and residence time as expected. The highest log inactivation was achieved when the temperature was the highest, 450 °C, but at just a modest residence time, 0.41 s. At temperatures near 150 °C, *E. coli* residence time appeared to have little effect on inactivation. Grinshpun et al. (2010a) also observed this in their study of UHT-treatment of bacterial spores and suggested that the biocidal effect may be characterized by temperature rather than residence time. For MS2, inactivation increased with temperature and residence time and like *E. coli*, the highest inactivation for MS2 was when the temperature was the greatest. It is difficult to directly compare the data here with the MS2 inactivation data of Grinshpun et al. (2010b) because of the different temperatures, flow conditions, and residence times tested. However, several consistencies are observed between the two data sets. First, both results showed that below a certain threshold temperature only

modest MS2 inactivation of about 1-log or less was obtained. Second, at nearly the same treatment temperature, an increase in residence time caused a sizeable increase in MS2 inactivation. This phenomenon can be seen in Figure 4-6 at about 270 °C where an increase in bioaerosol residence time of only 0.42 s increased inactivation by almost 2 orders of magnitude. Third, beyond some temperature (the value depends on residence time) inactivation reached the limit of detection which is about 4 to 5-log. Overall, although the exact values describing inactivation are different between studies, the trends are similar.

In future studies, the relationship between inactivation and residence time for a specific temperature can be established. A specific temperature can be obtained for different residence times by finding the proper combination of bulb voltage and flow rate. By plotting inactivation vs. residence time, the order of the rate equation for death kinetics can be determined and then the rate constant can be calculated for UHT treatment. The data will give more details about the specific temperatures/exposure times required for a certain level of disinfection and also clarify the difference in heat resistance among various types of bioaerosols. This is a possible use of the IR device upon further reduction of temperature gradients in the chamber.

**Inactivation Mechanism of *E. coli* Treated with UHT**

Figure 4-7 displays the SEM images of the samples collected by the BioSampler without heating (A) and with heating at 470 °C (B). In Figure 4-7 A, clear cells are visible which are rod shaped and have a length of 1.0-1.5 μm. The cells appear structurally intact after aerosolization, suspension in air, collection by the BioSampler, and centrifugation. Figure 4-7 B is drastically different as distinct bacterial cells are unidentifiable; instead, larger and more jagged-looking particles are present. These

particles are polydisperse with the largest particle having a length of 24 μm. Although the particles in B could be fragments of *E. coli* that have agglomerated during centrifuging, their strange morphology and the finding of no *E. coli* fragmenting in a previous study (Jung et al. 2009a) led to the hypothesis that these particles were emitted by the cloth during heating. To test this hypothesis, air downstream of the heated cloth was sampled with the SMPS without aerosolization of *E. coli*. Sampling found that the heated cloth emitted a total submicrometer particle concentration greater than $10^5$ particles/$cm^3$ which had a mode diameter of about 50 nm. Although nanoparticles were emitted, sampling with the APS revealed the absence of micrometer-sized particle emission. The micrometer-sized particles observed in Figure 4-7 B may then be *E. coli*/carbon nanoparticle agglomerations created during the centrifuging step of SEM sample preparation. Regardless of the identity of the particles viewed in the SEM images, evidence of particle emission highlights a potential disadvantage of UHT treatment especially when placing the heating element within the airflow. The emission of nanoparticles may be exclusive to heating of the carbon cloth (i.e. other materials may not emit particles), but the release of harmful byproducts must be considered when selecting a heating element or heating chamber in practical applications. Previous studies have not observed particle emissions from their UHT systems because they have sampled with an instrument incapable of detecting particles below 100 nm or they have not tested for emissions (Lee and Lee 2006; Jung et al. 2009a; Grinshpun et al. 2010a; Jung et al. 2010).

The gel electrophoresis results for *E. coli* exposed to three heating conditions are shown in Figure 4-7 C. In lane 1, the control, the observed band is likely the 4.6Mb-*E.*

*coli* genomic band because it has more base pairs than the largest band in the ladder (2,000bp). Although the band appears to have around 3,000bp, the size of DNA larger than the ladder cannot be estimated because the band is not between two known ladder values and because the migration of DNA is logarithmic. The size of a band above the ladder cannot be estimated by extrapolation. Agarose forms a matrix that acts as a sieve and makes it impossible for DNA molecules greater than a certain size to migrate easily through the gel. Depending on the percentage of agarose in the gel, an upper size threshold is reached in which the DNA molecule size cannot be resolved. All DNA molecules above this threshold - generally around the size of the largest ladder band - will migrate at very similar distances and consequently a Mb band would appear relatively close to a kb band. The ladder was added to the gel not for estimating the size of the DNA but rather to ensure that the bands that appeared were larger than the largest size on the ladder.

For the *E. coli* treated at 150 °C, the genomic band is only faintly visible suggesting that some of the genomic DNA had been broken and the resulting smaller fragments migrated further toward the positive electrode. Smearing of the genomic band cannot be observed because the fragments were of different sizes and at too low of a concentration. At temperatures of 310 °C and 470 °C, the genomic DNA are not visible and thus completely fragmented and spread throughout the gel. Overall, UHT treatment reduced the quantity of intact genomic DNA which proved DNA damage occurred and was a possible cause of UHT cell death.

Jung et al. (2009a) found that the UHT-treated *E. coli* were susceptible to structural damage by culturing *E. coli* on selective MacConkey agar. Greater than 80%

structural injury was found at their measured temperatures above 80 °C while the structural injury of Gram-positive *B. subtilis* was less. This difference in structural sensitivity was due to *E. coli*'s thin cell membrane compared to the Gram-positive cell wall. The specific contributions of various inactivation mechanisms (DNA damage, structural injury, etc.) for UHT-treated bioaerosols is likely strongly dependent on the microbe characteristics. For example, for thick-coated *B. subtilis* spores exposed to UHT there is a high association between inactivation and DNA mutational frequency (Johansson et al. 2011). In summary, the results here suggest that DNA degradation is one of the possible inactivation mechanisms although a combination of mechanisms is probably responsible for cell death particularly at high temperatures (Johansson et al. 2011).

**Ambient Bacteria and Fungi Concentration Reduction Using UHT**

Figure 4-8 shows the UHT reduction in outdoor concentration of the bacterial and fungal bioaerosols as a function of particle size. The cloth temperatures were lower here than in the lab setting because a higher flow rate of 28.3 LPM was used. Without heating, the aerodynamic particle size distribution of culturable bacteria was nearly uniform at about 100 CFU/$m^3$ for each size interval except for the smallest interval (0.65-1.1 μm) where it was about 10 CFU/$m^3$. The total concentration of culturable bacteria sampled was consistent with a previous study examining airborne bacteria in outdoor Beijing (Fang et al. 2007). In that study, of the 47 genera of culturable bacteria sampled, *Micrococcus* was the most common comprising 20-30% of the total concentration and was followed by *Staphylococcus*, *Bacillus*, *Corynebacterium*, and *Pseudomonas*. UHT treatment at 210 °C with the IR device reduced the bacteria concentration by about 1-2 orders of magnitude depending on particle size. At 60 °C,

the bacteria concentration was reduced by about 1 log for the larger sizes (4.7 - >7 μm) and the smallest size bin, but was less effective for particles between 1.1-4.7 μm. Because a size interval may be representative of a particular species or collection of species, differences in reduction among sizes may indicate different species sensitivity against biocidal treatment (Wu and Yao 2011). A two-way ANOVA test found that temperature was statistically significant (p-value < 0.05) while size was not. This means that for the temperatures tested in this study, inactivation was not statistically different among the sizes. Environmental bacteria consist of both Gram-positive and Gram-negative species which have different resistance to thermal stress due to differences in cell wall structure (Fang et al. 2007; Jung et al. 2009a). Because particle size was not found to be statistically significant, the different species could have a wide size distribution (aggregates, etc.) or simply have similar thermal resistance.

Figure 4-8 B displays the results of the concentration reduction of ambient fungi due to heat treatment. The culturable particle size distribution without treatment had a peak of about 470 CFU/$m^3$ at the 2.1-3.3-μm size interval and had zero CFU/$m^3$ for the smallest interval. Like the bacteria data, heating generally decreased the culturable concentration with the 210 °C temperature having the highest reduction. However, the magnitude of fungi inactivation was lower than bacteria inactivation at less than 1-log for all sizes. In a previous study in the lab setting, higher inactivation of greater than 2-log against two test fungal bioaerosols was found (Jung et al. 2009b). However, their exposure temperatures were greater than 350 °C compared to 210 °C used in this study. Additionally, in this study the environmental fungi (and bacteria) could have been attached to other non-biological particles like dust which offer protection against stress

(Woo et al. 2012a). While bacteria showed similar thermal resistance for different sizes, two-way ANOVA showed that fungi inactivation statistically differed among sizes. This may be because each fungi specie was exclusively associated with one size bin or that the fungi within a size bin had similar thermal resistance. As many different genera of fungi and their spores including *Aspergillus*, *Penicillium, and Cladosporium* (which have different aerodynamic sizes) can be sampled in the natural environment, finding size to be statistically significant is reasonable (Reponen et al. 2001; Lee and Jo 2006). Regardless, the results here indicate that temperature or exposure time must be increased for more adequate fungal aerosol inactivation.

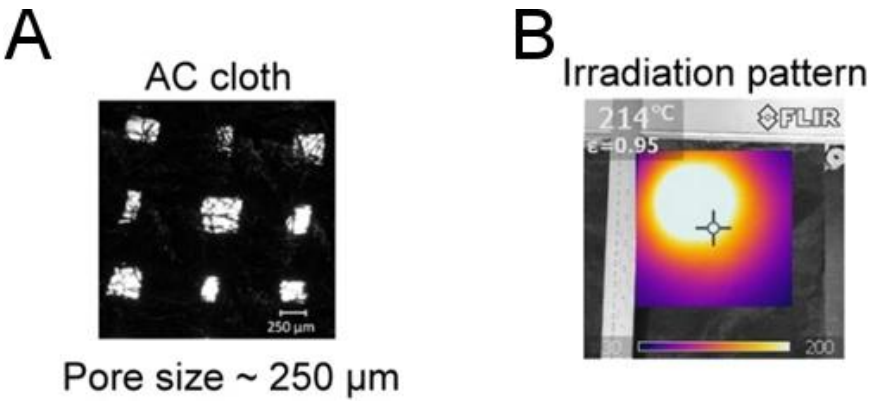


Figure 4-1. Images of the ACC and IR irradiation pattern. A) An image of the ACC displaying the pore size. B) The irradiation pattern produced by the IR bulb at a distance of about 5 cm from a surface.

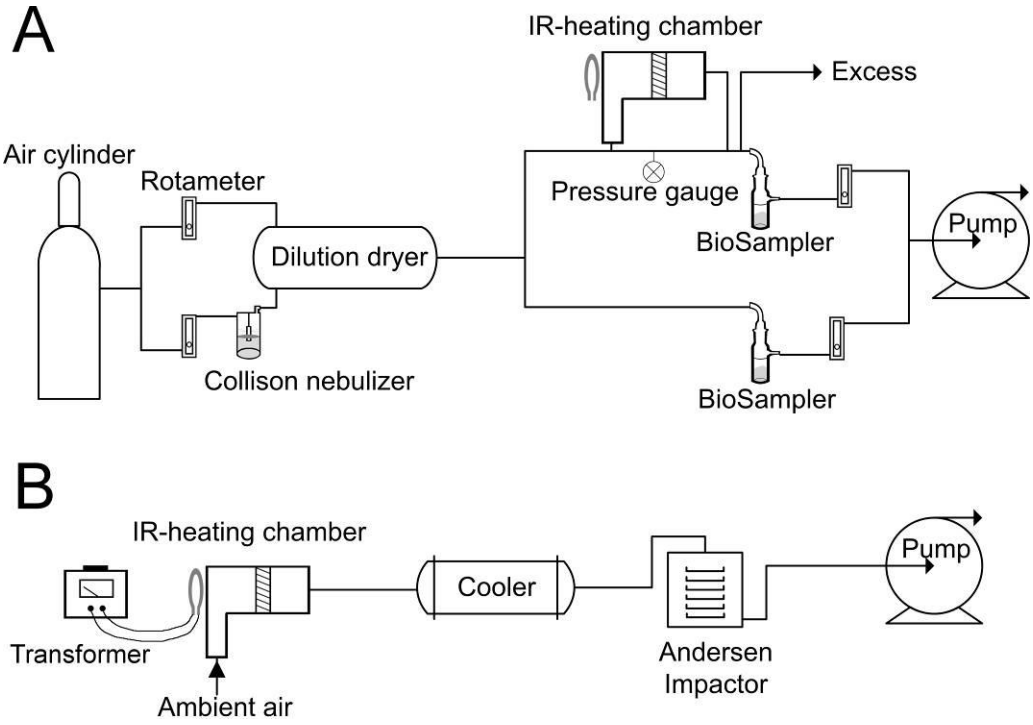


Figure 4-2. Experimental systems for the UHT bioaerosol testing. A) The lab testing system. B) The ambient bioaerosol testing system.

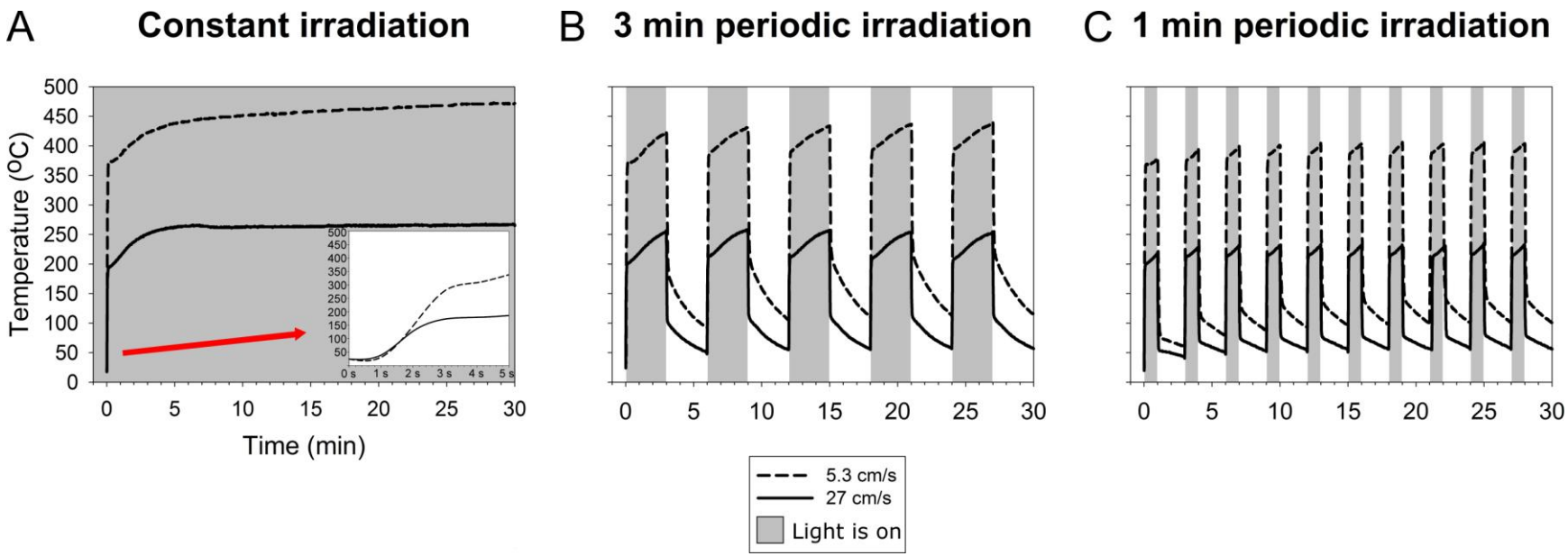


Figure 4-3. The cloth temperature vs. time as measured with the pyrometer. The temperatures are plotted for the three IR application cycles: A) constant irradiation, B) 3 min periodic, and C) 1 min periodic. The inset in the constant irradiation plot displays the increase in temperature during the first 5 s when the bulb was turned on.

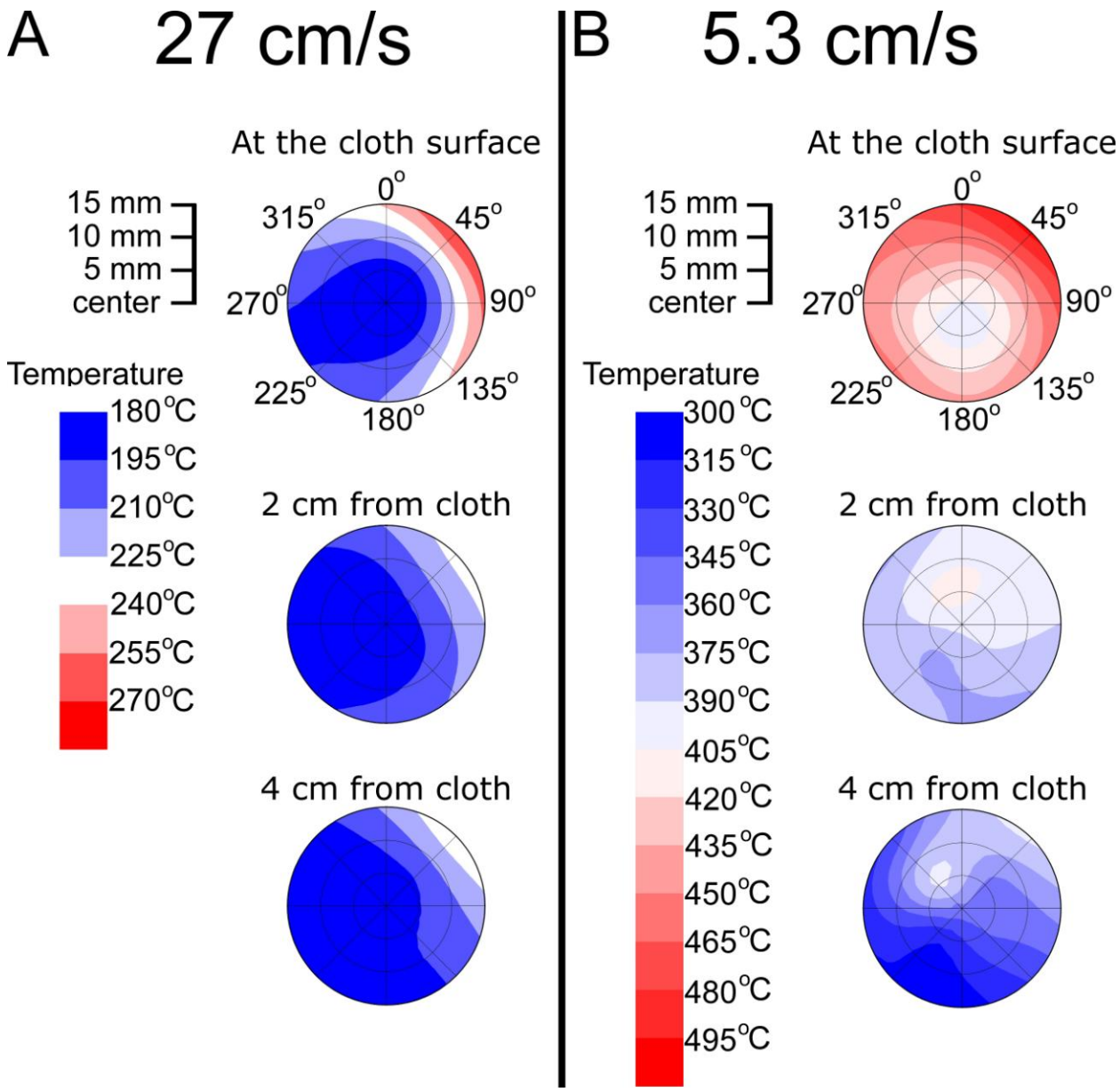


Figure 4-4. The airflow and cloth temperature at various positions within the heating chamber as measured with the thermocouple. The temperature is displayed for the two face velocities: A) 27 cm/s and B) 5.3 cm/s. Each circle represents the airflow temperature at different cross sections. The 0° label corresponds to the top of the heating chamber shown in Figure 1-1 C.

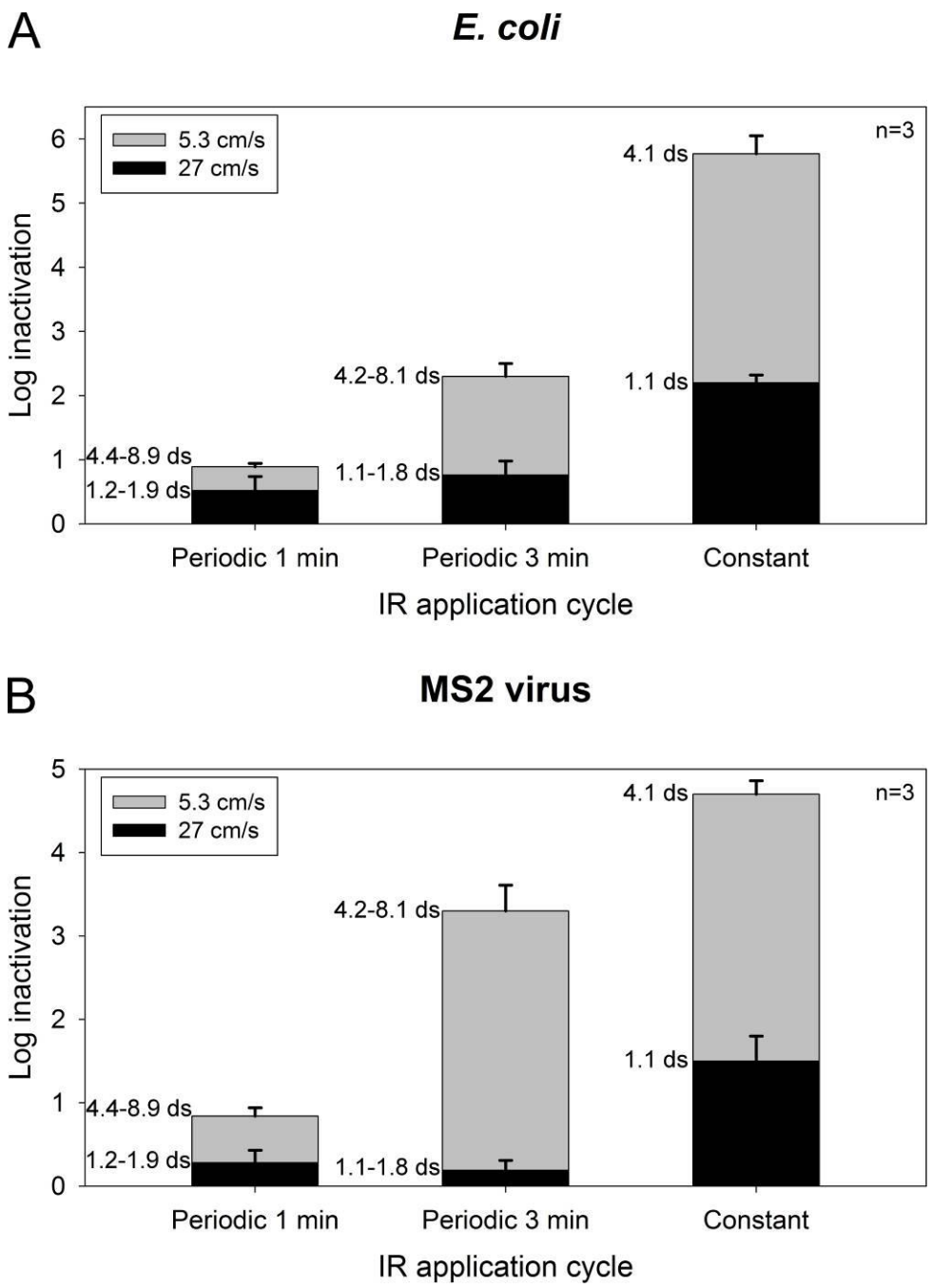


Figure 4-5. Log inactivation as a function of face velocity and IR application cycle. Results are displayed for A) *E. coli* and B) MS2 virus. The residence times are displayed for each condition in deciseconds (ds).

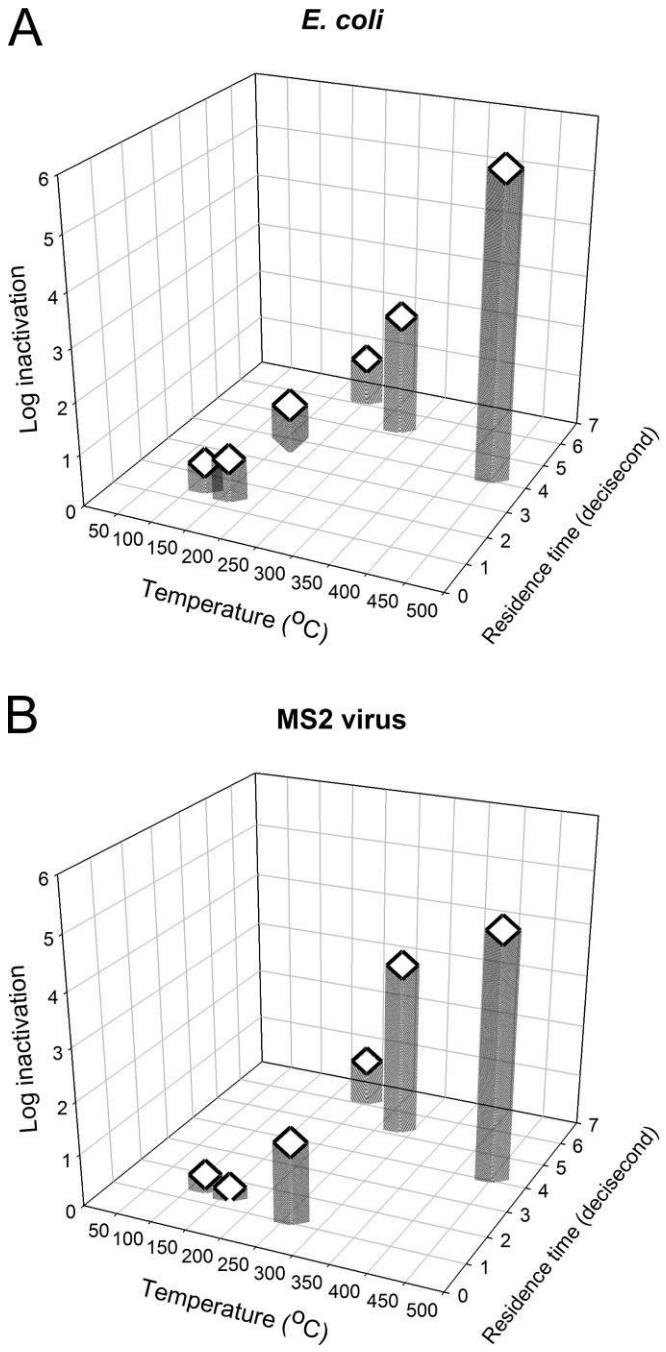


Figure 4-6. Log inactivation of bioaerosols as a function of temperature and residence time. The graphs display the inactivations for A) *E. coli* and B) MS2 virus.

A

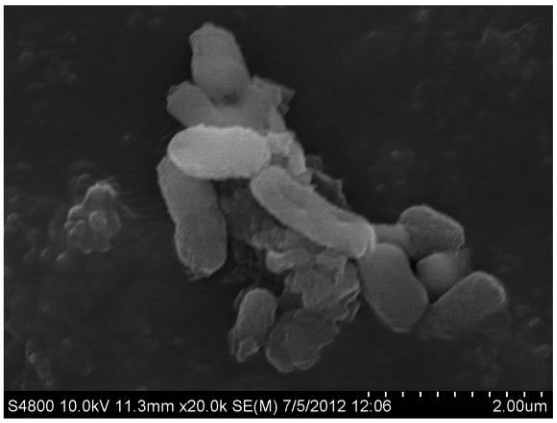


B

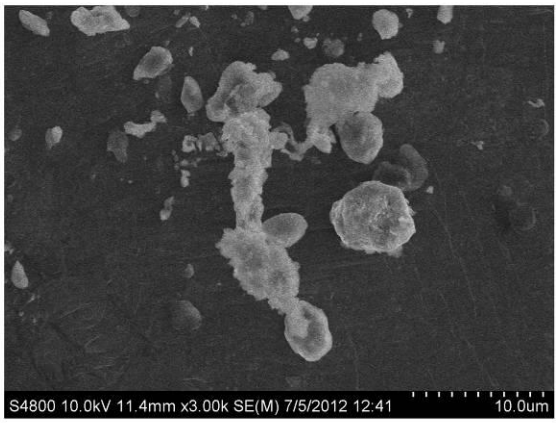


C

Lane 1: Control
Lane 2: 150 °C, 0.88 s
Lane 3: 310 °C, 0.64 s
Lane 4: 470 °C, 0.50 s
Lane 5: Ladder

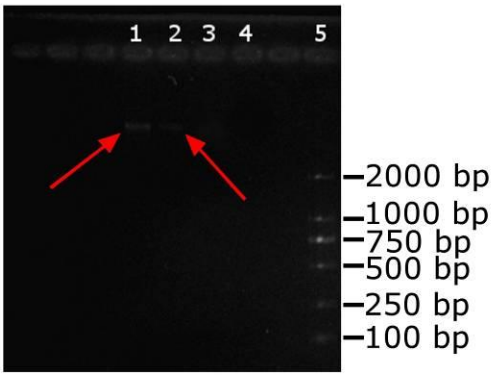


Figure 4-7. SEM and gel images from the samples collected with the BioSampler. A) SEM image of particles sampled without heating. B) Sampled particles with heating at 470 °C. C) Gel electrophoresis of the extracted genomic DNA at the test temperatures and residence times. The red arrows indicate the presence of visible bands.

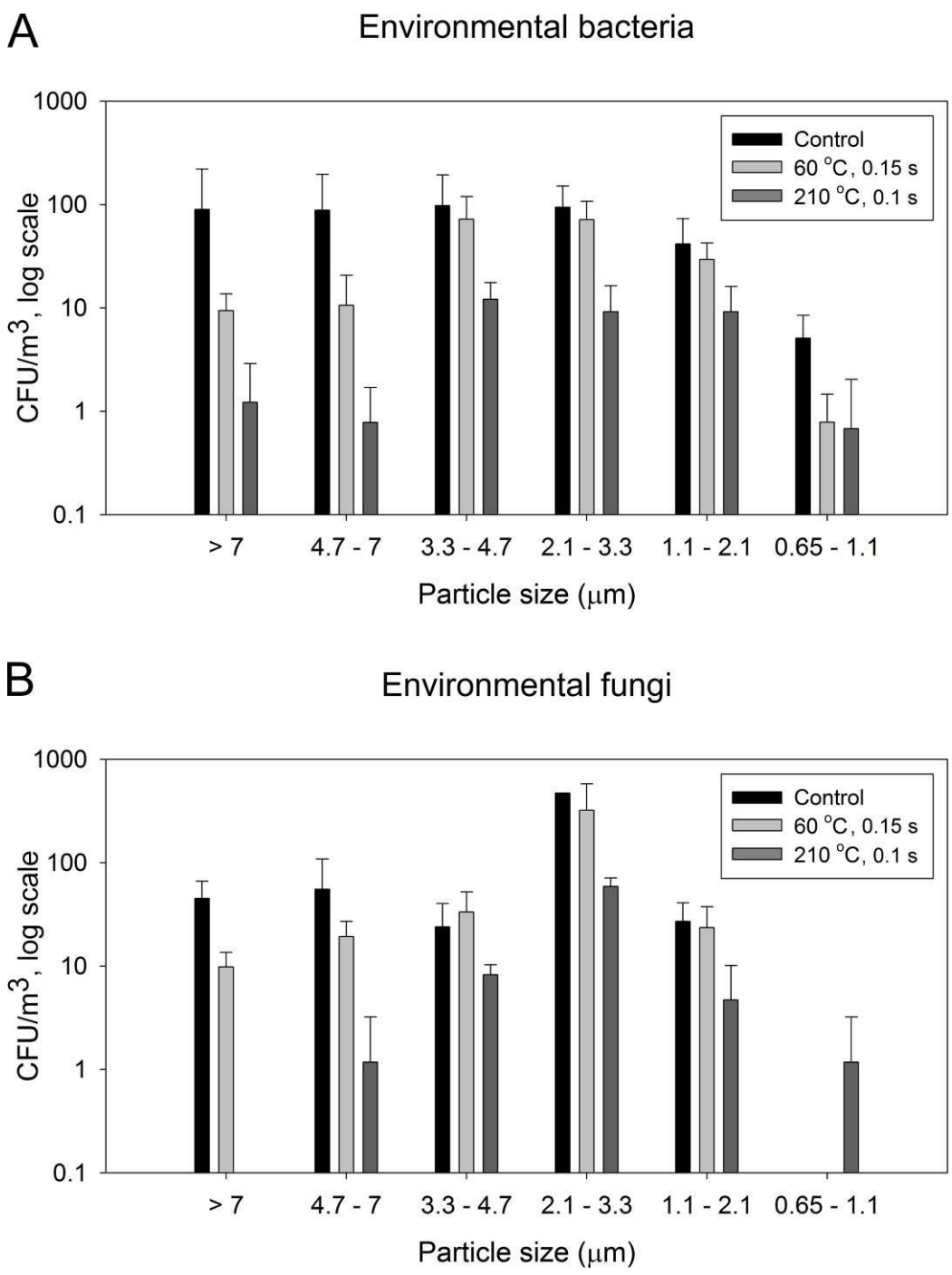


Figure 4-8. Culturable concentrations of ambient bioaerosols for the two heating conditions. The 60 °C and 210 °C temperatures were obtained with 83 and 250 W-bulb powers. A) Concentration of bacteria as a function of size. B) Concentration of fungi as a function of size.

# CHAPTER 5
# FILTRATION OF BIOAEROSOLS USING A GRANULAR METALLIC FILTER WITH MICROMETER-SIZED COLLECTORS*

## Objective

The objective of this study was to test the filtration performance of a granular metallic filter against challenging *B. subtilis* spore and MS2 virus bioaerosols. A testing system was constructed to assess the filter's physical removal efficiency (PRE), viable removal efficiency (VRE), and filter quality ($q_F$) as a function of face velocity and loading time. In addition, an extraction process was designed to remove collected microbes from the filter and the process' efficiency was determined.

## Materials and Methods

### The Experimental Metallic Filter

The experimental stainless steel filter was specially developed by ORNL and consisted of a larger pore-size support layer and a smaller pore-size primary layer. Once fabricated, the 5-µm thick primary layer consisted of unconsolidated micrometer-sized spherical granules while the 0.59-mm thick support layer had a sintered structure. The primary and support layers had measured pore sizes of 0.99 µm and 3.5 µm, respectively. The filter's overall porosity was found to be 37.5%; about 12.5% lower than that tested in previous studies (Endo et al. 2002; Marre et al. 2004).

Obtaining an SEM image of the test filter's primary layer would necessitate damaging the tubular filter and so an image of a similar filter's primary layer is shown instead in Figure 5-1 A. The SEM image of the support layer is displayed in Figure 5-1 B. The images show that the granules in the primary layer are polydisperse with size

* Reprinted with permission Damit, B., Bischoff, B., Phelps, T.J., Wu, C.Y. and Cheng, M.D. (2013) Filtration of bioaerosols using a granular metallic filter with micrometer-sized collectors. In review in *J Environ Eng-ASCE*.

from about 1 μm to greater than 20 μm, while the support layer contains sintered micrometer-sized granules which are larger than 10 μm. Macroscopically, the filter resembles a cylindrical pipe with length of 22 cm as shown in Figure 5-1 C.

### Physical Removal Efficiency (PRE) of Bioaerosols, Pressure Drop, and Filter Quality

The diagram of the PRE testing system is shown in Figure 5-2 A. *B. subtilis* spore and MS2 virus were selected as test bioaerosols. PRE indicates the effectiveness of the filter in removing bioaerosols whether they are viable or nonviable. To measure PRE, path A was used. Building-supplied compressed air passed through an in-line air supply (Model 3074, TSI Inc., MN) to provide air to the testing system. The dry, particle-free air was then split into parallel with dilution airflow sent to the mixing chamber and 5 LPM to a 6-jet Collison nebulizer (Model CN25, BGI Inc., MA). The dilution air was adjusted depending on the face velocity tested. Two face velocities were tested: 3.3 cm/s and 7.3 cm/s, to investigate its effect on efficiency and pressure drop. Face velocities near the tested face velocities are commonly tested in granular bed filter studies (Otani et al. 1989; Ruiz et al. 2000; Kuo et al. 2010). With a filter area of 69 $cm^2$, flow rates of about 14 LPM and 30 LPM were required for face velocities of 3.3 cm/s and 7.3 cm/s respectively.

After nebulization, the particles entered the mixing chamber (relative humidity ≤ 26%) where the water content evaporated. The flow was then directed into a charge neutralizer (Model 3054, TSI Inc., MN) to neutralize charge and ensure the charge distribution of particles followed a Boltzmann curve. The challenging bioaerosols encountered the primary layer before the support layer during filtration. The filtration efficiency was determined by measuring the particle concentration downstream of the

filter chamber with and without the filter in the chamber. Particle concentrations were measured with an Aerodynamic Particle Sizer (APS - Model 3320, TSI Inc., MN) for micrometer *B. subtilis* spore and an SMPS for sub-micrometer MS2. The physical removal efficiency, PRE, was then calculated from Eq. 5-1:

$$PRE = \left(1 - \frac{C_{filter}}{C_{no\ filter}}\right) \times 100\% \quad (5\text{-}1)$$

where $C_{filter}$ is the particle concentration with the filter and $C_{no\ filter}$ is the particle concentration without the filter in the chamber. Sampling was recorded for 0-4 min, 4-8 min and 8-12 min intervals during filter testing to determine the effect of loading time on filter performance. The filter's pressure drop was measured with a Magnehelic pressure gauge. Filter quality, $q_F$, was also calculated to evaluate the overall performance of the experimental filter against bioaerosols. Filter quality is defined as (Hinds 1999):

$$q_F = \frac{-\ln P}{\Delta p} \quad (5\text{-}2)$$

where $P$ is the penetration (1 – efficiency) and $\Delta p$ is the filter's pressure drop. Three trials were conducted for each experimental condition.

**Viable Removal Efficiency (VRE) of Bioaerosols**

Both penetrating viable and nonviable bioaerosols are included when calculating PRE. To determine only the number of viable bioaerosols penetrating the filter, VRE experiments were also conducted. Instead of an optical particle counting system, BioSamplers (Model No: 225-9595, SKC Inc., PA) filled with 15 mL DI water for spore sampling and 15 mL 1X phosphate buffered saline for virus sampling were used (Woo et al. 2011). The schematic of the VRE system is shown in path B in Figure 5-2. The BioSamplers were operated at a nominal flow rate of 12.5 LPM. Bioaerosols were

sampled for 30 min so that the filter could be challenged with a high number of particles and yield an accurate efficiency value. After sampling, the BioSampler liquid was removed and cultured with appropriate growth medium described in the previous chapters. VRE was calculated from Eq. 5-3.

$$VRE = \left(1 - \frac{N_{filter}}{N_{no\ filter}}\right) \times 100\% \quad (5\text{-}3)$$

*N* represents the counted CFU for spore or PFU for virus from the incubated cultures which were sampled with or without a filter present in the filter chamber. A serial dilution was performed and only plates with 30-300 CFU/PFU were included in the VRE calculation. Three trials were conducted for both microbes at the 3.3 cm/s face velocity.

**Filter Cleaning/Microbe Extraction Procedure**

After each experiment, the filter was thoroughly cleaned and restored to its initial condition. It was decided that the filter was sufficiently clean once its pressure drop returned to its original value before particle loading. The filter was subjected to a rigorous cleaning procedure involving the use of an ultrasonicator (UP200S, Hielscher, NJ). The seven-step procedure, detailed below, was developed specifically for the metallic filter and completed after each bioaerosol experiment.

1. A 300 mL 0.1% Tween 20 solution was prepared and poured into a cylindrical glass container with similar dimensions as the filter.
2. The bioaerosol-loaded filter was submerged in the solution and positioned upright in the glass container.
3. A 2-mm diameter finger sonotrode (S2, Hielscher, NJ) was inserted about 4 cm into the end of the filter and sonicated for 15 min at the highest acoustic power density (600 W/cm$^2$). For the first half of the 15 min, the ultrasonicator was operated at constant output. For the second half of the 15 min, the ultrasonicator was pulsed at half cycle.
4. The filter was removed from the container, flipped, and sonicated at the opposite end with an identical procedure using the same cleaning solution.

5. Afterwards the middle of the filter was cleaned by inserting the sonotrode about 10 cm into the filter and sonicating at the highest power density with constant output for 10 min.
6. The cleaning solution was removed and kept for culturing and the filter was then boiled for 10 min in turbulent water to remove any Tween 20 residue.

After boiling, the filter was dried in an oven at 100 ºC for 30 min. This cleaning procedure was able to return the filter's pressure drop to its initial value before bioaerosol loading. To determine viable extraction efficiency of the bioaerosols, the cleaning solution was cultured with appropriate growth medium and the CFU/PFU were counted after incubation. Provided the entering inlet count and penetrating count are known from sampling with the BioSamplers, the extraction efficiency, $E_E$, of the process was calculated by:

$$E_E = \left(\frac{N_E}{N_{no\ filter} - N_{filter}}\right) \times 100\ \% = \left(\frac{N_E}{VRE \times N_{no\ filter}}\right) \times 100\% \ . \quad (5\text{-}4)$$

$N_E$ is the CFU/PFU count extracted from the filter and VRE is the efficiency of the filter against the particular bioaerosol. The numerator of the ratio in Eq. 5-4 is the microbe count grown from the extraction solution while the denominator is the microbe count collected by the filter.

## Results and Discussions

### PRE of Bioaerosols, Pressure drop, and Filter Quality

Figure 5-3 displays the PSDs of the test bioaerosols. The *B. subtilis* spore PSD was nearly monodisperse with a geometric standard deviation of 1.28 and an aerodynamic mean, median, and mode of around 0.90 µm. On the other hand, the MS2 PSD was more polydisperse with a geometric standard deviation of 1.89 and mobility mean, median, and mode size of 64.3 nm, 48.4 nm, and 42.9 nm respectively - consistent with the PSDs obtained for nebulized MS2 virus in literature (Balazy et al.

2006; Eninger et al. 2009). Dissolved solutes and other impurities in the MS2 suspension yielded non-viral aerosols which are detectable with the CPC; this results in a more polydisperse PSD. The presence of these spurious aerosols, however, does not affect the results as it has been shown that MS2 penetration values are nearly identical with either a nebulized polydisperse PSD or a cleaner PSD obtained with electrospray (Eninger et al. 2009).

Figure 5-4 displays the results of the *B. subtilis* spore PRE experiments. The efficiency was relatively high and ranges from greater than 99.9% to almost 99.99%. It was unexpectedly higher at 3.3 cm/s than at 7.3 cm/s for the inertia-dominant spore, but the standard error bars indicated that the difference was not statistically significant (p-value>0.05). This observation is possibly because 10% of the spore PSD (by number) was greater than the 0.99-µm primary layer pore size and so were always collected regardless of face velocity. In other words, efficiency was not affected by face velocity for larger-than-pore-size particles in the spore PSD. Also, collection by interception is prevalent for spore and does not depend on face velocity; so, the efficiencies at two close face velocities would be similar. As loading time increased, the efficiency was shown to increase but the increase was not statistically significant. This was likely because the challenging spore concentration was relatively low at 100 #/cm$^3$ so that there was insufficient pore clogging over the 12 min period to cause higher efficiency.

The PRE of MS2 can also be seen in Figure 5-4. The filter's physical efficiency against MS2 was higher than its efficiency against *B. subtilis*. This is expected because *B. subtilis* has a higher percentage of particles in the most penetrating size range than MS2 which are highly diffusion-dominant particles. As expected, the diffusion-driven

collection efficiency for MS2 was higher with a lower face velocity. Unlike the spore results, face velocity for MS2 collection was a statistically significant factor (p-value<0.01). Particle loading was not sufficiently high to increase efficiency at 3.3 cm/s but it did increase efficiency at the higher velocity of 7.3 cm/s.

The pressure drop for the clean filter was 13.4, 23.7, and 30.5 kPa for face velocities of 3.3, 5.3, and 7.3 cm/s respectively. The increase in pressure drop with face velocity was nearly linear indicating laminar flow within the filter. Compared to fibrous or granular bed filters of similar or greater thickness, the tested filter exhibited a pressure drop that was 1-2 orders of magnitude greater at similar face velocities (Otani et al. 1989; Kuo et al. 2010; Zhang et al. 2010b). This higher pressure drop was also observed in literature for tested filters composed of micrometer-sized granules and is due likely to the filters' lower porosity (37.5% - 50%) and because pressure drop is inversely proportional to the square of the granule size (Endo et al. 2002). During filtration, pressure drop did not increase considerably during spore loading and increased only slightly during virus loading (83 Pa/min).

The bioaerosol filter quality corresponding to the efficiency in Figure 5-4 and the measured pressure drop is plotted in Figure 5-5. For both bioaerosols, filter quality ranged from about 0.25 $kPa^{-1}$ to 0.75 $kPa^{-1}$. It was higher at the 3.3 cm/s face velocity mainly due to the lower pressure drop. Filter quality generally remained stable with time because penetration changed only slightly with time while the pressure drop remained relatively constant. As apparent from previous studies, the filter quality for micrometer-sized granule filters tends to be lower than conventional filters (Endo et al. 2002). In this work, the tested filter exhibited a filter quality that was about 1 order of magnitude less

than fibrous filters used in MS2 testing (Lee et al., 2009). For the type of filter tested in this study, an increase in bioaerosol efficiency from smaller granules does not make up for a corresponding increase in pressure drop according to $q_F$ for air filtration.

**VRE of Bioaerosols**

In the VRE experiments, a VRE of slightly greater than 99.9996% was found for both spore and virus. This is greater than 5-log removal and indicated that the filter was highly effective in removing viable bioaerosols regardless of species and size. For some replicates for spore, no CFU were cultured from the sample downstream of the filter. A CFU value of 0.5 was then used and so the reported VRE is conservative. The VRE was higher than the reported PRE because PRE and VRE were measured for different timescales. PRE was only measured during a 0-12 min period while VRE was calculated over an integrated 30 min period. Additionally, VRE is not affected by the presence of nonviable aerosols so the challenging PSDs when determining PRE and VRE are different. Regardless, the high value of VRE provides practical evidence that the metallic filter offers protection against bioaerosols. Based on the value of VRE, the corresponding filter quality was about 0.928 $kPa^{-1}$ for both spore and virus - still 2 orders magnitude lower than the values found in literature for fibrous filtration of MS2 (Lee et al., 2009).

**Efficiency of the Extraction Process**

For spores, the designed extraction process was very effective with an extraction efficiency of about 99%. Considering all microbes, bacterial spores are among the most tolerant to an extraction process due to the highly resistance nature of the bacterial spore (Nicholson et al. 2000). For MS2, the extraction efficiency was much lower at about 1.2% even when assuming that the BioSampler sampled MS2 at an optimistic

10% efficiency (Hogan et al. 2005). The decreased extraction was likely a consequence of the sensitivity of MS2 to external stress. Inactivation may have occurred during the violent sonication process where shock waves, high shear forces, and greater temperatures and pressures were present (Lamminen et al. 2004). Furthermore, during sonication, it was noticed that the extraction solution became hot to the touch. If the ultrasonicator was operated at a lower power or the filter was sonitcated for less time, more viable viruses could have been recovered.

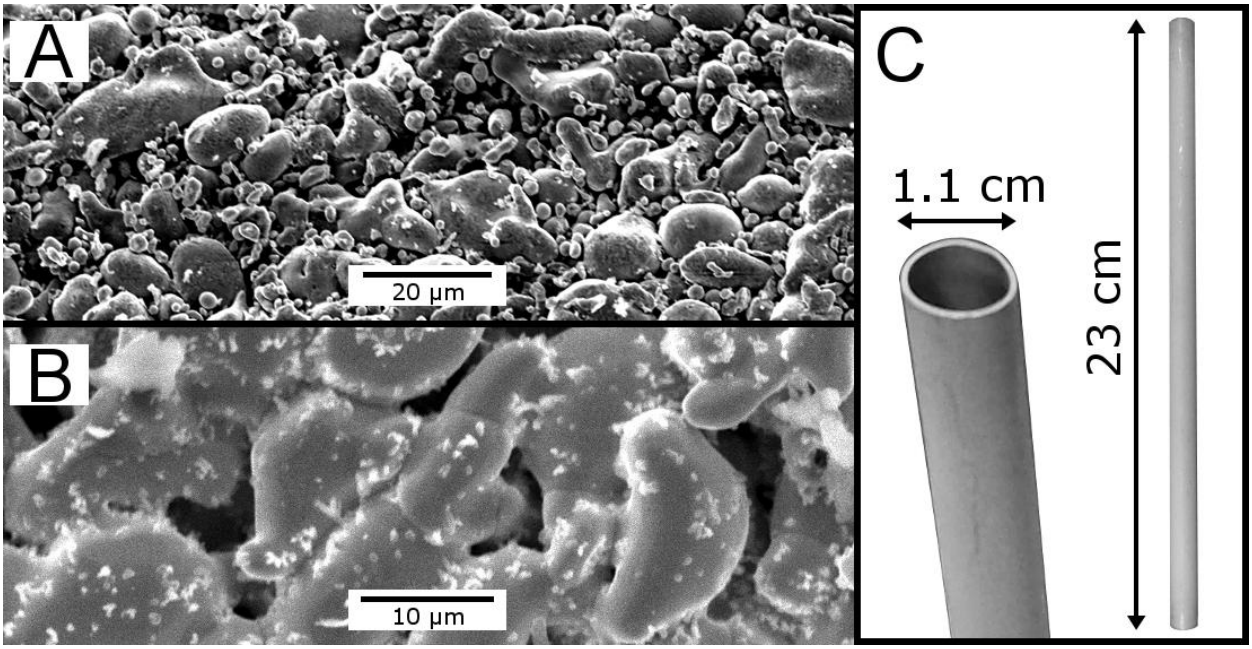


Figure 5-1. Images of the test granular metallic filter. A) SEM micrograph of the structure of the filter's primary layer under 950× magnification. B) Image of the support layer under 2,000× magnification. C) Macroscopic image of the filter. The filter resembles a metallic pipe.

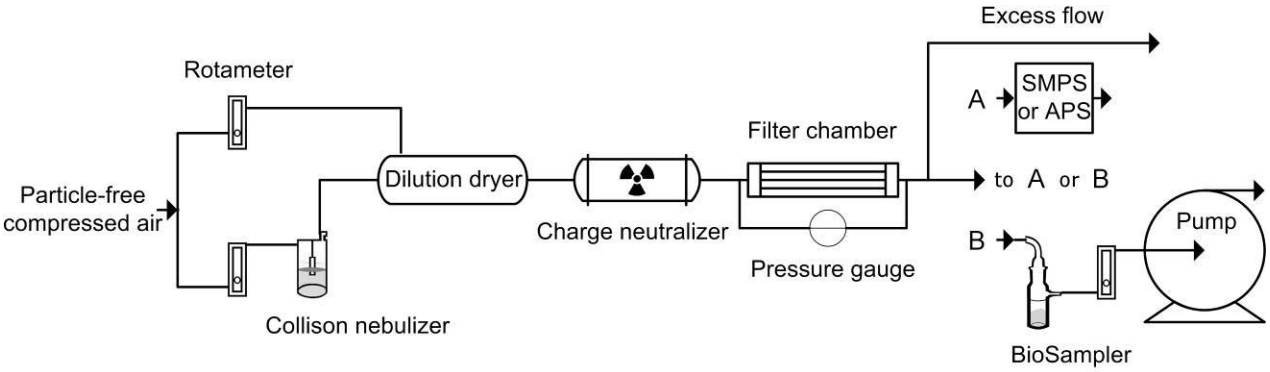


Figure 5-2. Diagram of the testing systems to evaluate the effectiveness of the granular metallic filter. Path A is the PRE testing system and path B is the VRE testing systems. For the filter tests, a filter was inserted in the filter chamber while for the control tests the filter was removed.

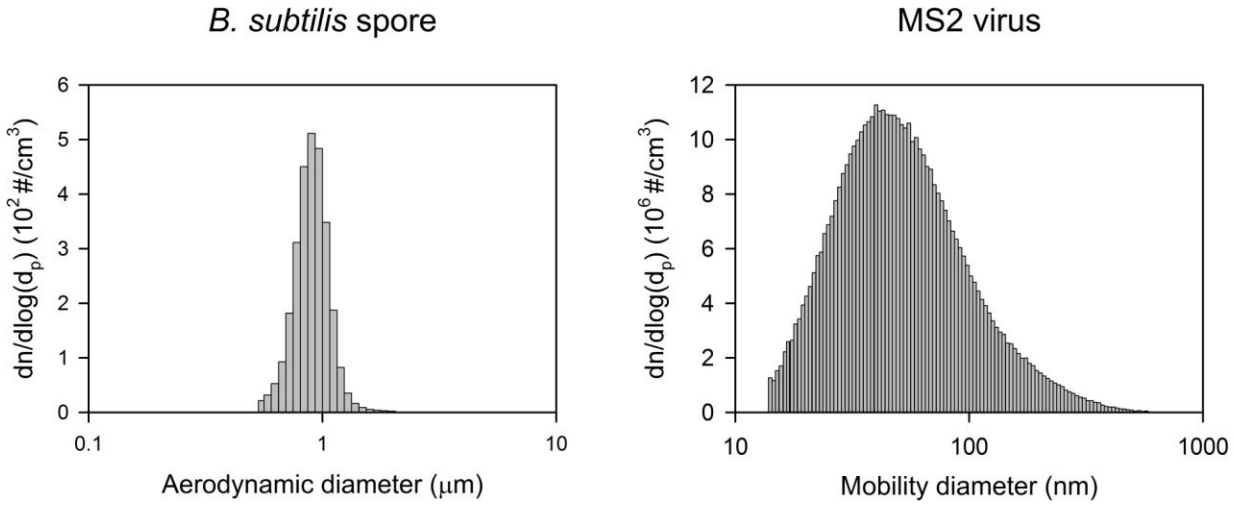


Figure 5-3. PSDs of the test bioaerosols.

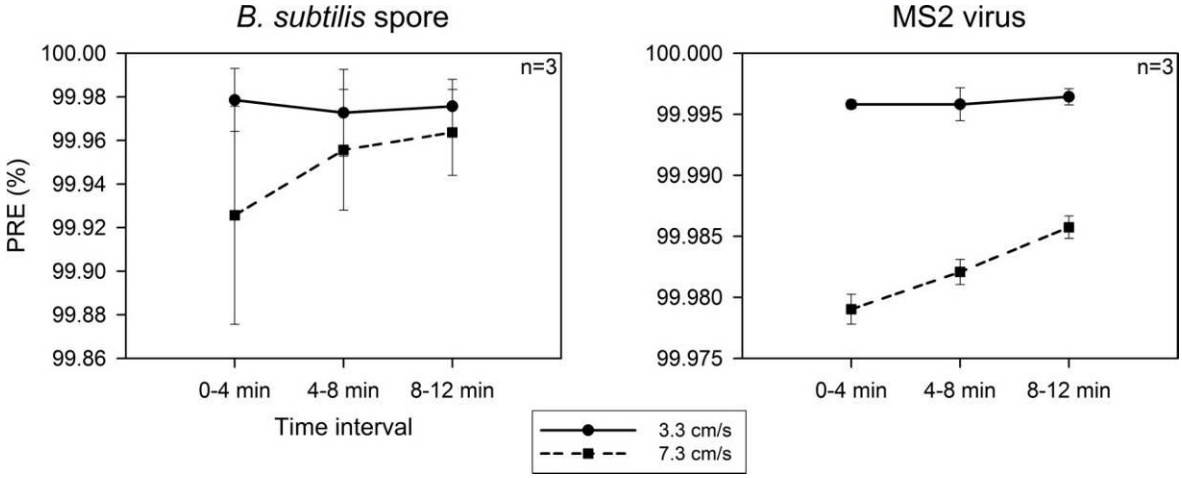


Figure 5-4. PRE of *B. subtilis* spore and MS2 virus as a function of face velocity and loading time. The error bars represent standard error.

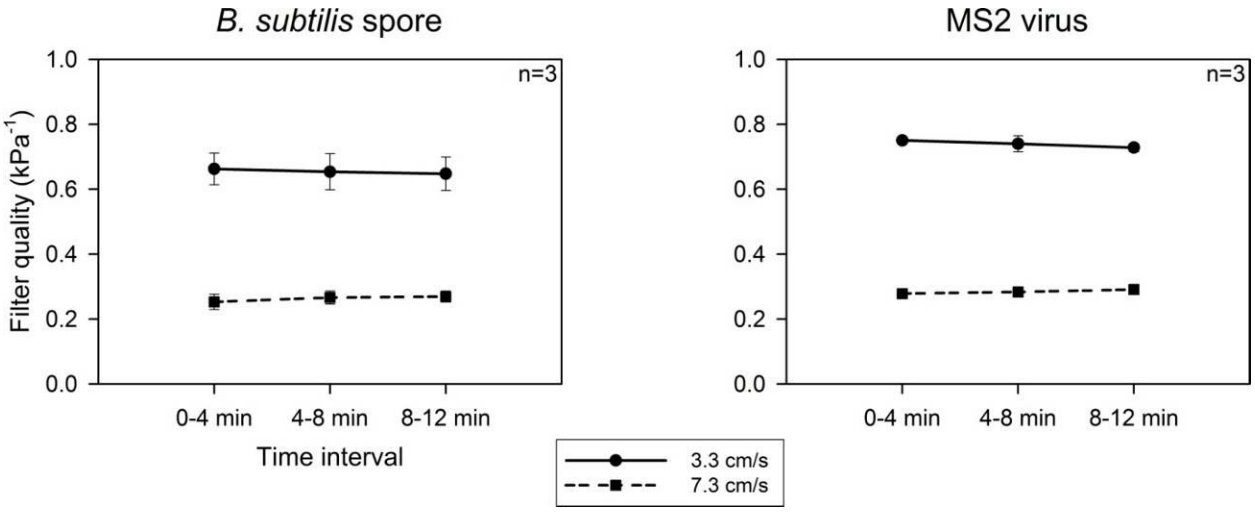


Figure 5-5. Filter quality for *B. subtilis* spore and MS2 virus as a function of face velocity and loading time. The error bars represent standard error.

# CHAPTER 6
# ON THE VALIDITY OF THE POISSON ASSUMPTION IN SAMPLING NANOMETER-SIZED AEROSOLS*

## Objective

The objective of this chapter was to determine whether nanometer-sized aerosol sampling follows a Poisson process. Times series of particle detections were obtained for four particle sizes - 10 nm, 25 nm, 50 nm and 100 nm - by sampling from indoor air. Five metrics were calculated from the data: pair-correlation function (PCF), time-averaged PCF, coefficient of variation, probability of measuring a concentration at least 25% greater than average, and posterior distributions from Bayesian inference. To identify departures from Poissonian behavior, the metrics calculated for the experimental time series were compared to the metrics calculated for 1,000 computer-generated Poisson time series.

## Materials and Methods

### Obtaining a Time Series of Nanometer-Sized Aerosol Counts from Indoor Air

An SMPS was used to obtain a time series of aerosol counts because it is able to accurately detect aerosols with sizes of tens of nanometers. Unlike an OPC, it is not limited by low light scattering produced by small aerosols. The SMPS consists of two subsystems: an electrostatic classifier (Model 3080) and a condensation particle counter (CPC; Model 3782). The air to be sampled first enters the classifier due to a vacuum applied by the CPC. Within the classifier, polydisperse aerosols are directed to a bipolar charge neutralizer where they obtain the Boltzmann equilibrium distribution. The aerosols then enter a differential mobility analyzer (DMA) that uses an electrostatic field to only allow aerosols with a specific electrical mobility to exit the classifier. Finally,

* Reprinted with permission Damit, B., Wu, C.Y. and Cheng, M.D. (2013) On the validity of the Poisson assumption in sampling nanometer-sized aerosols. In submission to *J Nanopart Res*.

these monodisperse aerosols are sent to the CPC where they are grown by condensation and counted with an optical detection setup. For nanometer-sized aerosols, the fraction of aerosols containing net charge is less than 40% at 50 nm and this fraction decreases with size (Hoppel and Frick 1986; Hinds 1999). Thus, the number of aerosols undergoing electrophoresis and are then counted decreases with size. In the scanning mode, an SMPS can obtain the PSD by automatically varying the electrophoresis voltage. In this study, however, the voltage was kept fixed so that the time series of particle detections for one specified size at a time could be obtained. In this manner, the validity of the Poisson assumption can be examined as a function of size. Aerosols with sizes of 10 nm, 25 nm, 50 nm and 100 nm were sampled and the resulting time series were analyzed.

The CPC recorded particle counts every 0.1 s (1 ds). This was the shortest sampling time available without creating custom software to extract the pulse signals recorded by the CPC's photodetector. Thus, the presence of non-Poisson behavior for scales shorter than the minimum sampling time (1 ds in this study) cannot be accurately identified. Also, as mentioned previously, when calculating the PCF, counts are measured and recorded over a 1-ds sampling period so that the exact arrival of a particle at the detector is not known (Larsen et al. 2003). With these limitations, a Poisson process cannot be determined from the data in the fullest sense; however, 1 ds is sufficient to investigate whether the Poisson distribution is practically appropriate (via the time-averaged PCF) because aerosol concentration measurements are usually taken with sampling periods greater than 1 ds. Nanometer-sized aerosol sampling is conducted in many different contexts (e.g. ambient aerosol measurements, filter testing,

etc.), but in this work, indoor air will be analyzed as a first study. Sampling was run overnight for about 12 hours for each particle size in an empty laboratory yielding a time series of $4.32\times10^5$ measurements from 0.432 $m^3$ of sampled air.

**Appropriate Use of the PCF and Check for Constant Concentration**

After obtaining the time series for each particle size, the data were plotted and a subset of data containing $10^4$ measurements (about 16.7 min) were selected which visually appeared to have constant concentration. The data sets were then scrutinized quantitatively for their validity of the following conditions: (1) the concentration is sufficiently dilute, (2) there are a high number of total counted particles in the subset, and (3) the underlying concentration does not change with time (it is stationary) (Larsen et al. 2005). The PCF is most meaningful when none of these conditions are violated - for the time-averaged PCF and other metrics (to be discussed in the paragraph below); however, only condition (3) needs to be met. Although the Poissonian assumption should theoretically be applicable even with a time-varying concentration, assessing its validity is most straightforward with a stationary time series.

To satisfy conditions (1) and (2), the following should be true respectively:

$$\mu^2 \ll 1 \quad (6\text{-}1)$$

$$N\mu \gg 1 \quad (6\text{-}2)$$

Examination of the data indicated that only the 10 nm- and 25 nm-time series were reasonably appropriate. In evaluating condition (3), although there have been attempts to establish criteria for constant-concentration data, no protocol exists that guarantees this. Calculation of the PCF and time-averaged PCF using a time series without constant concentration unintentionally yields the presence of positive correlations (i.e.

both η(t) and $\bar{\eta}(s)$ > 0) (Larsen 2012). In this study, the following necessary, but not sufficient criteria proposed by Larsen et al. (2005) were used in an effort to classify a data set as possibly stationary to address condition (3):

a. $\left|lim_{T\to\infty}\int_0^T \eta(t)dt\right| < \infty$ (6-3)

b. $q \neq q(T)$ (6-4)

c. $q \ll T$ (6-5)

where *q* is the minimum value of *t* for PCF equal to zero. Criterion (a) ensures that the PCF is not predominantly positive which would indicate the presence of varying underlying concentration. Violation of criterion (b) indicates that the value of *q* is dependent on the total sampling period while violation of (c) indicates that the PCF is not zero until *t* is similar to the total sampling period. Criteria (a)-(c) depend on the PCF which can only be meaningfully calculated for 10 nm and 25 nm. Thus, these criteria were not applicable for 50 nm and 100 nm and so the approach taken by Larsen (2007) was adopted to classify the time series as possibly having constant concentration. For 10-nm and 25-nm data, the PCF was calculated from the truncated, visually-stationary time series and was required to pass criteria (a)-(c) before continuing with analysis.

**Other Calculated Metrics**

Besides the PCF and time-averaged PCF, three other metrics - which are more practically meaningful - were calculated: the coefficient of variation (CV) for a sampling period, the probability of obtaining a concentration at least 25% greater than average, and the posterior distribution for the concentration from Bayesian inference. As mentioned in Chapter 1, Bayesian inference can be used to determine how likely the measured concentration is the actual concentration given a set of measurements. This

is the posterior density, $f(\mu|x_1,\ldots, x_m)$ (the density distribution of obtaining $\mu$, given $m$ samples), found using Bayes' theorem (Bolstad 2007):

$$f(\mu|x_1,\ldots,x_m) = \frac{f(x_1,\ldots,x_m|\mu)\, f(\mu)}{\int_0^\infty f(x_1,\ldots,x_m|\mu)\, f(\mu) d\mu} \quad (6\text{-}6)$$

where $f(x_1,\ldots, x_m|\mu)$ is the likelihood function, $f(\mu)$ is the prior distribution and the denominator of Eq. 6-6 is the normalizing constant. A positive uniform prior, $f(\mu) = 1$, was chosen to calculate the posterior distribution in this study.

To compare how the experimental data differed from Poisson data, the metrics were calculated for both the experimental data and for 1,000 Poisson simulations with the same mean and number of measurements as the experimental data. The Poisson simulation data were generated from MATLAB's poissrnd() function. For each metric, the maximum and minimum simulation values were plotted as well as the area of the graph containing 80% of the simulation-data values. The graphs present how typical the experimental data are to what are expected from a truly random process and signify departures from a Poisson process.

## Results and Discussions

Figure 6-1 displays the time series of particle counts that were analyzed for each particle size. The gray line indicates the mean count for each 100-ds sampling period within the 10,000 ds time series. For each particle size, the gray line remains relatively constant over the time series and no obvious trend in underlying concentration change can be seen. The average number of detected counts per ds increased with increasing particle size: 100 nm had the highest at 16.5 #/ds while 10 nm had the lowest at 0.159 #/ds. From ambient air, a higher concentration of smaller nanometer-sized aerosols (< 100 nm) is generally expected (Bukowiecki et al. 2002; Fromme et al. 2007), but the

lower average count was due to charge neutralization before electrophoresis within the classifier. The fraction of 10 nm aerosols with one positive net charge for a group of aerosols that have attained the Boltzmann distribution is 0.3% compared to 24.1% for 100 nm (Hinds 1999). This means that the CPC can theoretically count 80-times more 100 nm aerosols than 10 nm aerosols. Furthermore, the CPC used in this study has a counting efficiency of 50% for 10 nm aerosols compared to 100% for 100 nm aerosols (Liu et al. 2006). These causes explain the increase in counted aerosols with size. Overall, Figure 6-1 shows that the time series for each particle size has nearly constant concentration with seemly random behavior which is suitable for further analysis in this study.

The PCF for the experimental data and the simulations is displayed in Figure 6-2. Only the 10-nm and 25-nm PCFs were calculated due to the constraints described in the section above. For Figure 6-2 and the following figures, the dark gray area contains 80% of the simulation values, the light gray area contains 100% of the simulation values (i.e. the black edges of the light gray area represent the range of values obtained from the simulations), and the black dots represent experimental values. First, inspection of the experimental PCF for both sizes reveals that there is no prevailing positive PCF and criteria (a)-(c) outlined in the previous section were satisfied. In general, the PCF calculated from the experimental data is within the minimum and maximum simulation values for both aerosol sizes and are essentially indistinguishable from the simulations. Most of the experimental 25-nm PCF is within the area containing 80% of simulation values; on the other hand, the experimental 10-nm PCF has more data points outside the area. Besides this, the range for the 10-nm simulated PCF is greater than for the 25-

nm simulated PCF: about ±0.3 and ±0.08 for 10 nm and 25 nm respectively. This observation can be explained by examining the signal to noise ratio (SNR) for a purely Poisson process, which is displayed in Eq. 6-7:

$$SNR = \frac{\mu}{\sigma} = \frac{n}{\sqrt{n}} = \sqrt{n} \tag{6-7}$$

where $\sigma$ is the standard deviation and $n$ is the mean count in an arbitrary time period. By definition, a Poisson process must have an equal mean and variance, and so the SNR is equal to the square root of $n$. Equation 6-7 shows that the signal increases with increase in the count. Because 10 nm has a lower average count than 25 nm (see Figure 6-1), higher noise will be encountered and this is reflected in the range of the PCF. Regardless, the experimental values are consistent with what is expected from a Poisson process (via comparison to the simulations) for both sizes, and this provides first evidence that nanometer-sized aerosol sampling follows a Poisson process at least under the conditions tested here.

Figure 6-3 shows the time-averaged PCF. While the x-axis for the PCF represents the time separating two differential sampling periods, the time-averaged PCF x-axis represents the length (in ds) of the sampling period employed. The time-averaged PCF was calculated for sampling time periods up to 100 ds which is considerably longer than the time periods used for a single particle size during scanning with an SMPS. For all tested particle sizes, the experimental time-averaged PCF falls within the area containing 80% of the simulations. An overall trend of positive values for the experimental data is not observed here suggesting that the aerosol concentration remains stable during the time series for all particle sizes. The 10-nm particle size has the largest range of values again due to its lower average count and lower SNR as

explained in the above paragraph. Like with the PCF, the experimental values of the time-averaged PCF are indistinguishable from the simulations.

Further evidence to support the Poisson assumption is displayed in Figure 6-4 and Figure 6-5. Figure 6-4 is the CV of counts vs. the sampling time period length. Practically, the CV describes how a measured concentration would change from sample to sample (for a specified sampling period) due to random fluctuations. The experimental CV values generally fall within the range of the simulations for all sizes except 10 nm where there is a lower CV than what is expected. This occurs when the sampling time period is about 250 ds but it is not sustained for longer sampling time periods. A CV lower than a CV for a Poisson process indicates that an aerosol concentration measured on multiple occasions would yield more consistent results than expected. For some purposes, this may be beneficial because the concentration fluctuation is not as extreme; however, the Poisson distribution cannot be used in determining confidence in a measurement. The event occurs at 250 ds - much larger than the sampling period for optical sampling instruments - so it may not be practically relevant.

Figure 6-5 is a concrete example of how a non-Poissonian process could possibly affect a concentration measurement. The figure displays the probability (for a specific sampling period length) of measuring a concentration at least 25% greater than the average concentration calculated over the 10,000-ds time series. For all tested particle sizes, the experimental data generally falls within the range of 80% of the simulated values. The zigzag pattern of the curves in Figure 6-5 is due to the relationship between the aerosol detection rate and the length of the sampling period.

As an example, consider 10 nm which has an aerosol detection rate of 0.159/ds. The probability that 1 particle is detected (among particles that can be detected by the CPC) within 1 ds is thus about 16% - and a detection within this period would yield a measured concentration at least 25 % greater than average. A particle detection in a sampling period of 2 ds would also yield a measured concentration at least 25% greater than average but a single detection is twice as likely as occurring. This increasing trend continues until a sampling period of 5 ds, where 1 particle is not sufficient to yield a measured concentration at least 25% greater than average (2 particle detections are required) and so the probability returns to about 16%. Essentially, this cycle length is proportional to the inverse of the average detection rate. Regardless of the trend, most importantly, Figure 6-5 shows that measured extreme concentrations were not more likely than what is expected from a Poisson process.

Figure 6-6 and Figure 6-7 show the normalized posterior distributions obtained from Bayesian inference. A total of 100 measurements were used to form the posterior distributions - the likelihood that a measured concentration is the actual (population) mean concentration. Sampling time periods of 1 ds and 10 ds were used in Figure 6-6 and Figure 6-7 respectively. The population mean concentration, $\mu$, is listed underneath the particle size. In both figures, the experimental posterior distributions are within the 80%-range of the simulation values. Thus, Bayesian inference using experimental data does not produce results that are noticeably different from a Poisson simulation.

For accurate inference of $\mu$, the posterior distribution should have a peak at $\mu$ and as minimal spread as possible. There is wider spread in the posterior distributions for the 1-ds sampling period than the 10-ds sampling period since more counts can be

accumulated in 10-ds sampling period. The SNR will be increased, and there will be a better prediction of the population mean. A more appropriate prior could have been chosen (e.g. Jeffery's prior or Gamma distribution), but the goal of this study was to compare the output produced by the experimental and simulated data without respect to the prior chosen.

By examining Figures 6-2 to 6-7, this study has shown evidence to support the Poisson assumption in sampling of nanometer-sized aerosols. A caveat is that the conclusions may only be valid for the tested environmental conditions (temperature, humidity, etc.), location (indoor air), particle sizes, and sampling instrument (SMPS). Furthermore, the results may only be valid for the 16.7 minute time series examined. Nothing can be said definitively about the applicability of the Poisson assumption in other situations (e.g. laboratory generated aerosols, outdoor aerosols, etc.) (Larsen 2007).

Results from previous works with ambient micrometer-sized aerosols show that sampling does not follow a Poisson process and positive correlations exist (both PCF and time-averaged PCF > 0) (Larsen et al. 2003; Larsen 2007). Those findings could be produced by two causes: (1) there was a change in underlying aerosol concentration that could not be identified (2) sampling of micrometer-sized aerosols simply cannot be described by a Poisson process. Cause (1) is possible because the previous studies observed positive correlations (not negative correlations) which is what occurs from underlying change in concentration. As mentioned previously, a change in underlying concentrations results in a higher variance and $\eta(t)>0$; thus, a finding of positive correlations cannot be unequivocally interpreted as non-Poisson sampling behavior.

However, if no underlying concentration change exists, then (2) is valid and there may be a fundamental difference in how micrometer-sized and nanometer-sized aerosols are sampled: nanometer-sized aerosols are sampled according to a Poisson process while micrometer-sized aerosols are not.

The reason for this phenomenon may be explained by Brownian motion - the random motion of aerosols due to collisions with air molecules - which affects both aerosols in flow and in still air. Smaller aerosols have less mass and so Brownian motion is more influential for smaller aerosols than for larger aerosols. Ambient nanometer-sized aerosols with spatial correlations may be decorrelated by Brownian motion. During sampling, nanometer-sized aerosols follow the streamlines in the air flow, but their path resembles a “random walk” with a mean transport direction. This movement may cause aerosols to be detected in a random Poisson manner. The results presented in Larsen (2007) and here show that greater correlations occur for larger micrometer-sized aerosols (> 1 μm) than for smaller aerosols suggesting that Brownian motion causes the Poissonian detection of aerosols. Besides Brownian motion, other mechanisms (e.g. electrostatic forces) which are size dependent may also be responsible for determining the sampling nature.

It should be noted that the original goal of previous studies was to determine whether the Poisson process correctly describes the position of ambient aerosols in space (Larsen et al. 2003; Larsen 2007). An important assumption of these studies was that a time series of particle detections by an OPC could be inverted to infer the spatial distribution of aerosols. However, this premise seems dubious; it is very doubtful that the sampling process does not affect the position of the aerosols relative to each other.

Aerosols entering an OPC are subjected to the laminar parabolic flow inside the sampling tube causing aerosols at the center of the tube to travel faster than aerosols near the walls. Aerosols will change their positions (and detection time) with respect to each other simply because of the very act of drawing air into the OPC and the parabolic flow. Furthermore, light-scattering instruments rely on a variant of an aerosol focusing lens to make particles converge to the focal point of the laser beam. Thus, the relative spatial structure will not be preserved, and the time series of detections is not an accurate surrogate for spatial distribution. There is the possibility that aerosols initially uncorrelated in space will become correlated because of the position changes or vice-versa. Consequently, here, no attempt will be made to infer results about the spatial distribution of ambient nanometer-sized aerosols from the time series data. This study simply investigated the assumption of whether aerosol sampling - regardless of instrument or how aerosols are manipulated before detection - follows a Poisson process. For the conditions tested, this assumption was proven to be valid. Essentially, Poissonian sampling behavior was evaluated directly and so there are no possible artifacts to consider.

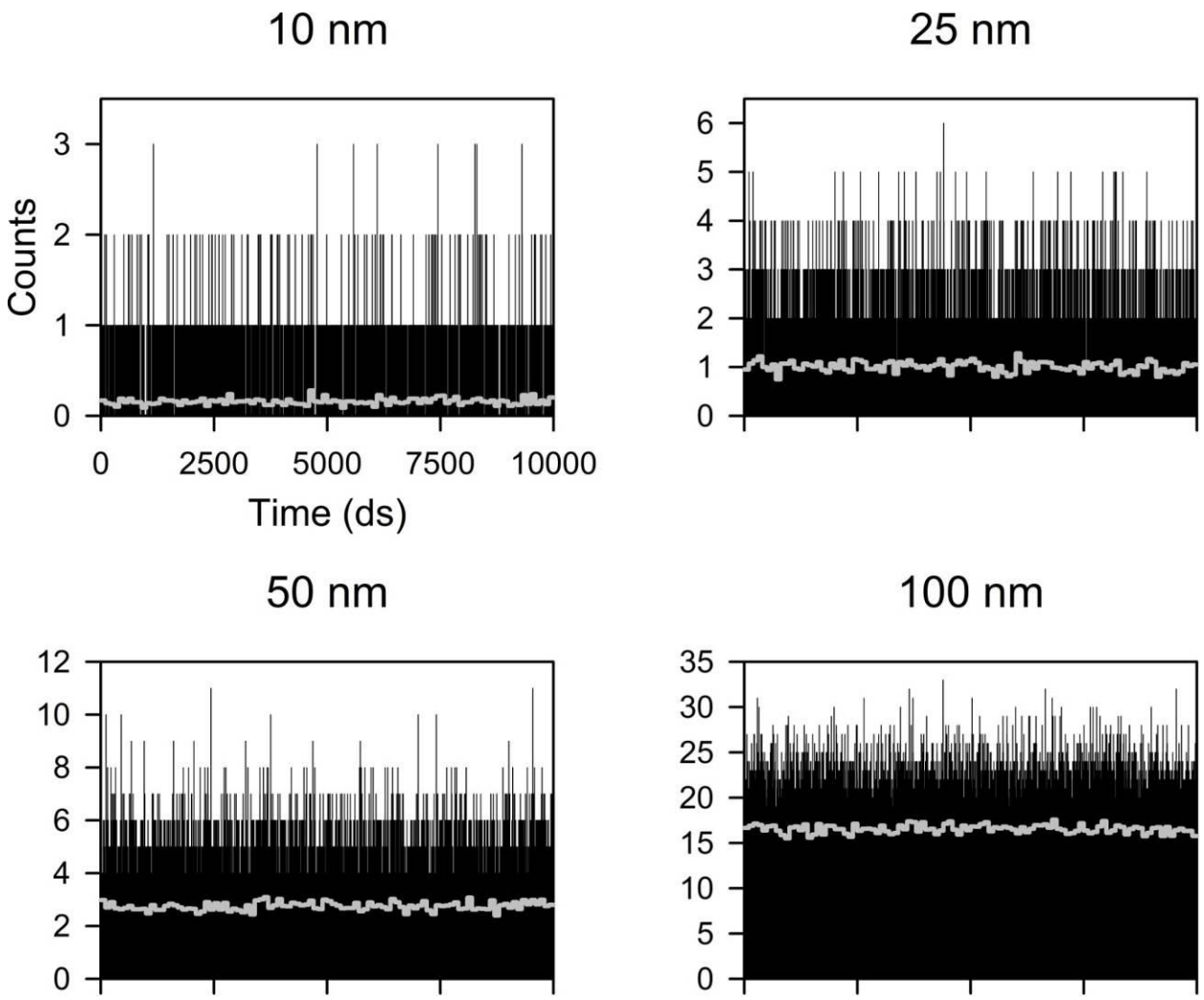


Figure 6-1. Count vs. sampling time for the tested particle sizes. The gray line indicates the mean concentration over a 100-ds period.

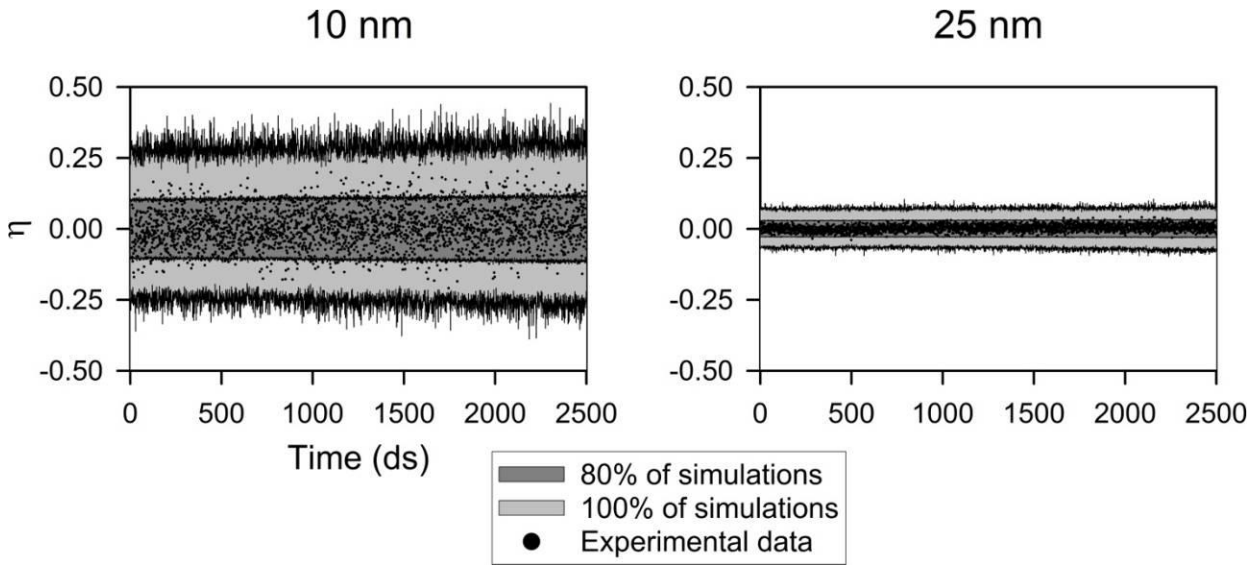


Figure 6-2. The PCF for the 10 nm and 25 nm sizes. The area containing 80% of the simulation values is shown in dark gray while the area containing 100% of the simulation values is shown in light gray. The experimental PCF is represented by the black dots.

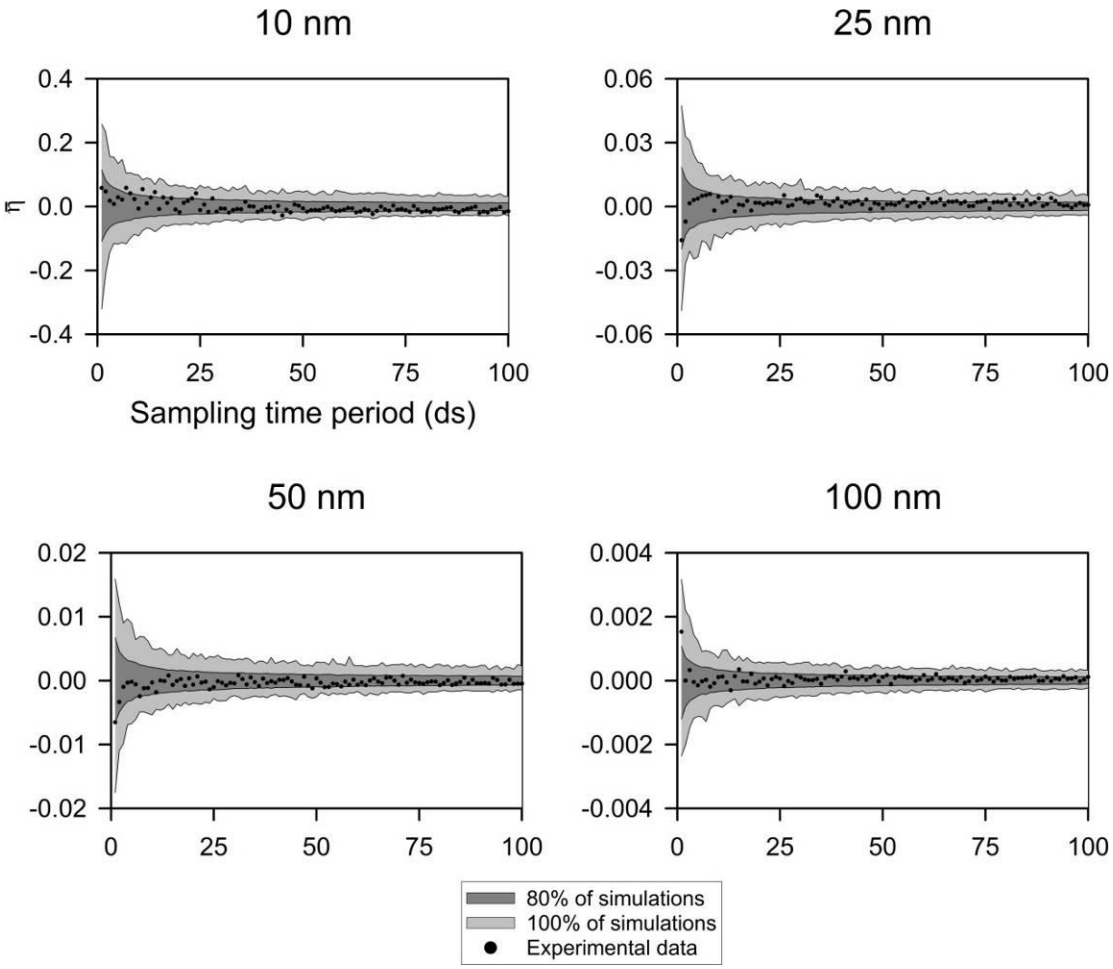


Figure 6-3. The time-averaged PCF for each particle size.

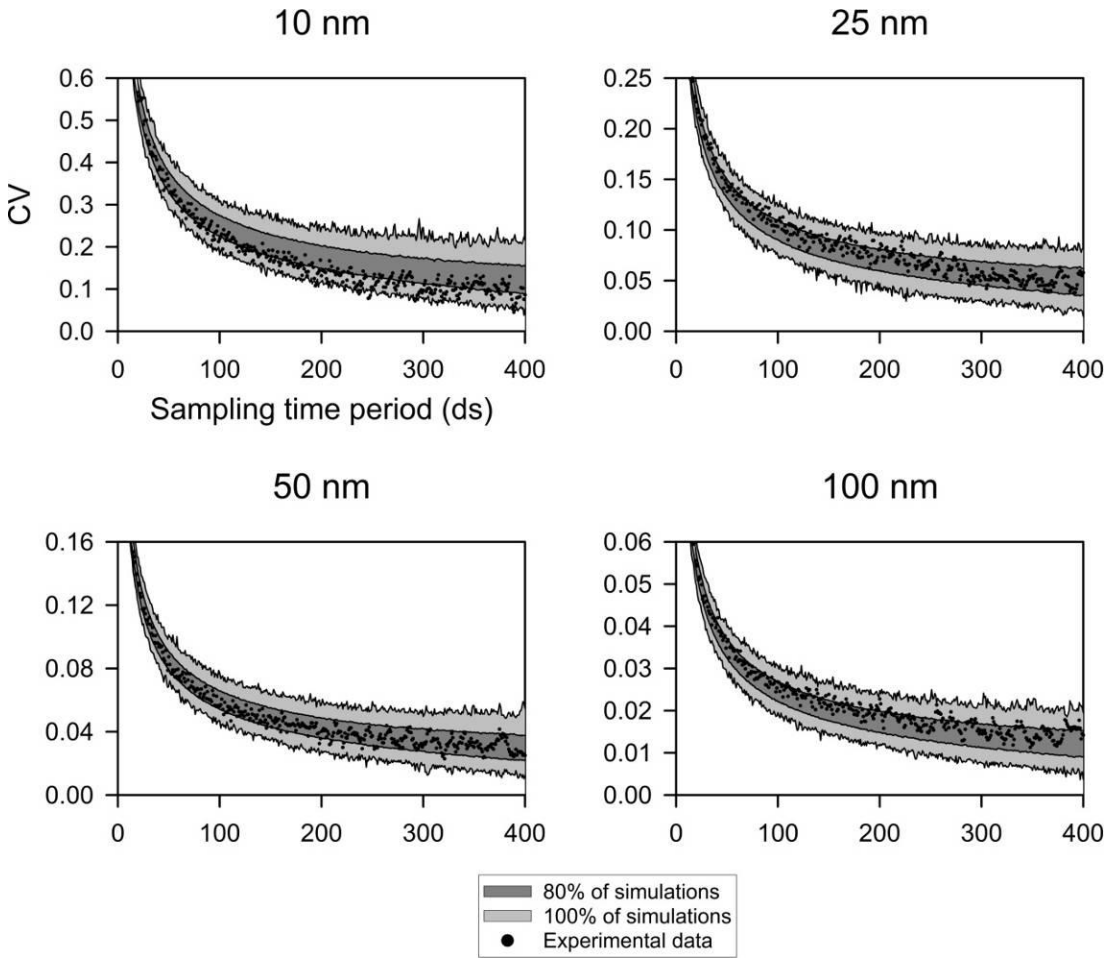


Figure 6-4. The CV values vs. sampling time period for the tested particle sizes.

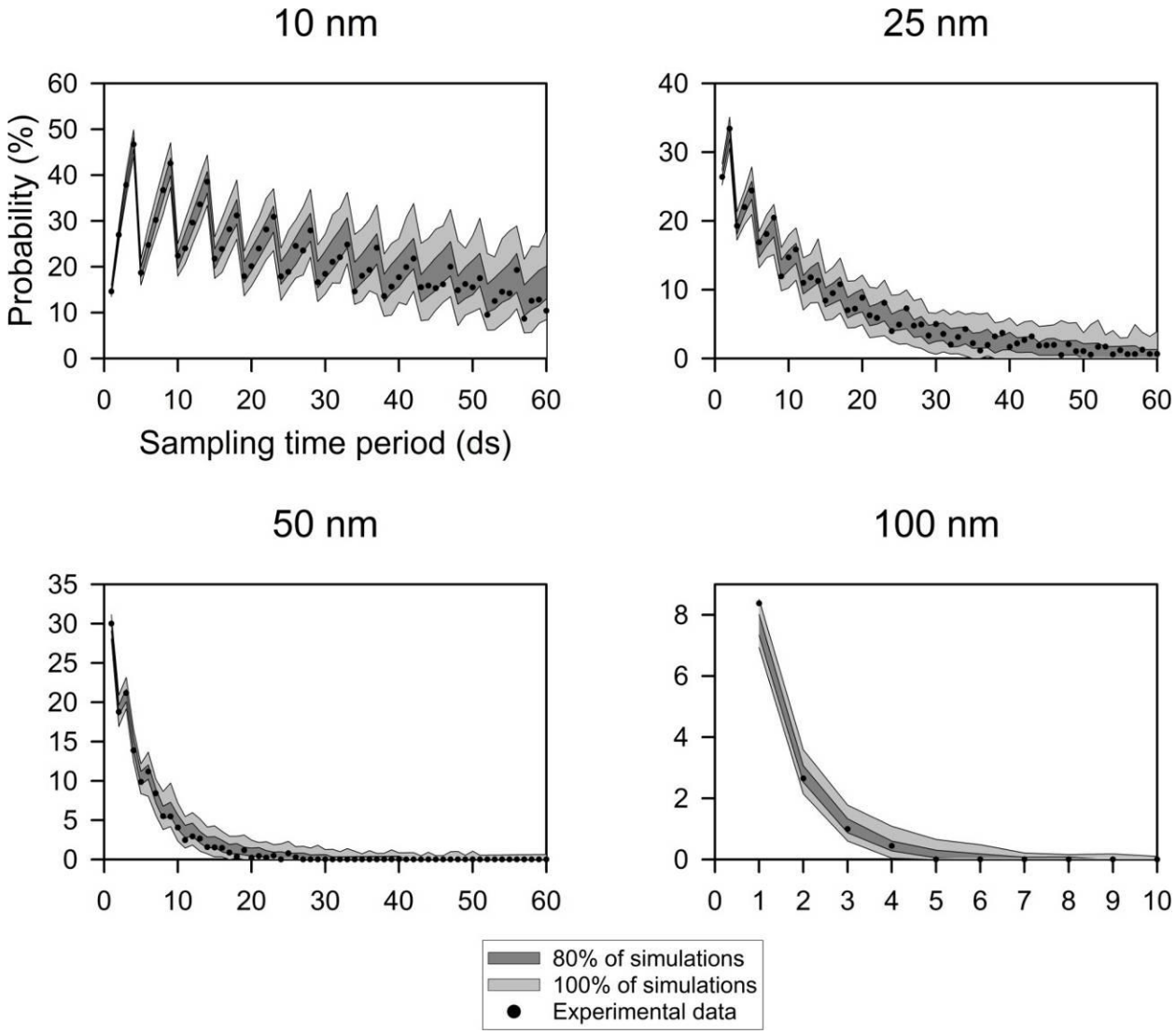


Figure 6-5. The probability of observing a concentration at least 25% greater than the average concentration for the time series. The probabilities are presented as a function of sampling time period.

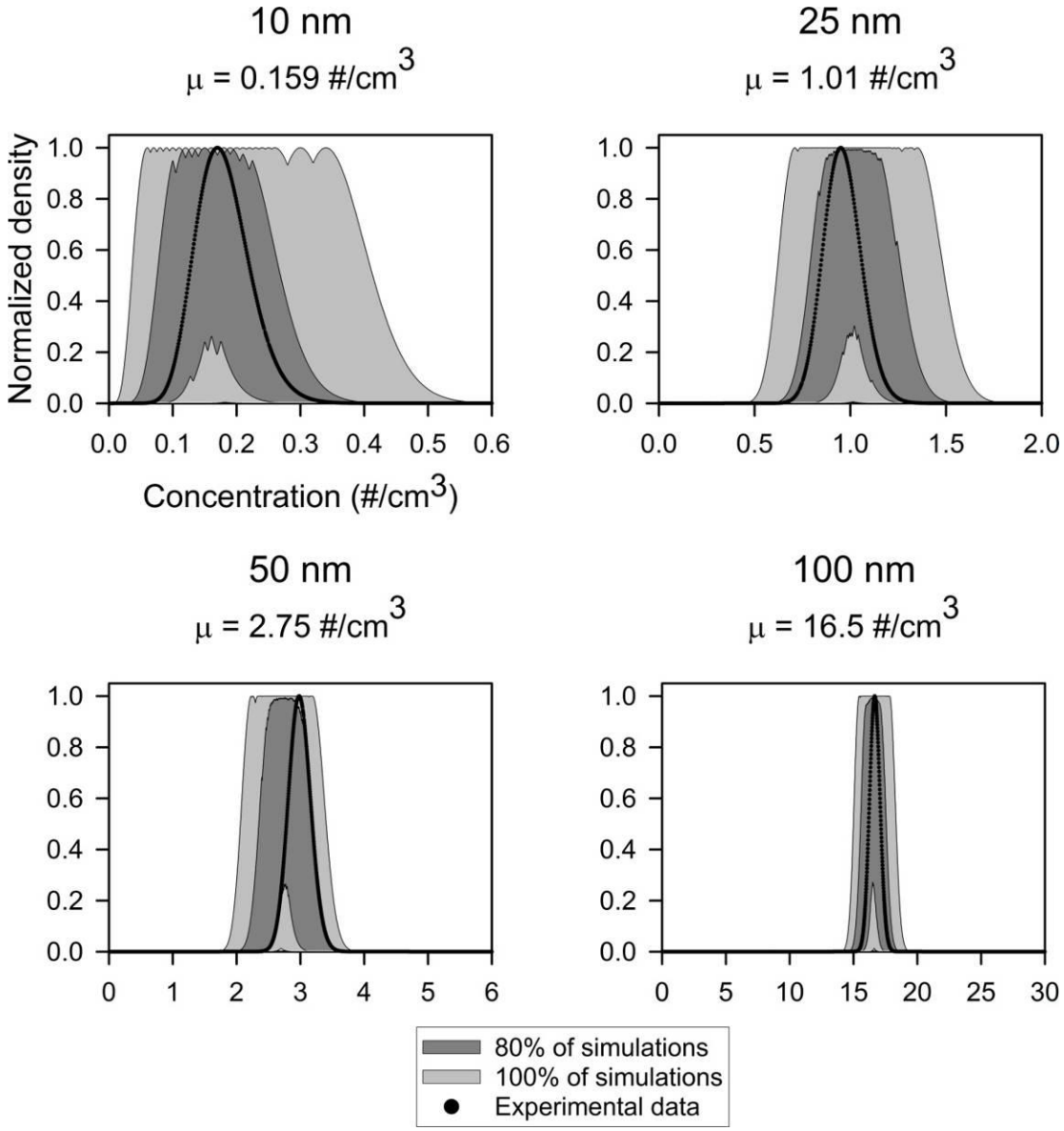


Figure 6-6. The normalized posterior distribution from Bayesian inference with sampling time period of 1 ds. A total of 100 measurements were used to form the posterior distributions.

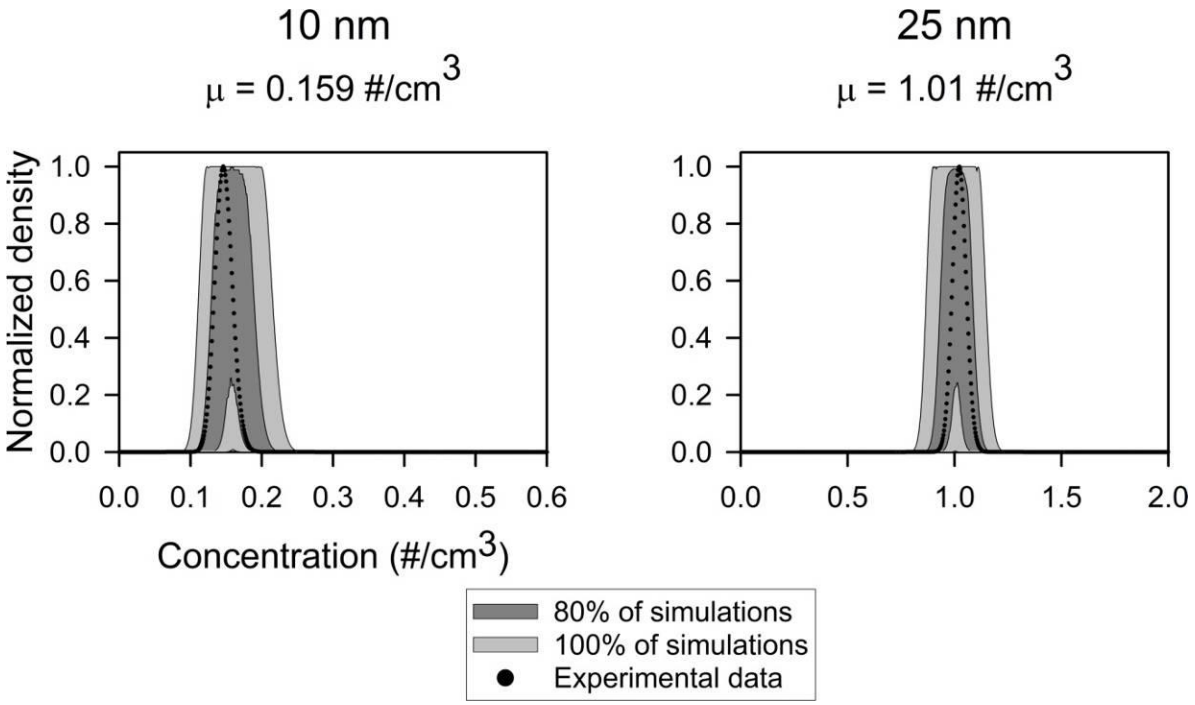


Figure 6-7. The normalized posterior distribution from Bayesian inference with sampling time period of 10 ds. A total of 100 measurements were used to form the posterior distributions.

# CHAPTER 7
# INFRARED REGENERATION OF ACTIVATED CARBON CLOTH SATURATED WITH TOLUENE

## Objective

The objective of the study in this chapter was to evaluate the feasibility of IR in regenerating activated carbon cloth (ACC). The test volatile organic compound (VOC), toluene, was first adsorbed on the ACC until saturation. Then, the ACC was irradiated with IR to desorb the toluene in an attempt to return the ACC to its initial adsorption capacity. Regeneration was performed a second time to investigate adsorption performance after repeated IR regeneration.

## Materials and Methods

ACC Model ACC-507-15 used in Chapter 4 was used here and Table 7-1 lists its properties. Circular ACC swatches with a diameter of 37 mm were cut from a 2 $m^2$ fabric sheet supplied by the manufacturer. Again, the ACC was held perpendicularly to the challenging flow using the same custom quartz reactor described in Chapter 4 and shown in Figure 1-1 C. In this case, toluene vapor was the challenging pollutant instead of bioaerosols. The diagram of the testing setup is shown in Figure 7-1 and consisted of a vapor generation section, the IR reactor containing the ACC swatch, and a vapor measurement system. Toluene was selected for testing because it is one of the most commonly found VOCs in the indoor environment (Lee et al. 2002). Toluene has a molecular weight of 92.14 g/mol, boiling point of 110.7 °C, and a relatively moderate vapor pressure for a VOC of 28.47 mmHg (Yao et al. 2009). Compressed, ultrahigh purity nitrogen from a gas cylinder was supplied to one mass flow controller to generate vapor from a bubbler and another mass flow controller for dilution air. The bubbler containing liquid toluene was immersed in a temperature-controlled 27-°C water bath.

By adjusting the flow rates of the dilution air and toluene carrier flow to the bubbler, a 1-LPM airstream with 2,500 ppmv and corresponding to a mass flow rate of 2.2 g/min was created for testing. The test vapor stream then entered the reactor for adsorption and the concentration of toluene exiting the reactor was measured with a gas chromatography (GC) system (7820 A; Agilent Technologies, Santa Clara CA). The effect of water vapor, which competes for adsorption sites with insoluble VOCs like toluene (Cal et al. 1996), was out of the scope of this study and so water vapor was not introduced in the test vapor stream. Because the testing system was closed and nitrogen was supplied by an ultrahigh purity nitrogen cylinder, there was no unintentional addition of water vapor into the test stream. After breakthrough was observed from the chromatogram, the test vapor stream was shut off and regeneration was performed.

Three test voltages of 27.5 V, 55 V, and 110 V (corresponding to bulb powers of 62.5 W, 125 W, and 250 W, respectively) were supplied to the bulb using an electrical transformer (TDGC-0.5KM, Variac) to examine the relationship between bulb power, ACC temperature, and regeneration performance. With the 12 $cm^2$ area of ACC irradiated by the bulb and an approximate bulb efficiency of 87.5%, the estimated power densities at the ACC surface were 4.56 $W/cm^2$, 9.10 $W/cm^2$, and 18.2 $W/cm^2$ for bulb powers of 62.5 W, 125 W, and 250 W, respectively. The regeneration step lasted for 1 h which was similar to previous studies (Hashisho et al. 2005; Yao et al. 2009). Nitrogen at a flow rate of 0.25 LPM (25% of the adsorption flow rate) served as the regeneration flow to remove desorbed molecules from the ACC surface during regeneration. Nitrogen flow, rather than a flow containing oxygen, is usually used in heat regeneration because

it is safer (Sullivan et al. 2001; Sullivan et al. 2004; Hashisho et al. 2005). Desorption flow was passed through the ACC in the reverse direction of toluene loading to optimize regeneration. The temperature of the ACC was measured without adsorbate but with the 0.25-LPM nitrogen flow using the pyrometer method described previously in Chapter 4.

The effectiveness of IR regeneration was tested with the following five step procedure: (1) toluene adsorption with a fresh swatch of ACC until breakthrough, (2) regeneration at a prescribed bulb power, (3) adsorption again until breakthrough, (4) second regeneration with the same power, (5) final adsorption step until breakthrough. The adsorption profile was measured and the total mass of toluene adsorbed at each adsorption step (steps 1,3, and 5) was calculated to determine the ability of IR regeneration in restoring ACC to its initial capacity.

The concentration of vapor exiting the reactor was measured every 30 s until ACC saturation. The entire run time was divided into 30-s intervals containing each measurement (a 15-s interval for the first measurement) and the mass of toluene adsorbed in each interval, $m_n$, was calculated by Eq. 7-1:

$$m_n = \dot{m}\left(1 - \frac{C_o}{C_i}\right)\Delta t \tag{7-1}$$

where $\dot{m}$ is the mass flow rate of toluene, $C_o$ is the outlet toluene concentration in interval $n$, $C_i$ is the inlet toluene concentration, and $\Delta t$ is the length of the interval. The mass adsorbed in each interval was then summed to yield the total mass adsorbed by the ACC:

$$m = \sum_{n=1}^{n_{sat}} m_n \tag{7-2}$$

where $n_{sat}$ is the number of intervals until saturation (i.e. $C_o$ is equal to $C_i$). To compare the ACC's adsorption capacity after regeneration to its fresh adsorption capacity, the capacity ratio, $q_r$, was calculated from Eq. 7-3:

$$q_r = \frac{m_r}{m_f} \tag{7-3}$$

where $m_f$ is the mass of toluene adsorbed with fresh ACC and $m_r$ is the mass of toluene adsorbed with regenerated ACC. For an ideal regeneration process, the $q_r$ will be 1 so that the mass adsorbed after regeneration is equal to the mass adsorbed with fresh ACC. In addition to the capacity ratio, length of unused bed (LUB) and throughput ratio (TPR) were calculated to see how the ACC's adsorption behavior changed after IR regeneration.

$$LUB = 1 - \frac{m_{5\%}}{m_{100\%}} \tag{7-4}$$

$$TPR = \frac{t_{5\%}}{t_{50\%}} \tag{7-5}$$

In Eq. 7-4, $m_{5\%}$ and $m_{100\%}$ are the masses of toluene adsorbed on the ACC at the time of 5% and 100% breakthrough. Similarly, in Eq. 7-5, $t_{5\%}$ and $t_{50\%}$ are the times for when 5% and 50% breakthrough occurs. LUB represents the effective fraction of the ACC bed that is not used at $t_{5\%}$ while TPR describes how quickly the mass transfer zone develops (Hashisho et al. 2005; Luo et al. 2006). An ideal adsorber has LUB approaching zero and TPR approaching unity. Like with adsorption capacity, the ratios of regenerated LUB ($LUB_r$) and TPR ($TPR_r$) to fresh LUB ($LUB_f$) and TPR ($TPR_f$) were calculated to show how the values changed after regeneration. LUB ratio ($R_{LUB}$) and TPR ratio ($R_{TPR}$) were calculated by Eq. 7-6 and Eq. 7-7 respectively.

$$R_{LUB} = \frac{LUB_r}{LUB_f} \tag{7-6}$$

$$R_{TPR} = \frac{TPR_r}{TPR_f} \tag{7-7}$$

For each bulb power, three trials were run by starting adsorption testing with a new, fresh swatch of ACC. Using OriginPro 8.5 software, paired t-tests were performed to construct confidence intervals (CI) of the difference between fresh ACC and regenerated ACC capacity, LUB, and TPR. The pairing minimized intrinsic variability between ACC swaths cut from the source sheet and isolated the effects of IR regeneration on adsorption performance.

Besides adsorption performance, modification of the ACC by IR heating was investigated. As shown in Chapter 4, elevated ACC temperatures caused the ACC to release nanoparticles which likely changed the ACC's microscopic structure and possibly its adsorption characteristics. The presence of oxygen during heating may have contributed to particle emission in those results and this is because oxygen is used to modify the ACC's properties during the activation step of fabrication. As nitrogen was the regeneration flow here, a separate study was conducted to determine if particle emission occurred during heating under nitrogen flow. To accomplish this, an SMPS was attached downstream of the cloth during regeneration to sample emitted nanoparticles. An additional nitrogen flow of 0.35 LPM was added before sampling and combined with the 0.25-LPM regeneration flow to obtain the required 0.60-LPM CPC sampling flow rate. The particle number concentration and PSD were recorded every 2 min during a 17-min period of heating for the 125-W and 250-W bulb powers.

## Results and Discussions

### ACC Regeneration Temperature

Figure 7-2 displays the ACC temperature vs. regeneration time for the three bulb powers. The ACC temperature was greater as bulb power increased; the peak (equilibrium) temperatures reached were 74 °C, 152 °C, and 277 °C for 62.5-W, 125-W, and 250-W powers, respectively. The temperatures for the 125-W and 250-W powers were similar or higher than the temperatures used for successful VOC desorption in previous studies and indicated that the IR setup would be suitable for regeneration (Yao et al. 2009; Sidheswaran et al. 2012). The 62.5-W ACC temperature of 74 °C, which is lower than the boiling point of toluene, may not be as effective. Temperatures above the boiling point of the adsorbate are traditionally used for regeneration (Subrenat and Le Cloirec 2004; Sullivan et al. 2004; Hashisho et al. 2005). Like in Chapters 3 and 4 with IR heating of ACC (see Figure 3-3 and Figure 4-3), the ACC temperature profiles here were characterized by rapid initial temperature increases, a subsequent reduced heating rate, and finally a stable equilibrium temperature. The average rates of temperature increase during the first 10 s were 53 °C/min, 158 °C/min, and 930 °C/min and heating to 90% of the equilibrium temperature were reached in 5.15 min, 4.75 min, and 3.73 min, for the 62.5-W, 125-W, and 250-W powers, respectively. During heating of VOC-saturated ACC, this rate will be lower because the received energy will be used to heat the adsorbate as well as the ACC.

Besides heating the ACC to a high temperature, Figure 7-2 highlights the stability of IR heating with time and the potential for a controlled and predictable desorption rate. This stability is in contrast to microwave heating which can be unstable and has the potential for thermal runaway; Hashisho and coauthors had to manually control power to

the microwave generator to obtain a constant temperature between 110-140°C (Hashisho et al. 2005). Using electrothermal regeneration, Sullivan et al. (2001) employed a rectifier to control the voltage across the ACC and obtained rapid heating of ACC although fluctuations were present. Other heating methods like steam and hot gases also make regeneration difficult to control (Luo et al. 2006).

**Adsorption Capacity, Breakthrough Curves, LUB, and TPR of Regenerated ACC**

Figure 7-3 is a graph of the capacity ratios obtained after the first and second regenerations for each bulb power. The error bars represent standard deviation and above each power is the peak temperature measured during the 1-h desorption period. Figure 7-7 A shows the CIs of the difference in adsorbed mass between fresh and regenerated ACC ($m_f$ - $m_r$) as determined by paired t-test. The 90% and 95% CIs are displayed. When a CI does not include zero, it indicates that the regenerated ACC is statistically different from fresh ACC (at that confidence level). At the 62.5-W power, which corresponds to a peak temperature of 74 °C, the adsorption capacity was just 54.8%±2.41% and 50.9%±0.343% of fresh ACC for the first and second regenerations respectively. Fresh ACC adsorbed about 7 g more toluene than regenerated ACC. The CIs were indeed greater than zero which indicated that the mass adsorbed with fresh ACC was statistically greater than the mass adsorbed with regenerated ACC. This finding was likely a result of the 72-°C ACC temperature which was lower than the toluene boiling point and not high enough to completely desorb all the molecules within 1 h. The overlap of the first-regeneration and second-regeneration CIs suggests that although the 62.5-W regeneration was incomplete it was consistent at around 50%.

For the 125-W and 250-W regenerations, the capacity ratios were near 1. The CIs include zero at both confidence levels and this means that the adsorbed mass for fresh and regenerated ACC was not statistically different. Therefore, the IR regeneration essentially restored saturated ACC to its fresh capacity. Given that 125 W was able to restore the capacity, the heating condition at 250 W was excessive and less energy efficient. However, the desorption rate at 250 W will be higher and in this case the regeneration step could have been shortened. Specific regeneration conditions depend on the goal of the user conducting desorption (Subrenat and Le Cloirec 2004). If a 1-h regeneration period is preferred, the optimal power density is between 4.56-9.10 W/cm$^2$ corresponding to an ACC temperature somewhere in the range of 72 °C-152 °C. This temperature range includes the boiling point of toluene which supports that temperatures near or greater than the adsorbate's boiling point are most effective for practical regeneration periods (≤ 1 h).

The capacity ratio was found to be slightly greater than 1 (about 7% greater) for the 250-W regeneration indicating that the ACC was able to adsorb more toluene after IR regeneration than when fresh. A lower capacity for fresh ACC may be due to the adsorption of environmental water vapor during storage of the adsorbent before experiments. The high 277-°C regeneration temperature at 250 W may have desorbed water as well as toluene causing an increased capacity after regeneration.

Like at 62.5 W, at the higher bulb powers the first and second regeneration capacities were nearly the same. A decrease in capacity after the second regeneration may signal that the ACC had been degraded in some way by IR. The IR heating mechanism is different from the established regeneration methods of electrothermal and

steam because it is associated with radiation-induced molecular vibrations of the absorbing target molecule (Workman and Weyer 2008). IR photons, however, do not have sufficient energy to break bonds and cause modifications to adsorption sites. Thus, IR should not be destructive simply by radiation interaction with the adsorbent.

Figure 7-4 displays the breakthrough curves at each adsorption step (overlaid for comparison). Three trials were run for each bulb power and the resulting curves showed high reproducibility. Therefore, only one representative trial is shown here. The x-axis is dimensionless time, $t/t_{50\%}$. For each bulb power, the shapes of the curves at each adsorption step were generally very similar. Breakthrough began at about 0.8 and was nearly complete at slightly greater than 3. Although complete regeneration was not achieved at the 62.5-W power, the shape of the breakthrough curves after the first and second regenerations were still very similar to the fresh curve.

Figure 7-5 and Figure 7-6 display $R_{LUB}$ and $R_{TPR}$ respectively and describe the change in the nature of adsorption for each condition. The corresponding CIs of the difference between the fresh and regenerated values (e.g. $LUB_f$ - $LUB_r$ and $TPR_f$ - $TPR_r$) are shown in Figure 7-7 B and C. The fresh LUB had a range of 0.168-0.339 and was dependent on the swatch of ACC used in the testing. This range was near the guideline of LUB<0.30 suggested by Sullivan et al. (2001). For all bulb powers, the regenerated LUB was lower than the fresh LUB (i.e. $R_{LUB}<1$). This is reflected in Figure 7-7 B where most of the CIs contain values greater than zero. Although the regenerated LUB was not statistically different from fresh using a 95% CI, it was close and actually statistically lower using a 90% level at the higher bulb powers. Thus, there is some evidence to suggest that the regeneration decreased the LUB or improved the

performance of the ACC. The decrease was most notable at the higher bulb powers when complete regeneration was found. As with capacity ratio, the lower LUB after regeneration was likely due to desorbed water which had been adsorbed onto the ACC during storage.

The TPR of fresh ACC ranged 0.569-0.777 which, for the lower bound, was less than the recommended guideline of TPR>0.70. The regenerated TPR was found to be higher than the fresh TPR for every condition (i.e. $R_{TPR}$>1). According to Figure 7-7 C, the regenerated TPRs were statistically greater for the higher bulb powers (at the 90% level) and again this may be attributed to water desorption from fresh ACC. To determine the effect of IR regeneration on LUB and TPR without the confounding influence of water, the adsorption periods after the first and second regenerations can be compared at 250 W. For these periods, the ACC swatch had undergone regeneration and water had been desorbed. Paired t-tests between these adsorption periods produced CIs (not shown) that included zero and suggested that LUB and TPR remained statistically the same after regeneration. Overall, the LUB and TPR results here indicated that IR regeneration did not decrease the performance of the ACC.

To summarize the results, the 125-W and 250-W regenerations completely restored the adsorption capacity of toluene-saturated ACC while retaining or slightly improving the LUB and TPR. Essentially, at these bulb powers, IR-regenerated ACC had very similar performance as fresh ACC. For 62.5-W regeneration, only about 50% of the fresh capacity was restored. A power density greater than 4.56 W/cm$^2$ is needed for more effective regeneration with this system.

With sufficient power density, the results here prove that IR is able to successfully regenerate toluene-saturated ACC. Table 7-2 displays a list of ACC regeneration methods tested in previous studies, the pollutant tested in those studies, and the restoration of fresh adsorption capacity (or regeneration efficiency) obtained. The works show between 1-100% restoration using electrothermal, unheated outdoor air, and microwave regeneration. It is difficult to directly compare between studies because of different conditions and system designs but the table provides a general overview. Regardless of the method, effective regeneration is possible upon careful consideration of adsorbate volatility and regeneration conditions. Of the heating methods, electrothermal heating is theoretically the most energy efficient because all the dissipated electrical energy is converted to heat. For microwave and IR heating, energy waste occurs during radiation generation, from radiation not being directed onto the target (i.e. poor waveguide or ray tracing design), and from transmission through the target.

**Emission of Particles from ACC during Heating**

Figure 7-8 displays the total concentration of nanoparticles for the baseline (no heating) and six sampling periods during heating with the 250-W and 125-W bulb powers. The 125-W ACC temperature of 152°C was similar to the temperatures used in literature while the 250-W temperature was considerably higher at 277 °C (Sullivan et al. 2001; Hashisho et al. 2005; Sidheswaran et al. 2012). In the previous studies, no degradation of the ACC or emission of nanoparticles were noted at around 150 °C. With no heating, the total concentration of nanoparticles exiting the reactor was about 30 #/cm$^3$. These particles likely originated from the compressed gas cylinder that supplied

nitrogen to the system. In the first heating period (0-2 min) for both bulb powers, the total concentration was less than the baseline; this may be because (1) the ACC was not sufficiently hot to release particles and (2) heating of the flow created a greater flow volume which diluted the number of baseline particles. In the 3-5 min period, a negligible change in concentration was observed for 125-W power but the 250-W power produced a concentration of $3.86\times10^{5}$ #/cm$^{3}$. The concentration of particles in the next period was about one order of magnitude less but still relatively high at $2.46\times10^{4}$ #/cm$^{3}$.

Figure 7-9 displays the emitted PSDs for the two periods in which high concentrations were measured at the 250-W power. The emitted particles during the 3-5 min period had a median, geometric mean, mode, and geometric standard deviation of 23.1 nm, 22.9 nm, 22.5 nm, and 1.35 respectively. The PSD for the 6-8 min period shifted toward smaller sizes with a geometric mean of 17.7 nm and became slightly more polydisperse with a geometric standard deviation of 1.43. The smaller sizes and lower concentration correspond to a lower mass loss from the ACC during this period. For the remaining time periods, as shown in Figure 7-8, the concentration returned approximately to the baseline level which suggested that a higher temperature would be needed for further emission of particles.

Although nanoparticles were emitted during the 250-W heating, there was no accompanying change in capacity as determined from the adsorption experiments. The hole left by a released nanoparticle could either decrease or increase the ACC surface area depending on where/how the particle was released. A particle released from a flat surface on the microporous structure would leave a cavity and increase the surface area, while a released particle initially present as an extrusion would decrease the

surface area. Regardless, any change in surface area here was low and not detectable. To change the surface area considerably, the ACC activation procedure, which consists of heating ACC to around 850 °C or greater under a $CO_2$ or steam environment, needs to be replicated (Subrenat et al. 2001). Especially, the lack of oxygen during regeneration here prohibits thermal oxidation and allows for retention of adsorption properties.

Table 7-1. Properties, as provided by the manufacturer, of the tested ACC, American Kynol model ACC-507-15.

| Thickness | Weight | Specific surface area | Mass available in reactor for adsorption |
|---|---|---|---|
| 0.5 mm | 120 g/m$^2$ | 1,500 m$^2$/g | 0.14 g |

Table 7-2. List of regeneration techniques and details of their performance in different studies.

| ACC regeneration technique | Test adsorbate | Restoration of fresh capacity/regeneration efficiency | Heating conditions |
|---|---|---|---|
| Electrothermal (Sullivan et al. 2001) | Methyl ethyl ketone (MEK) | 92% | 150-200 °C for 55 min |
| Electrothermal regeneration (Sidheswaran et al. 2012) | Benzene, butanol, toluene, O-xylene, undecane, formaldehyde | 31-88% | ~150 °C for 15 min |
| Unheated outdoor air (Sidheswaran et al. 2012) | Same as above | 1-73% | Room temperature, 12 h, 6.2 m/min face velocity |
| Electrothermal regeneration (Subrenat et al. 2001) | Ethanol | 100% | 100-150 °C for 30 min |
| Microwave regeneration (Hashisho et al. 2005) | MEK | 60-74% | 120-160 °C for 1 h |
| | Tetrachloroethylene (PERC) | 65% | Peak temperature of 150 °C for 1 h |

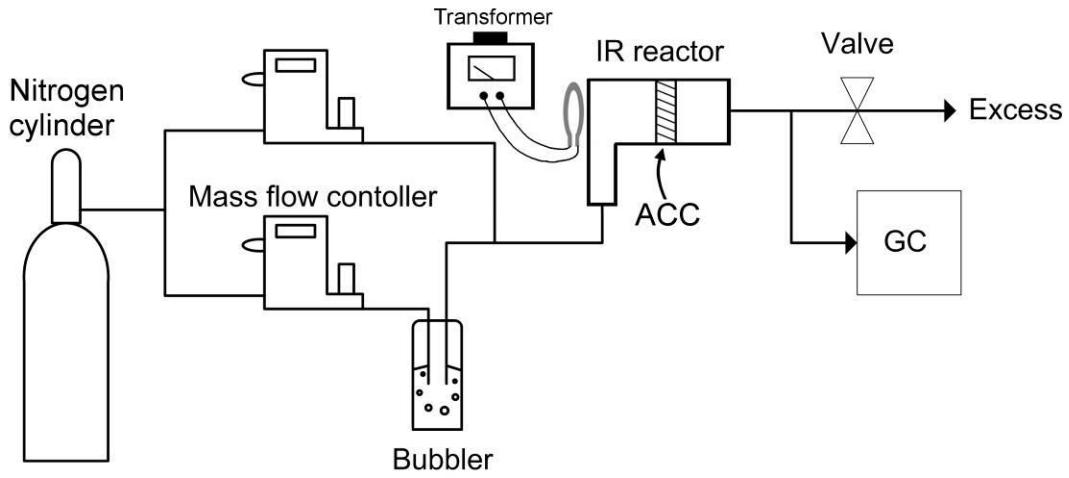


Figure 7-1. Diagram of the adsorption/IR regeneration testing system.

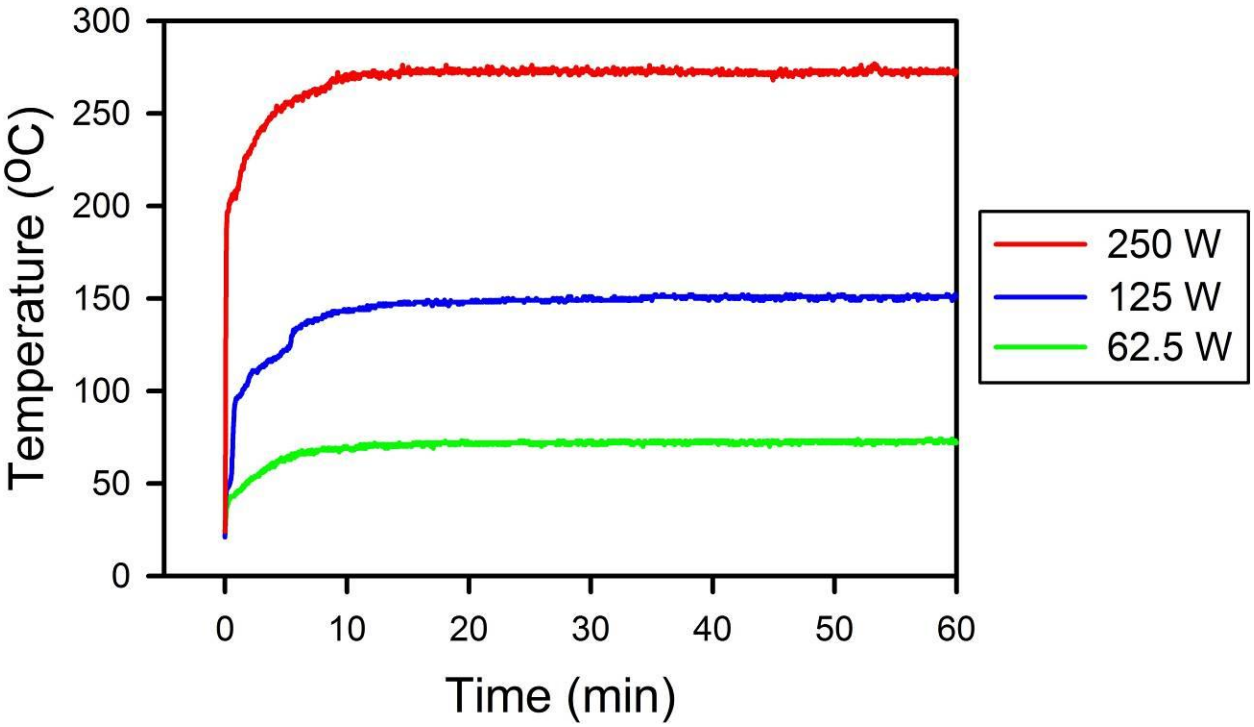


Figure 7-2. ACC temperature vs. heating time for the three tested bulb powers.

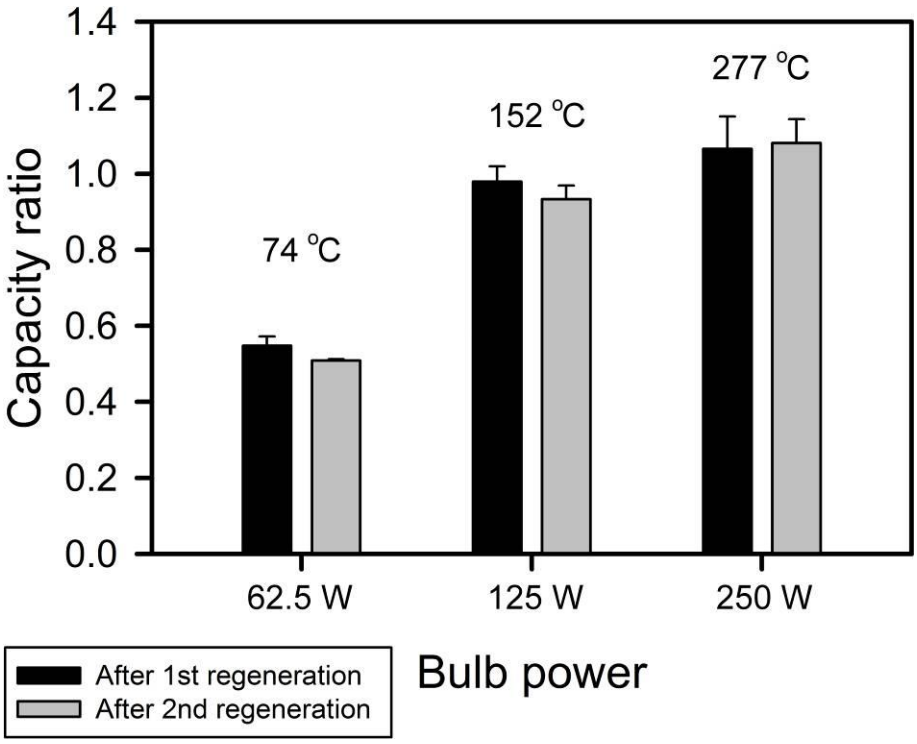


Figure 7-3. Capacity ratios for the adsorption after the first and second regenerations. The peak ACC temperatures reached during the regeneration period (from data in Figure 7-2) are also displayed above the bars for each bulb power.

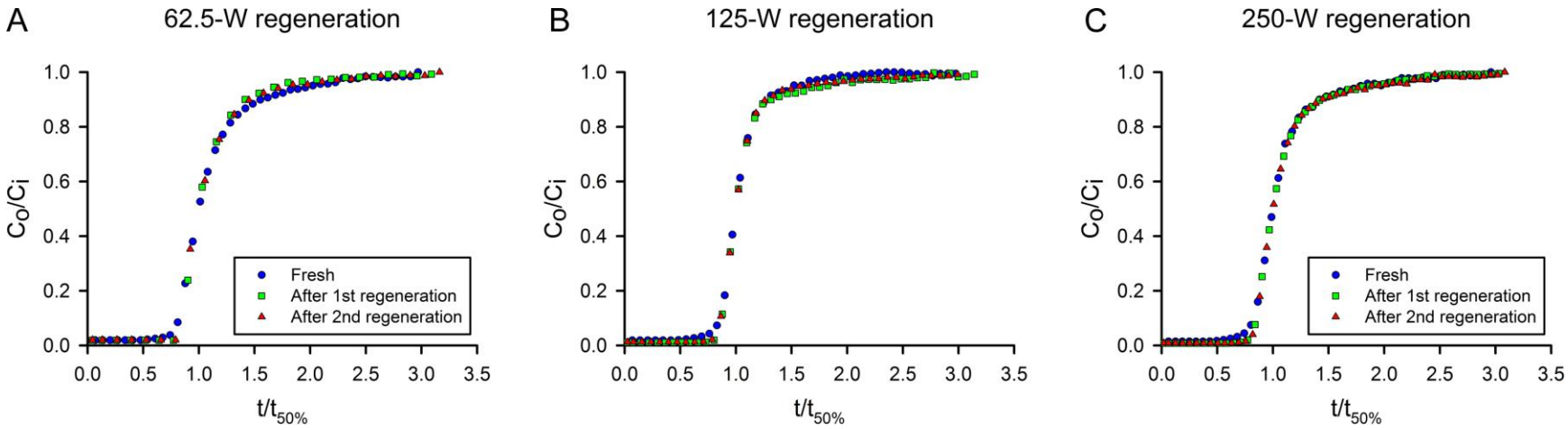


Figure 7-4. Dimensionless breakthrough curves for fresh ACC, after the first regeneration, and after the second regeneration. The breakthrough curves are displayed for the three bulb powers: A) 62.5 W, B) 125 W, and C) 250 W.

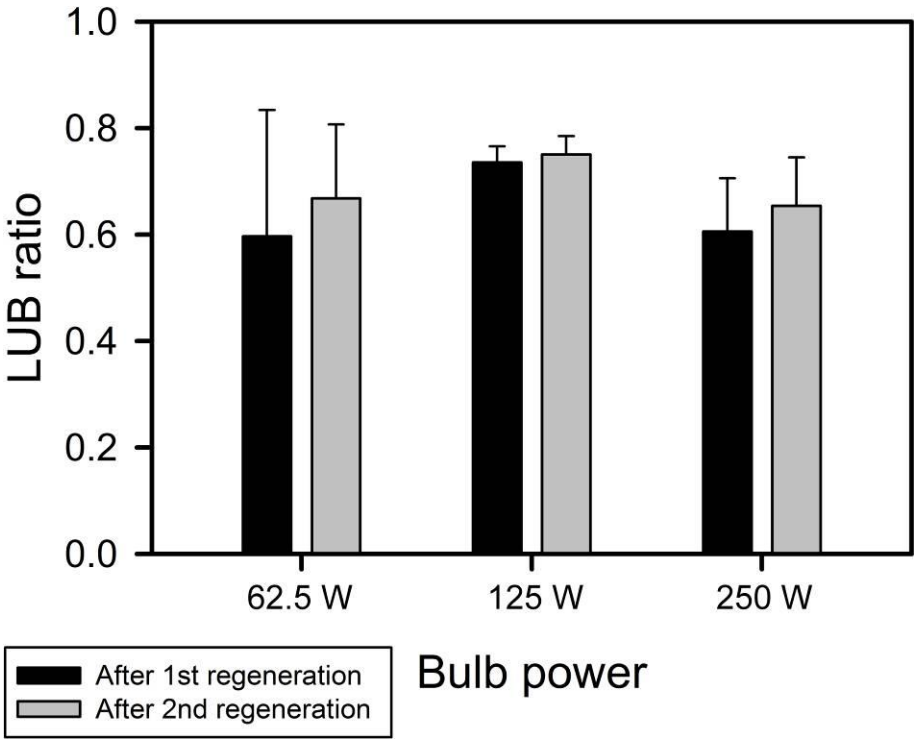


Figure 7-5. LUB ratio for adsorption after the first and second regenerations for the three bulb powers.

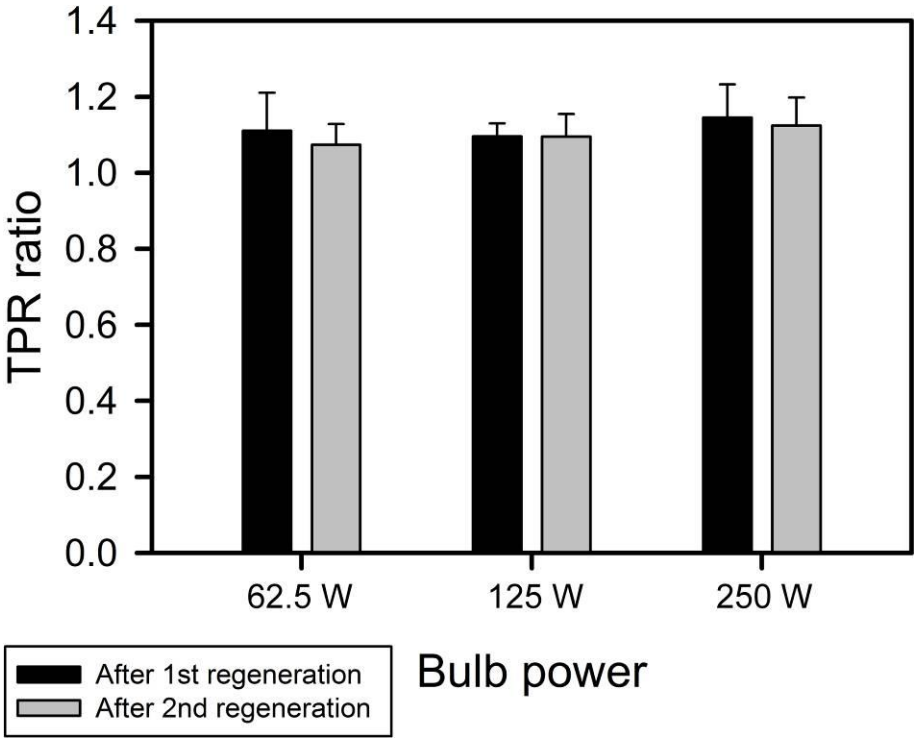


Figure 7-6. TPR ratio for adsorption after the first and second regenerations for the three bulb powers.

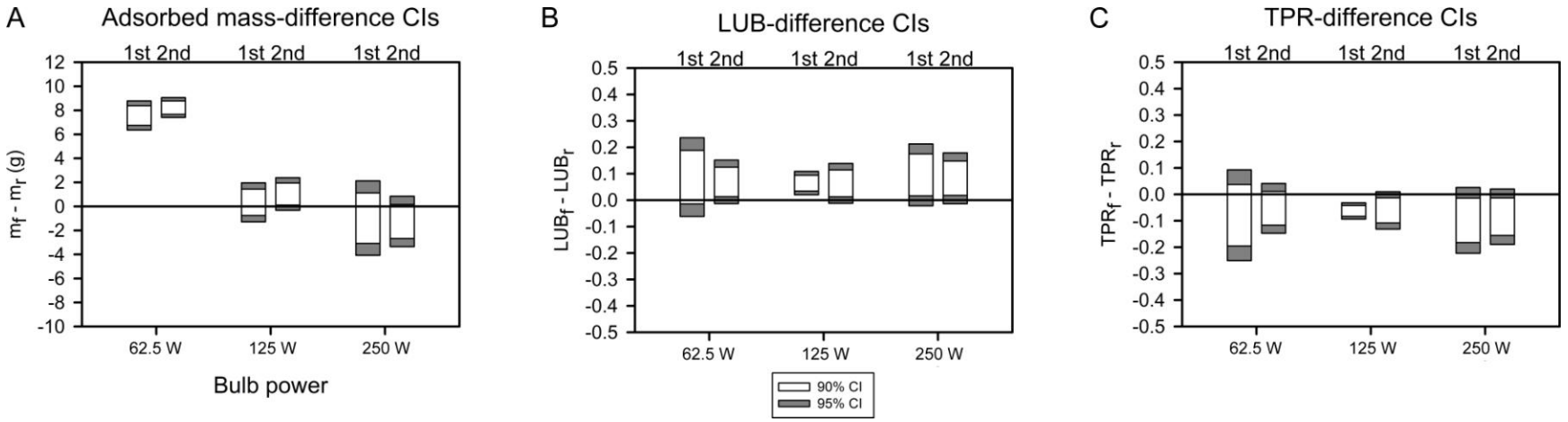


Figure 7-7. Confidence intervals (CI) describing the difference in performance between fresh and regenerated ACC. The CIs are shown for A) adsorbed mass, B) LUB, and C) TPR. The label “1st” corresponds to the adsorption period after the first regeneration while the label “2nd” corresponds to the adsorption period after the second regeneration.

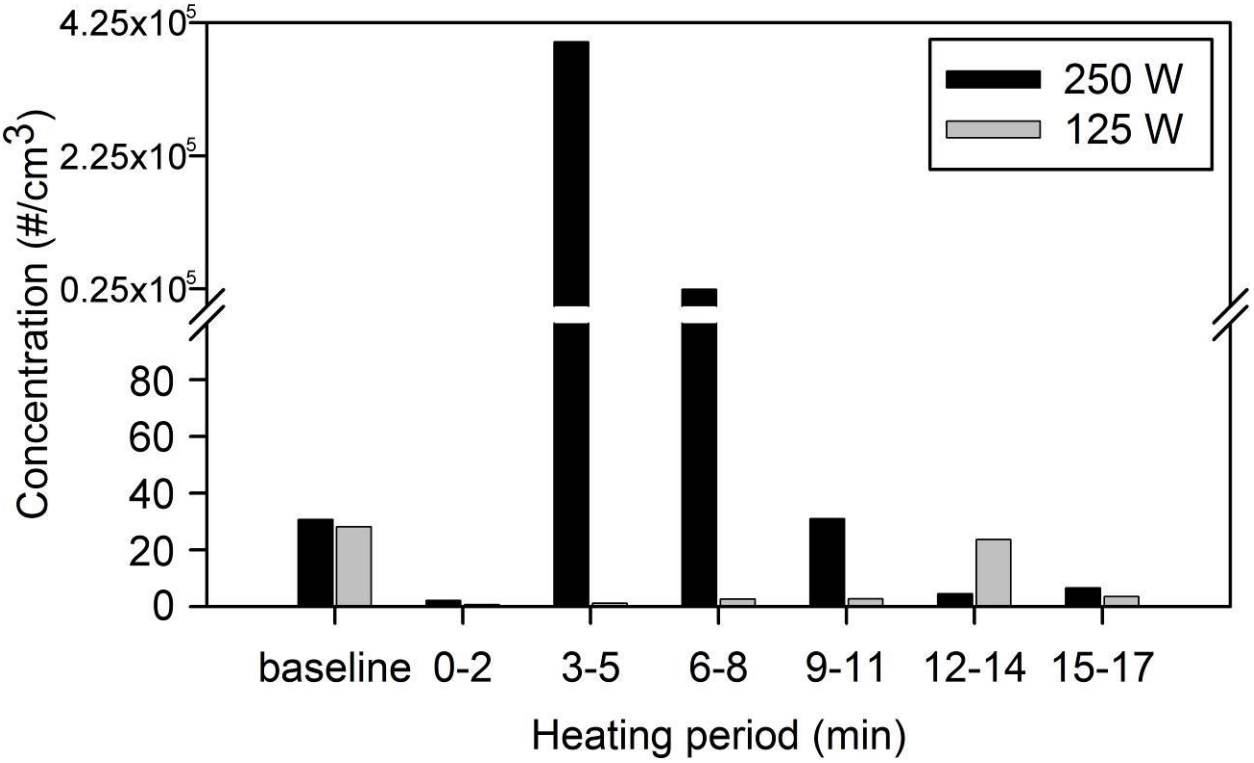


Figure 7-8. The emitted particle concentrations from the ACC during heating with 250-W and 125-W bulb powers.

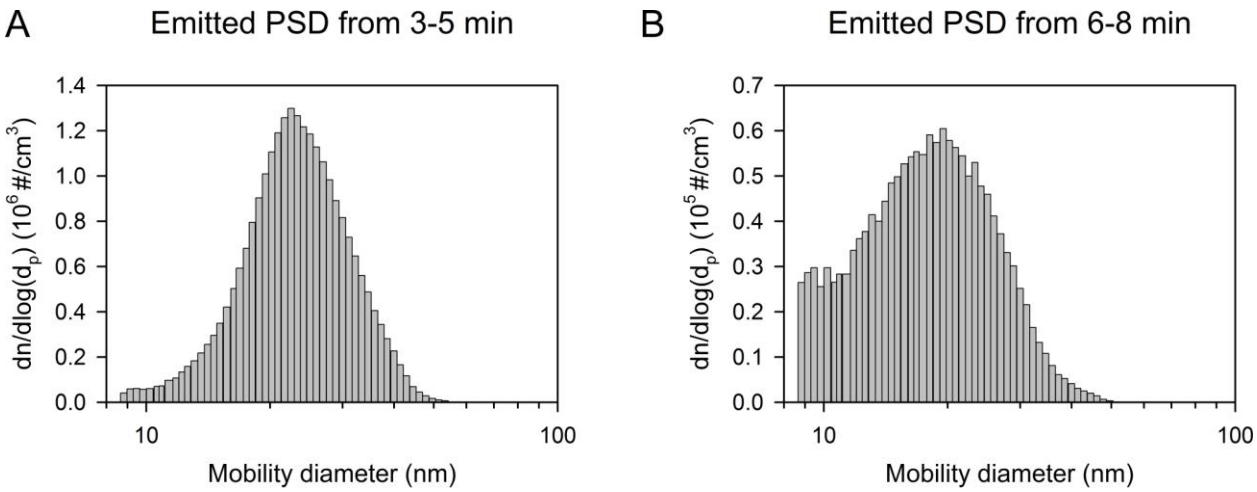


Figure 7-9. Emitted PSDs from the ACC using the 250-W power. A) Emitted PSD during the 3-5 min period. B) Emitted PSD during the 6-8 min period.

# CHAPTER 8
# CONCLUSIONS

In microwave filter disinfection experiments, irradiation at 750 W for 90 s was able to inactivate 98.8% of collected bacterial spores. On-line experiments showed 2.8-log inactivation with continuous microwave irradiation at 750 W during the 30-min filtration period. A decreased overall effectiveness in the on-line tests suggested that airflow passing through the filter reduced the filter temperature and thus the inactivation. By reducing the flow rate through the filter by 50%, a 0.636-log increase in spore inactivation was observed. Besides increasing disinfection, this finding supported that the thermal effect of microwave irradiation may be more dominant than a non-thermal effect. From the microwave experiments, it was determined that the filter disinfection process could be improved by using IR radiation, measuring filter temperature, and realizing UHT treatment.

An irradiation device was constructed considering the unique characteristics of IR and the physical dimensions and radiative properties of air filters to achieve UHT. A maximum of 3.77-, 4.38-, and 5.32-log inactivation of *B. subtilis* spores, *E. coli*, and MS2 viruses respectively were achieved within 5 s of irradiation. Inactivation was highest with the 250-W power bulb and a threshold temperature greater than 200 ºC was found necessary to successfully inactivate the test microorganisms. SEM analysis of the filter showed no visible damage from the heat treatment that would affect filtration efficiency and that the collected *E. coli* aerosols shrank in size from the heating. Although it was shown that air filters can be flash disinfected with IR given sufficient incident power density, the results demonstrate that the 125-°C temperature used for

the UHT treatment of liquids was not sufficiently high to disinfect air filters. This was likely because the disinfection was a dry heat process.

Besides filter disinfection, UHT generated by IR successfully inactivated microbes suspended in air. To address the undesirable non-uniform airflow temperatures noted in previous studies, the IR-UHT system was designed so that air flow passed through a heating element (in contrast to axial heating) and the Fourier number of the air was analyzed. In temperature measurements, high temperatures (near 450 °C) were obtained at the cloth surface and for downstream air. Airflow temperatures were more axially uniform and less so radially/azimuthally due to the parabolic velocity profile at the cloth surface. In lab testing, both *E. coli* and MS2 virus were inactivated at greater than 4.7-log for a temperature of about 450 °C and residence time of 0.41 s during constant irradiation of the cloth. When the cloth was heated periodically for half or a third of the time, the inactivation was orders of magnitude less indicating that the residual cloth temperature was not sustained for long enough. Most importantly, having heat conduct from a heating element held perpendicularly to the flow and considering the Fourier number in the design here improved temperature uniformity and advanced UHT bioaerosol disinfection systems.

Gel electrophoresis suggested that DNA degradation may contribute to *E. coli* inactivation although a combination of death mechanisms is possibly responsible at higher temperatures. For using UHT in practical applications, SEM imaging and sampling with an SMPS showed that care must be taken to ensure that harmful materials are not released (from the heating element, wall, etc.) during heating. Finally, UHT treatment at 210 °C with a 0.1-s exposure time was found to reduce the

concentration of ambient bacteria bioaerosols by 1-2 log depending on particle size although it was less effective against ambient fungi. The results proved that an UHT treatment process can inactivate a variety of bioaerosols in a real world environment and give motivation for further research on this topic.

In assessing the performance of the metallic granular bed filter with small collectors against bioaerosols, a PRE greater than 99.9% and a VRE greater than 5-log were observed for both *B. subtilis* spore and MS2 virus. A lower face velocity produced higher collection efficiency for virus but was not statistically significant for spore filtration. Although the filter had high filtration efficiency of the test bioaerosols, the filter's high pressure drop (caused by its small granules) resulted in a low filter quality (0.25-0.75 $kPa^{-1}$). In short, filters with micrometer-sized collectors capture bioaerosols effectively but their applications in aerosol filtration may be limited by their high pressure drop.

The Poisson assumption was found to be valid for nanometer-sized aerosol sampling. Analysis of the time series with the PCF and time-averaged PCF showed that the experimental data generally produced values within the range of 80% of the Poisson-simulation values. The same result was observed for the metrics related to concentration measurements (CV, probability of measuring a concentration at least 25% greater than average, and posterior distribution) which indicates that a Poisson process describes nanometer-sized aerosol sampling at least for the tested conditions. Non-Poissonian behavior found in previous studies for micrometer-sized aerosols may be due to the inability of Brownian motion to decorrelate the detection of larger particles.

Further studies are required to confirm the validity of the Poisson assumption in a variety of aerosol sampling circumstances.

IR regeneration for 1 h completely restored the adsorption capacity of toluene-saturated ACC at the 250-W and 125-W powers (corresponding to ACC temperatures of 277 °C and 152 °C, respectively). Furthermore, LUB and TPR remained unchanged or were slightly improved after regeneration. The adsorption performance of ACC after one and two regenerations was found to be nearly the same as fresh ACC with these bulb powers. Regeneration with the 62.5-W power, however, was only able to restore about 50% of the fresh ACC capacity. For complete regeneration, an IR power density greater than 4.56 $W/cm^2$ at the ACC surface is needed with the experimental setup. It was observed that nanoparticles were emitted from ACC heated to 277 °C under the nitrogen regeneration flow. However, the effect of the emitted particles was likely small because there was little to no change in adsorption performance for regenerated ACC. Overall, the success of regeneration with broadband IR provides a basis for future work using different IR wavelengths for pollutant desorption.

In this dissertation, IR radiation-based technologies were successfully developed to control bioaerosol and VOC air pollutants. The technologies offer unique advantages over existing technologies, namely: IR air filter disinfection is faster and provides enhanced inactivation, on-line IR-UHT yields more uniform airflow temperatures, and IR desorption provides stable and controlled regeneration. In future research, the flash IR filter disinfection technology can be scaled-up and incorporated in a disinfection device for respirator filters. For the on-line system, a flow straightener can be added to further reduce temperature gradients and realize an even more stable and predictable UHT

process. The system can also be used to obtain detailed information about the death kinetics of airborne microbes. Future work with IR regeneration can examine the use of tuned IR light in targeting a particular adsorbate to achieve selective desorption. This can significantly lower regeneration power consumption because energy will be delivered directly to targeted molecules. The research completed in this study and future research with radiation-based control devices can improve control strategies and reduce the negative effects of bioaerosol and VOC air pollutants.

# APPENDIX A
# MATLAB SOURCE CODE FOR CALCULATING THE METRICS PRESENTED IN CHAPTER 6 FROM TIME SERIES DATA

```
clear
fileid=fopen('datatry.log');
n=fscanf(fileid, '%d');

lower_limit=1.64E5;
upper_limit=1.74E5;

% 0.1E5 measurements or 1E4

T=size(n,1);

for i=1:T
   if i<lower_limit || i>=upper_limit
      n(i)=-999;
   end
end

n(n==-999)=[];
clearvars -except n

test_per=0.75; %the sampled conc. is 1-test_per greater than the average
removed_minus_one=n;
removed_minus_one(removed_minus_one==-1)=[];
averaged_n=mean(removed_minus_one);

T=size(n,1);

no_minus_one=size(find(n==-1),1);

%=========================================================================
%==================================Data===================================
%=========================================================================

% calculate the averaged PCF, etc for the data
disp(['calculating the averaged PCF, prob, CV, and Po for data...  '...
   , datestr(now,13)])

for time=1:T

   clear x;
   Nsi=floor(T/time);
   sum_=0;
   counter=0;
   flag=0;

   if (Nsi-no_minus_one)>10

      for i=1:(Nsi*time)
```

```
    sum_=sum_+n(i);
    counter=counter+1;

    if n(i)==-1
        flag=1;
    end

    if counter==time

        j=i/time;
        if flag==1
            x(j)=-1;
        else
            x(j)=sum_;
        end

        sum_=0;
        counter=0;
        flag=0;
    end

end

x(x==-1)=[];
% x is a row vector, STWMO - sampling times without minus one
STWMO(time)=size(x,2);


%--- probability of having a sampled conc. (from the samples)
% that is 1-test_per greater than the global average

prob_sum=0;

for l=1:STWMO(time)

    if (averaged_n/(x(l)/time))<=test_per
        prob_sum=prob_sum+1;
    end

end

prob(time)=100*(prob_sum/STWMO(time));


%--- calcualte the CV

average=mean(x);
standard_deviation=std(x);
CV(time)=standard_deviation/average;


%--- calcualte the averaged PCF
```

```
variance=standard_deviation^2;
eta_avg(time)=(variance/(average^2))-(1/average);


%--- calcualte the posterior distribution using bayes theorem

if time==1 || (time==10 && averaged_n<5)

    v=average/variance;
    r=(average^2)/variance;

    dm=1E-3;
    disp_num_si=100;

    Sa=[0:(dm*time):(averaged_n*5*time)];

    L=length(Sa);
    Po=ones(1,L); % initialize

    for j=1:disp_num_si;

        m=0*Po; % initialize

        for i=1:L  % loops me
            me=Sa(i);

            if j==1
                Pr=1;%(v^r)*(me^(r-1))*(exp(-v*me))/gamma(r);
            else
                Pr=Po(i);
            end

            m(i)=((me^x(j))*exp(-me))/...
                 (factorial(x(j))); % likelihood
            m(i)=m(i)*Pr;
        end
        Po=m/(sum(m));
    end

    if time==1
        disp(['calculating the posterior distribution for data'...
            ' for time==1...  ', datestr(now,13)])
        Po_one=Po/(max(Po));
        a=find(Po==max(Po));
        max_one=Sa(a);
    else
        Po_ten=Po/(max(Po));
        a=find(Po==max(Po));
        max_ten=Sa(a);
    end

end % Po
```

```
    end % if Nsi-no_minus_one>10

end


% pair correlation function for data
disp(' ')
disp(['calculating the PCF for data...  ',...
    datestr(now,13)])

for time=1:T

    evaluations=T-time;
    clear x;

    if (evaluations-(2*no_minus_one))>2000
% actual number of evaluations always greater than 2000

      for i=1:evaluations

          if n(i)==-1 || n(i+time)==-1
              x(i)=-1;
          else
              x(i)=n(i)*n(i+time);
          end

      end

      x(x==-1)=[];
      % x is a row vector, EWMO - evaluations without minus one
      EWMO(time)=size(x,2);

      numerator=mean(x);
      eta(time)=(numerator/(averaged_n^2))-1;

    end

end

prob=prob';
CV=CV';
eta_avg=eta_avg';
Po_one=Po_one';
if averaged_n<5
    Po_ten=Po_ten';
end
eta=eta';

%=========================================================================
%============================Simulation===================================
%=========================================================================
```

```
total_no_sim=1000; % 1000
lower_lim=100; % 100
upper_lim=900; % 900

prob_sim=zeros(total_no_sim,length(prob));
CV_sim=zeros(total_no_sim,length(CV));
eta_avg_sim=zeros(total_no_sim,length(eta_avg));
Po_one_sim=zeros(total_no_sim,length(Po_one));
if averaged_n<5
   Po_ten_sim=zeros(total_no_sim,length(Po_ten));
end
eta_sim=zeros(total_no_sim,length(eta));
max_one_sim=zeros(total_no_sim,1);
max_ten_sim=zeros(total_no_sim,1);

for f=1:total_no_sim

   n_sim=poissrnd(averaged_n,T,1);
   disp(' ')
   disp(['calculating the averaged PCF, prob, CV, and Po for sim ',...
      num2str(f), ' ', datestr(now,13)])

   for time=1:T

      clear x;
      Nsi=floor(T/time);
      sum_=0;
      counter=0;

      if (Nsi-no_minus_one)>10

         for i=1:(Nsi*time)

            sum_=sum_+n_sim(i);
            counter=counter+1;

            if counter==time

               j=i/time;
               x(j)=sum_;

               sum_=0;
               counter=0;
            end
         end

         x_size=size(x,2);
         remove=x_size-STWMO(time);

         for k=1:remove
            x(1)=[];
         end
```

```
%--- probability of having a sampled conc. (from the samples)
% that is 1-test_per greater than the average

prob_sum=0;

for l=1:STWMO(time)
   if (averaged_n/(x(l)/time))<=test_per
      prob_sum=prob_sum+1;
   end
end

prob_sim(f,time)=100*(prob_sum/STWMO(time));


%--- calcualte the CV

average=mean(x);
standard_deviation=std(x);
CV_sim(f,time)=standard_deviation/average;


%--- calcualte the averaged PCF

variance=standard_deviation^2;
eta_avg_sim(f,time)=(variance/(average^2))-(1/average);

%--- calcualte the posterior distribution using bayes theorem

if time==1 || (time==10 && averaged_n<5)

   v=average/variance;
   r=(average^2)/variance;

   dm=1E-3;
   disp_num_si=100;

   Sa=[0:(dm*time):(averaged_n*5*time)];

   L=length(Sa);
   Po=ones(1,L); % initialize

   for j=1:disp_num_si;

      m=0*Po; % initialize

      for i=1:L  % loops me
         me=Sa(i);

         if j==1
            Pr=1;%(v^r)*(me^(r-1))*(exp(-v*me))/gamma(r);
         else
```

```
                Pr=Po(i);
            end

            m(i)=((me^x(j))*exp(-me))/...
                (factorial(x(j))); % likelihood
            m(i)=m(i)*Pr;
        end
        Po=m/(sum(m));
    end

    if time==1
        disp(['calculating the posterior distribution '...
            'for sim ', num2str(f),...
            ' for time==1...  ', datestr(now,13)])
        Po_one_sim(f,:)=Po/(max(Po));
        a=find(Po==max(Po));
        max_one_sim(f)=Sa(a);
    else
        Po_ten_sim(f,:)=Po/(max(Po));
        a=find(Po==max(Po));
        max_ten_sim(f)=Sa(a);
    end

  end % Po

end % if Nsi-no_minus_one>10

end


% pair correlation function for sim

disp(' ')
disp(['calculating the sim PCF for ', num2str(f), ' ... ',...
    datestr(now,13)])

for time=1:T

    evaluations=T-time;
    clear x;

    if (evaluations-(2*no_minus_one))>2000
% actual number of evaluations always greater than 2000

      for i=1:evaluations
          x(i)=n_sim(i)*n_sim(i+time);
      end

      x_size=size(x,2);
      remove=x_size-EWMO(time);

      for k=1:remove
          x(1)=[];
```

```
        end

        numerator=mean(x);
        eta_sim(f,time)=(numerator/(averaged_n^2))-1;

      end

    end

end % f

% prob_sim
sorted_prob_sim=sort(prob_sim,1);
lower_prob_sim=(sorted_prob_sim(1,:))';
upper_prob_sim=(sorted_prob_sim(total_no_sim,:))';
lower_inter_prob_sim=(sorted_prob_sim(lower_lim,:))';
upper_inter_prob_sim=(sorted_prob_sim(upper_lim,:))';

% CV_sim
sorted_CV_sim=sort(CV_sim,1);
lower_CV_sim=(sorted_CV_sim(1,:))';
upper_CV_sim=(sorted_CV_sim(total_no_sim,:))';
lower_inter_CV_sim=(sorted_CV_sim(lower_lim,:))';
upper_inter_CV_sim=(sorted_CV_sim(upper_lim,:))';

% eta_avg_sim
sorted_eta_avg_sim=sort(eta_avg_sim,1);
lower_eta_avg_sim=(sorted_eta_avg_sim(1,:))';
upper_eta_avg_sim=(sorted_eta_avg_sim(total_no_sim,:))';
lower_inter_eta_avg_sim=(sorted_eta_avg_sim(lower_lim,:))';
upper_inter_eta_avg_sim=(sorted_eta_avg_sim(upper_lim,:))';

% Po_one_sim
sorted_Po_one_sim=sort(Po_one_sim,1);
lower_Po_one_sim=(sorted_Po_one_sim(1,:))';
upper_Po_one_sim=(sorted_Po_one_sim(total_no_sim,:))';
lower_inter_Po_one_sim=(sorted_Po_one_sim(lower_lim,:))';
upper_inter_Po_one_sim=(sorted_Po_one_sim(upper_lim,:))';

% Po_ten_sim
if averaged_n<5
   sorted_Po_ten_sim=sort(Po_ten_sim,1);
   lower_Po_ten_sim=(sorted_Po_ten_sim(1,:))';
   upper_Po_ten_sim=(sorted_Po_ten_sim(total_no_sim,:))';
   lower_inter_Po_ten_sim=(sorted_Po_ten_sim(lower_lim,:))';
   upper_inter_Po_ten_sim=(sorted_Po_ten_sim(upper_lim,:))';
end

% eta_sim
sorted_eta_sim=sort(eta_sim,1);
lower_eta_sim=(sorted_eta_sim(1,:))';
upper_eta_sim=(sorted_eta_sim(total_no_sim,:))';
lower_inter_eta_sim=(sorted_eta_sim(lower_lim,:))';
upper_inter_eta_sim=(sorted_eta_sim(upper_lim,:))';
```

```
% max_one_sim and max_ten_sim
median_max_one_sim=median(max_one_sim);
median_max_ten_sim=median(max_ten_sim);
```

LIST OF REFERENCES


Aizenberg, V., Reponen, T., Grinshpun, S.A. and Willeke, K. (2000) Performance of Air-O-Cell, Burkard, and Button samplers for total enumeration of airborne spores. *AIHAJ* **61**, 855-864.

Aranha-Creado, H. and Brandwein, H. (1999) Application of bacteriophages as surrogates for mammalian viruses: A case for use in filter validation based on precedents and current practices in medical and environmental virology. *PDA J Pharm Sci Tech* **53**, 75-82.

Balazy, A., Toivola, M., Adhikari, A., Sivasubramani, S., Reponen, T. and Grinshpun, S.A. (2006) Do N95 respirators provide 95% protection level against airborne viruses, and how adequate are surgical masks? *Am J Infect Control* **34**, 51-57.

Basso, M.F.M., Giampaolo, E.T., Vergani, C.E., Machado, A.L., Pavarina, A.C. and Compagnoni, M.A. (2010) Influence of microwave disinfection on the linear dimensional stability of complete dentures: a clinical study. *Int J Prosthodont* **23**, 318-320.

Bird, R.B., Steward, W.E. and Lightfoot, E.N. (2007) *Transport Phenomena*. New York: John Wiley & Sons, Inc.

Bolstad, W.M. (2007) *Introduction to Bayesian Statistics*. Hoboken, N.J.: John Wiley & Sons, Inc.

Brandl, M.T., Pan, Z., Huynh, S., Zhu, Y. and McHugh, T.H. (2008) Reduction of Salmonella Enteritidis population sizes on almond kernels with infrared heat. *J Food Protect* **71**, 897-902.

Brasquet, C. and Le Cloirec, P. (1997) Adsorption onto activated carbon fibers: Application to water and air treatments. *Carbon* **35**, 1307-1313.

Bukowiecki, N., Dommen, J., Prevot, A., Richter, R., Weingartner, E. and Baltensperger, U. (2002) A mobile pollutant measurement laboratory-measuring gas phase and aerosol ambient concentrations with high spatial and temporal resolution. *Atmos Environ* **36**, 5569-5579.

Burton, N.C., Adhikari, A., Iossifova, Y., Grinshpun, S.A. and Reponen, T. (2008) Effect of gaseous chlorine dioxide on indoor microbial contaminants. *J Air Waste Manage* **58**, 647-656.

Burton, N.C., Grinshpun, S.A. and Reponen, T. (2007) Physical collection efficiency of filter materials for bacteria and viruses. *Ann Occup Hyg* **51**, 143-151.

Cal, M.P., Larson, S.M. and Rood, M.J. (1994) Experimental and modeled results describing the adsorption of acetone and benzene onto activated carbon fibers. *Environ Prog* **13**, 26-30.

Cal, M.P., Rood, M.J. and Larson, S.M. (1996) Removal of VOCs from humidified gas streams using activated carbon cloth. *Gas Sep Purif* **10**, 117-121.

Cañumir, J.A., Celis, J.E., de Bruijn, J. and Vidal, L.V. (2002) Pasteurisation of apple juice by using microwaves. *LWT-Food Sci Technol* **35**, 389–392.

Casanova, L., Alfano-Sobsey, E., Rutala, W., Weber, D. and Sobsey, M. (2008) Virus transfer from personal protective equipment to healthcare employees skin and clothing. *Emerg Infect Dis* **14**, 1291–1293.

Celandroni, F., Longo, I., Tosoratti, N., Giannessi, F., Ghelardi, E., Salvetti, S., Baggiani, A. and Senesi, S. (2004) Effect of microwave radiation on *Bacillus subtilis* spores. *J Appl Microbiol* **97**, 1220-1227.

Chu, C., Cheng, V.C.C., Hung, I.F.N., Chan, K., Tang, B.S.F., Tsang, T.H.F., Chan, K. and Yuen, K. (2005) Viral load distribution in SARS outbreak. *Emerg Infect Dis* **11**, 1882-1886.

Chuaybamroong, P., Chotigawin, R., Supothina, S., Sribenjalux, P., Larpkiattaworn, S. and Wu, C.Y. (2010) Efficacy of photocatalytic HEPA filter on microorganism removal. *Indoor Air* **20**, 246-254.

Cox, C.S. (1987) *The Aerobiological Pathway of Microogranisms*. Chichester, UK: John Wiley & Sons.

Cox, C.S. (1995) Stability of airborne microbes and allergens. In *Bioaerosols Handbook* eds. Cox, C.S. and Wathes, C.M. pp.77-100. Boca Raton, FL: CRC Press LLC.

Cox, C.S. (1998) The microbiology of air. In *Topley & Wilson's Microbiology and Microbial Infections* eds. Collier, L., Balows, A. and Sussman, M. pp.339-350. London: Arnold, Oxford University Press.

Cox, C.S. and Wathes, C.M. (1995) Editors' introduction. In *Bioaerosols Handbook* eds. Cox, C.S. and Wathes, C.M. pp.3-4. Boca Raton, FL: CRC Press LLC.

Damit, B., Lee, C. and Wu, C.Y. (2011) Flash infrared radiation disinfection of fibrous filters contaminated with bioaerosols. *J Appl Microbiol* **110**, 1074-1084.

Des Prez, R.M. and Heim, C.R. (1990) *Mycobacterium tuberculosis*. In *Principles and practices of infectious diseases* eds. Mandell, G.L., Douglas, R.G. and Bennett, J.E. pp.1877–1906. New York: Churchill Livingstone.

Douwes, J., Thorne, P., Pearce, N. and Heederik, D. (2003) Bioaerosol health effects and exposure assessment: Progress and prospects. *Ann Occup Hygiene* **47**, 187-200.

Dovigo, L.N., Pavarina, A.C., Ribeiro, D.G., De Oliveira, J.A., Vergani, C.E. and Machado, A.L. (2009) Microwave disinfection of complete dentures contaminated in vitro with selected bacteria. *J Prosthodont* **18**, 611–617.

Ehrlich, R., Miller, S. and Walker, R.L. (1970) Relationship between atmospheric temperature and survival of airborne bacteria. *Appl Microbiol* **19**, 245–249.

Endo, Y., Chen, D. and Pui, D. (2002) Collection efficiency of sintered ceramic filters made of submicron spheres. *Filtr Separat* **41**, 40-40.

Eninger, R.M., Hogan, C.J., Biswas, P., Adhikari, A., Reponen, T. and Grinshpun, S.A. (2009) Electrospray versus nebulization for aerosolization and filter testing with bacteriophage particles. *Aerosol Sci Tech* **43**, 298-304.

Fang, Z., Ouyang, Z., Zheng, H., Wang, X. and Hu, L. (2007) Culturable airborne bacteria in outdoor environments in Beijing, China. *Microb Ecol* **54**, 487-496.

Farnsworth, J.E., Goyal, S.M., Kim, S.W., Kuehn, T.H., Raynor, P.C., Ramakrishnan, M.A., Anantharaman, S. and Tang, W.H. (2006) Development of a method for bacteria and virus recovery from heating, ventilation, and air conditioning (HVAC) filters. *J Environ Monitor* **8**, 1006-1013.

Franklin, J.G., Williams, D.J., Chapman, H.R. and Clegg, L.F.L. (1958) Methods of assessing the sporicidal efficiency of an ultrahigh-temperature milk sterilizing plant. II. Experiments with suspensions of spores in milk. *J Appl Bacteriol* **21**, 47-50.

Franz, D.R., Jahrling, P.B., Friedlander, A.M., McClain, D.J., Hoover, D.L., Bryne, W.R., Pavlin, J.A., Christopher, G.W. and Eitzen, E.M. (1997) Clinical recognition and management of patients exposed to biological warfare agents. *JAMA* **278**, 399-411.

Friedel, R. and Hofer, L. (1970) Spectral characterization of activated carbon. *J Phys Chem* **74**, 2921–2922.

Fromme, H., Twardella, D., Dietrich, S., Heitmann, D., Schierl, R., Liebl, B. and Rüden, H. (2007) Particulate matter in the indoor air of classrooms—exploratory results from Munich and surrounding area. *Atmos Environ* **41**, 854-866.

Gangneux, J., Noussair, L., Bouakline, A., Roux, N., Lacroix, C. and Derouin, F. (2004) Experimental assessment of disinfection procedures for eradication of *Aspergillus fumigatus* in food. *Blood* **104**, 2000-2002.

George, D.F., Bilek, M.M. and McKenzie, D.R. (2008) Non-thermal effects in the microwave induced unfolding of proteins observed by chaperone binding. *Bioelectromagnetics* **29**, 324-330.

Golmohammadi, R., Valegard, K., Fridborg, K. and Liljas, L. (1993) The refined structure of bacteriophage MS2 at 2.8 Å resolution. *J Mol Biol* **234**, 620-639.

Gonzalez-Juarrero, M., Turner, O.C., Turner, J., Marietta, P., Brooks, J.V. and Orme, I.M. (2001) Temporal and spatial arrangement of lymphocytes within lung granulomas induced by aerosol infection with Mycobacterium tuberculosis. *Infect Immun* **69**, 1722-1728.

Goswami, D.Y., Trivedi, D.M. and Block, S.S. (1997) Photocatalytic disinfection of indoor air. *J Sol Energ-T ASME* **119**, 92-96.

Green, H.S. (1969) *The Molecular Theory of Fluids*. New York: Dover.

Griffiths, W.D. and Decosemo, G.A.L. (1994) The assessment of bioaerosols - a critical review. *J Aerosol Sci* **25**, 1425-1458.

Grinshpun, S.A., Adhikari, A., Li, C., Reponen, T., Yermakov, M., Schoenitz, M., Dreizin, E., Trunov, M. and Mohan, S. (2010a) Thermal inactivation of airborne viable Bacillus subtilis spores by short-term exposure in axially heated air flow. *J Aerosol Sci* **41**, 352-363.

Grinshpun, S.A., Adhikari, A., Li, C., Yermakov, M., Reponen, L., Johansson, E. and Trunov, M. (2010b) Inactivation of aerosolized viruses in continuous air flow with axial heating. *Aerosol Sci Tech* **44**, 1042-1048.

Guo, H. (2000) Evaluation of total volatile organic compound emissions from adhesives based on chamber tests. *J Air Waste Manage* **50**, 199-206.

Guo, H., Lee, S., Chan, L. and Li, W. (2004) Risk assessment of exposure to volatile organic compounds in different indoor environments. *Environ Res* **94**, 57-66.

Guo, H. and Murray, F. (2000) Characterisation of total volatile organic compound emissions from paints. *Clean Prod Process* **2**, 28-36.

Guo, H. and Murray, F. (2001) Determination of total volatile organic compound emissions from furniture polishes. *Clean Prod Process* **3**, 42-48.

Haas, D., Unteregger, M., Habib, J., Galler, H., Marth, E. and Reinthaler, F.F. (2010) Exposure to bioaerosol from sewage systems. *Water Air Soil Poll* **207**, 49-56.

Hamanaka, D., Uchino, T., Furuse, N., Han, W. and Tanaka, S. (2006) Effect of the wavelength of infrared heaters on the inactivation of bacterial spores at various water activities. *Int J Food Microbiol* **108**, 281-285.

Hamanaka, D., Uchino, T., Hu, W., Eriko, Y. and H.M., S. (2003) Effects of infrared radiation on the disinfection for wheat and soybean. *J Jpn Soc Agr Mach* **65**, 64-70.

Hashisho, Z., Rood, M. and Biotech, L. (2005) Microwave-swing adsorption to capture and recover vapors from air streams with activated carbon fiber cloth. *Environ Sci Technol* **39**, 6851-6859.

Heddleson, R.A. and Doores, S. (1994) Factors affecting microwave heating of foods and microwave induced destruction of foodborne pathogens - a review. *J Food Protect* **57**, 1025-1037.

Heinrich, J., Holscher, B., Douwes, J., Richter, K., Koch, A., Bischof, W., Fahlbusch, B., Kinne, R., Wichmann, H. and Grp, I.S. (2003) Reproducibility of allergen, endotoxin and fungi measurements in the indoor environment. *J Expo Anal Env Epid* **13**, 152-160.

Hinds, W.C. (1999) *Aerosol Technology: Properties, Behavior, and Measurement of Airborne Particles*. New York: John Wiley & Sons, Inc.

Hirst, J.M. (1995) Bioaerosols: introduction, retrospect, and prospect. In *Bioaerosols Handbook* eds. Cox, C.S. and Wathes, C.M. pp.5-14. Boca Raton, FL: CRC Press LLC.

Hiti, K., Walochnik, J., Faschinger, C., Haller-Schober, E. and Aspöck, H. (2001) Microwave treatment of contact lens cases contaminated with Acanthamoeba. Cornea **20**, 467-470.

Hogan, C.J., Kettleson, E.M., Lee, M.H., Ramaswami, B., Angenent, L.T. and Biswas, P. (2005) Sampling methodologies and dosage assessment techniques for submicrometre and ultrafine virus aerosol particles. *J Appl Microbiol* **99**, 1422-1434.

Hoppel, W.A. and Frick, G.M. (1986) Ion-aerosol attachment coefficients and the steady-state charge distribution on aerosols in a bipolar ion environment. *Aerosol Sci Tech* **5**, 1-21.

Ijaz, M.K., Brunner, A.H., Sattar, S.A., Nair, R.C. and Johnson-Lussenburg, C.M. (1985) Survival characteristics of airborne human coronavirus 229E. *J Gen Virol* **66**, 2743-2748.

Inoué, S. and Kabaya, M. (1989) Biological activities caused by far-infrared radiation. *Int J Biometeorol* **33**, 145-150.

Jankowska, E., Reponen, T., Willeke, K., Grinshpun, S.A. and Choi, K.J. (2000) Collection of fungal spores on air filters and spore reentrainment from filters into air. *J Aerosol Sci* **31**, 969–978.

Jaques, P.A., Hsiao, T.C. and Gao, P. (2011) A recirculation aerosol wind tunnel for evaluating aerosol samplers and measuring particle penetration through protective clothing materials. *Ann Occup Hyg* **55**, 784-796.

Jia, C., Batterman, S. and Godwin, C. (2008) VOCs in industrial, urban and suburban neighborhoods, Part 1: Indoor and outdoor concentrations, variation, and risk drivers. *Atmos Environ* **42**, 2083-2100.

Jo, W. and Kang, J. (2006) Workplace exposure to bioaerosols in pet shops, pet clinics, and flower gardens. *Chemosphere* **65**, 1755–1761.

Johansson, E., Adhikari, A., Reponen, T., Yermakov, M. and Grinshpun, S. (2011) Association between increased DNA mutational frequency and thermal inactivation of aerosolized Bacillus spores exposed to dry heat. *Aerosol Sci Tech* **45**, 376-381.

Johnsen, D.L., Mallouk, K.E. and Rood, M.J. (2011) Control of electrothermal heating during regeneration of activated carbon fiber cloth. *Environ Sci Technol* **45**, 738-743.

Jung, J., Lee, J., Kim, S. and Bae, G. (2010) Size reduction of Aspergillus versicolor fungal bioaerosols during a thermal heating process in continuous-flow system. *J Aerosol Sci* **41**, 602-610.

Jung, J.H., Lee, J.E. and Kim, S.S. (2009a) Thermal effects on bacterial bioaerosols in continuous air flow. *Sci Total Environ* **407**, 4723-4730.

Jung, J.H., Lee, J.E., Lee, C.H., Kim, S.S. and Lee, B.U. (2009b) Treatment of fungal bioaerosols by a high-temperature, short-time process in a continuous-flow system. *Appl Environ Microb* **75**, 2742-2749.

Kalogerakis, N., Paschali, D., Lekaditis, V., Pantidou, A., Eleftheriadis, K. and Lazaridis, M. (2005) Indoor air quality - bioaerosol measurements in domestic and office premises. *J Aerosol Sci* **36**, 751-761.

Karol, M.H. (1991) Allergic reactions to indoor air pollutants. *Environ Health Persp* **95**, 45–51.

Kemp, P.C., Neumeister-Kemp, H.G., Lysek, G. and Murray, F. (2001) Survival and growth of micro-organisms on air filtration media during initial loading. *Atmos Environ* **35**, 4739-4749.

Knight, V. (1973) Airborne transmission and pulmonary deposition of respiratory viruses. In *Viral and Mycoplasmal Infections of the Respiratory Tract* ed. Knight, V. pp.1-9. Philadelphia: Lea & Febiger.

Knight, V. (1980) Viruses as agents of airborne contagion. *Ann NY Acad Sci* **353**, 147-156.

Kostiainen, R. (1995) Volatile organic compounds in the indoor air of normal and sick houses. *Atmos Environ* **29**, 693–702.

Kostinski, A.B. and Jameson, A.R. (2000) On the spatial distribution of cloud particles. *J Atmos Sci* **57**, 901-915.

Kreith, F., R.M., M. and Bohn, M.S. (2011) *Principles of Heat Transfer*. Stamford, CT: Cengage Learning.

Kujundzic, E., Matalkah, F., Howard, C., Hernandez, M. and Miller, S. (2006) UV air cleaners and upper-room air ultraviolet germicidal irradiation for controlling airborne bacteria and fungal spores. *J Occup Environ Hyg* **3**, 536-546.

Kummer, V. and Thiel, W.R. (2008) Bioaerosols - sources and control measures. *Int J Hyg Envir Heal* **211**, 299-307.

Kuo, Y.M., Huang, S.H., Lin, W.Y., Hsiao, M.F. and Chen, C.C. (2010) Filtration and loading characteristics of granular bed filters. *J Aerosol Sci* **41**, 223-229.

Lacey, J. and Dutkiewicz, J. (1994) Bioaerosols and occupational lung disease. *J Aerosol Sci* **25**, 1371-1404.

Lamminen, M.O., Walker, H.W. and Weavers, L.K. (2004) Mechanisms and factors influencing the ultrasonic cleaning of particle-fouled ceramic membranes. *J Membr Sci* **237**, 213-223.

Larsen, M.L. (2007) Spatial distributions of aerosol particles: Investigation of the Poisson assumption. *J Aerosol Sci* **38**, 807-822.

Larsen, M.L. (2012) Scale localization of cloud particle clustering statistics. *J Atmos Sci* **69**, 3277-3289.

Larsen, M.L., Cantrell, W., Kannosto, J. and Kostinski, A.B. (2003) Detection of spatial correlations among aerosol particles. *Aerosol Sci Tech* **37**, 476-485.

Larsen, M.L., Kostinski, A.B. and Tokay, A. (2005) Observations and analysis of uncorrelated rain. *J Atmos Sci* **62**, 4071-4083.

Lee, B., Yun, S., Jung, J. and Bae, G. (2010) Effect of relative humidity and variation of particle number size distribution on the inactivation effectiveness of airborne silver nanoparticles against bacteria bioaerosols deposited on a filter. *J Aerosol Sci* **41**, 447-456.

Lee, B.U. (2011) Life comes from the air: A short review on bioaerosol control. *Aerosol Air Qual Res* **11**, 921-927.

Lee, J.H. and Jo, W.K. (2006) Characteristics of indoor and outdoor bioaerosols at Korean high-rise apartment buildings. *Environ Res* **101**, 11-17.

Lee, J.H., Wu, C.Y., Lee, C.N., Anwar, D., Wysocki, K.M., Lundgren, D.A., Farrah, S., Wander, J. and Heimbuch, B.K. (2009) Assessment of iodine-treated filter media

for removal and inactivation of MS2 bacteriophage aerosols. *J Appl Microbiol* **107**, 1912-1923.

Lee, J.H., Wu, C.Y., Wysocki, K.M., Farrah, S. and Wander, J. (2008) Efficacy of iodine-treated biocidal filter media against bacterial spore aerosols. *J Appl Microbiol* **105**, 1318–1326.

Lee, K.W. and Mukand, R. (2001) Filter collection. In *Aerosol Measurement: Principles, Techniques, and Applications* eds. Baron, P.A. and Willeke, K. p.213. New York: John Wiley and Sons, Inc.

Lee, S.C., Li, W.M. and Ao, C.H. (2002) Investigation of indoor air quality at residential homes in Hong Kong - case study. *Atmos Environ* **36**, 225-237.

Lee, Y.H. and Lee, B.U. (2006) Inactivation of airborne E. coli and B. subtilis bioaerosols utilizing thermal energy. *J Microbiol Biotechn* **16**, 1684-1689.

Li, C.S., Hao, M.L., Lin, W.H., Chang, C.W. and Wang, C.S. (1999) Evaluation of microbial samplers for bacterial microorganisms. *Aerosol Sci Techn* **30**, 100-108.

Li, Y., Duan, S., Yu, I.T. and Wong, T.W. (2005) Multi-zone modeling of probable SARS virus transmission by airflow between flats in Block E, Amoy Gardens. *Indoor Air* **15**, 96-111.

Li, Y., Leung, G.M., Tang, J.W., Yang, X., Chao, C.Y., Lin, J.Z., Lu, J.W., Nielsen, P.V., Niu, J., Qian, H., Sleigh, A.C., Su, H.J., Sundell, J., Wong, T.W. and Yuen, P.L. (2007) Role of ventilation in airborne transmission of infectious agents in the built environment - a multidisciplinary systematic review. *Indoor Air* **17**, 2-18.

Lia, C. and Wena, Y. (2003) Control effectiveness of electrostatic precipitation on airborne microorganisms. *Aerosol Sci Tech* **37**, 933-938.

Liang, Y., Wu, Y., Sun, K., Chen, Q., Shen, F., Zhang, J., Yao, M., Zhu, T. and Fang, J. (2012) Rapid inactivation of biological species in the air using atmospheric pressure nonthermal plasma. *Environ Sci Technol* **46**, 3360-3368.

Lin, C.Y. and Li, C.S. (2002) Control effectiveness of ultraviolet germicidal irradiation on bioaerosols. *Aerosol Sci Tech* **36**, 474-478.

Liu, W., Kaufman, S.L., Osmondson, B.L., Sem, G.J., Quant, F.R. and Oberreit, D.R. (2006) Water-based condensation particle counters for environmental monitoring of ultrafine particles. *J Air Waste Manage* **56**, 444-455.

Love, W. (1995) Magnetrons. In *Handbook of Microwave Technology* ed. Ishii, T.K. pp.33-55. San Diego, CA: Academic Press, Inc.

Luo, L., Ramirez, D., Rood, M.J., Grevillot, G., Hay, K.J. and Thurston, D.L. (2006) Adsorption and electrothermal desorption of organic vapors using activated carbon adsorbents with novel morphologies. *Carbon* **44**, 2715-2723.

Marre, S., Palmeri, J., Larbot, A. and Bertrand, M. (2004) Modeling of submicrometer aerosol penetration through sintered granular membrane filters. *J Colloid Interf Sci* **274**, 167-182.

Martin, J.H., Harper, W.J. and Gould, I.A. (1966) Ultra-high temperature effects on selected Bacillus species. *J Dairy Sci* **49**, 1367–1370.

Maus, R., Goppelsröder, A. and Umhauer, H. (1997) Viability of bacteria in unused air filter media. *Atmos Environ* **31**, 2305–2310.

Maus, R., Goppelsröder, A. and Umhauer, H. (2001) Survival of bacterial and mold spores in air filter media. *Atmos Environ* **35**, 105–113.

McDonnell, G.E. (2007) *Antisepsis, Disinfection, and Sterilization*. Washington, DC: ASM Press.

McMurry, P.H. (2000) A review of atmospheric aerosol measurements. *Atmos Environ* **34**, 1959-1999.

Mendell, M.J., Fisk, W.J., Kreiss, K., Levin, H., Alexander, D., Cain, W.S., Girman, J.R., Hines, C.J., Jensen, P.A., Milton, D.K., Rexroat, L.P. and Wallingford, K.M. (2002) Improving the health of workers in indoor environments: Priority research needs for a national occupational research agenda. *Am J Public Health* **92**, 1430-1440.

Miaskiewicz-Peska, E. and Lebkowsk, M. (2012) Comparison of aerosol and bioaerosol collection on air filters. *Aerobiologia* **28**, 185-193.

Mishra, U. and Singh, J. (2008) *Semiconductor Device Physics and Design*. Dordrecht: Springer.

Molin, G. and Östlund, K. (1976) Dry-heat inactivation of Bacillus subtilis var. niger spores with special reference to spore density. *Can J Microbiol* **22**, 359-363.

Montville, T.J., Dengrove, R., De Siano, T., Bonnet, M. and Schaffner, D.W. (2005) Thermal resistance of spores from virulent strains of Bacillus anthracis and potential surrogates. *J Food Prot* **68**, 2362-2366.

Morawska, L. (2006) Droplet fate in indoor environments, or can we prevent the spread of infection? *Indoor Air* **16**, 335-347.

Neppelenbroek, K., Pavarina, A., Spolidorio, D., Massucato, E., Spolidorio, L. and Vergani, C. (2008) Effectiveness of microwave disinfection of complete dentures

on the treatment of Candida-related denture stomatitis. *J Oral Rehabil* **35**, 836-846.

Nicholson, W.L., Munakata, N., Horneck, G., Melosh, H.J. and Setlow, P. (2000) Resistance of Bacillus endospores to extreme terrestrial and extraterrestrial environments. *Microbiol Mol Biol Rev* **64**, 548-572.

Oliveira, E.A., Nogueira, N.G.P., Innocentini, M.D.M. and Pisani, R. (2010) Microwave inactivation of Bacillus atrophaeus spores in healthcare waste. *Waste Manage* **30**, 2327–2335.

Otani, Y., Kanaoka, C. and Emi, H. (1989) Experimental-study of aerosol filtration by the granular bed over a wide-range of Reynolds-numbers. *Aerosol Sci Tech* **10**, 463-474.

Otto, D., Hudnell, H., House, D., Mølhave, L. and Counts, W. (1992) Exposure of humans to a volatile organic mixture. In behavioral assessment. *Arch Environ Health* **47**, 23-30.

Pal, A., Min, X., Yu, L.E., Pehkonen, S.O. and Ray, M.B. (2005) Photocatalytic inactivation of bioaerosols by $TiO_2$ coated membrane. *Int J Chem React Eng* **3**, Article A45.

Pan, J., Sun, K., Liang, Y., Sun, P., Yang, X., Wang, J., Zhang, J., Zhu, W., Fang, J. and Becker, K.H. (2013) Cold plasma therapy of a tooth root canal infected with Enterococcus faecalis biofilms in vitro. *J Endodont* **39**, 105-110.

Pappas, G.P., Herbert, R.J., Henderson, W., Koenig, J., Stover, B. and Barnhart, S. (2000) The respiratory effects of volatile organic compounds. *Int J Occup Env Heal* **6**, 1-8.

Park, J., Yoon, K., Kim, Y., Byeon, J. and Hwang, J. (2009) Removal of submicron aerosol particles and bioaerosols using carbon fiber ionizer assisted fibrous medium filter media. *J Mech Sci Technol* **23**, 1846-1851.

Pflug, I.J., Holcomb, R.G. and Gomez, M.M. (2001) Principles of the thermal destruction of microorganisms. In *Disinfection, Sterilization, and Preservation* ed. Block, S. pp.79-124. Philadelphia, PA: Lippincott Williams & Wilkins.

Phelps, T.J., Palumbo, A.V., Bischoff, B.L., Miller, C.J., Fagan, L.A., McNeilly, M.S. and Judkins, R.R. (2008) Micron-pore-sized metallic filter tube membranes for filtration of particulates and water purification. *J Microbiol Meth* **74**, 10-16.

Qian, Y., Willeke, K., Grinshpun, S. and Donnelly, J. (1997) Performance of N95 respirators: Reaerosolization of bacteria and solid particles. *Am Ind Hyg Assoc J* **58**, 876-880.

Ramachandran, G. and Cooper, D.W. (2011) Size Distribution Data Analysis and Presentation. In *Aerosol Measurement: Principles, Techniques, and Applications* eds. Kulkarni, P., Baron, P.A. and Willeke, K. p.488. Hoboken, New Jersey: John Wiley & Sons, Inc.

Ratnesar-Shumate, S., Wu, C.Y., Wander, J., Lundgren, D., Farrah, S., Lee, J.H., Wanakule, P., Blackburn, M. and Lan, M.F. (2008) Evaluation of physical capture efficiency and disinfection capability of an iodinated biocidal filter medium. *Aerosol Air Qual Res* **8**, 1-18.

Rengasamy, S., Fisher, E. and Shaffer, R. (2010) Evaluation of the survivability of MS2 viral aerosols deposited on filtering face piece respirator samples incorporating antimicrobial technologies. *Am J Infect Control* **38**, 9-17.

Reponen, T., Grinshpun, S., Conwell, K., Wiest, J. and Anderson, W. (2001) Aerodynamic versus physical size of spores: Measurement and implication for respiratory deposition. *Grana* **40**, 119-125.

Reponen, T., Wang, Z., Willeke, K. and Grinshpun, S.A. (1999) Survival of Mycobacteria on N95 personal respirators. *Infect Cont Hosp Ep* **20**, 237-241.

Riemenschneider, L., Woo, M.H., Wu, C.Y., Lundgren, D., Wander, J., Lee, J.H., Li, H.W. and Heimbuch, B. (2010) Characterization of reaerosolization from impingers in an effort to improve airborne virus sampling. *J Appl Microbiol* **108**, 315-324.

Robbins, C., Swenson, L., Nealley, M., Gots, R. and Kelman, B. (2000) Health effects of mycotoxins in indoor air: A critical review. *Appl Occup Environ Hyg* **15**, 773-784.

Robinette, C.D., Silverman, C. and Jablon, S. (1980) Effects upon health of occupational exposure to microwave radiation (radar). *Am J Epidemiol* **112**, 39-53.

Ruiz, J., Blanc, P., Prouzet, E., Coryn, P., Laffont, P. and Larbot, A. (2000) Solid aerosol removal using ceramic filters. *Sep Purif Technol* **19**, 221-227.

Sawai, J., Sagara, K., Hashimoto, A., Igarashi, H. and Shimizu, M. (2003) Inactivation characteristics shown by enzymes and bacteria treated with far-infrared radiative heating. *Int J Food Sci Tech* **38**, 661-667.

Schieke, S.M., Schroeder, P. and Krutmann, J. (2003) Cutaneous effects of infrared radiation: from clinical observations to molecular response mechanisms. *Photodermatol Photo* **19**, 228–234.

Sehulster, L. and Chinn, R.Y.W. (2003) *Guidelines for environmental infection control in health-care facilities: recommendations of CDC and the Healthcare Infection Control Practices Advisory Committee (HICPAC)*: Centers for Disease Control and Prevention.

Shamis, Y., Taube, A., Shramkov, Y., Mitik-Dineva, N., Vu, B. and Ivanova, E.P. (2008) Development of a microwave treatment technique for bacterial decontamination of raw meat. *Int J Food Eng* **4**, Article 8.

Shaw, R., Kostinski, A. and Larsen, M. (2002) Towards quantifying droplet clustering in clouds. *Q J Roy Meteor Soc* **128**, 1043-1057.

Sidheswaran, M.A., Destaillats, H., Sullivan, D.P., Cohn, S. and Fisk, W.J. (2012) Energy efficient indoor VOC air cleaning with activated carbon fiber (ACF) filters. *Build Environ* **47**, 357-367.

Siegel, R. and Howell, J.R. (2002) *Thermal Radiation Heat Transfer*. New York: Taylor and Francis.

Smith, D.W., Wiegeshaus, E., Navalkar, R. and Grover, A.A. (1966) Host-parasite relationships in experimental airborne tuberculosis. I. Preliminary studies in BCG-vaccinated and nonvaccinated animals. *J Bacteriol* **91**, 718-724.

Smith, D.W. and Wiegeshaus, E.H. (1989) What animal models can teach us about the pathogenesis of tuberculosis in humans. *Rev Infect Dis* **11**, 5385-5393.

Stewart, E.J. (2012) Growing unculturable bacteria. *J Bacteriol* **194**, 4151-4160.

Stock, T.H. and Morandi, M.T. (1988) A characterization of indoor and outdoor microenvironmental concentrations of pollen and spores in two Houston neighborhoods. *Environ Int* **14**, 1-9.

Subrenat, A., Baleo, J.N., Le Cloirec, P. and Blanc, P.E. (2001) Electrical behaviour of activated carbon cloth heated by the joule effect: desorption application. *Carbon* **39**, 707-716.

Subrenat, A. and Le Cloirec, P. (2004) Adsorption onto activated carbon cloths and electrothermal regeneration: Its potential industrial applications. *J Environ Eng-ASCE* **130**, 249-257.

Sullivan, P.D., Rood, M.J., Grevillot, G., Wander, J.D. and Hay, K.J. (2004) Activated carbon fiber cloth electrothermal swing adsorption system. *Environ Sci Technol* **38**, 4865-4877.

Sullivan, P.D., Rood, M.J., Hay, K.J. and Qi, S. (2001) Adsorption and electrothermal desorption of hazardous organic vapors. *J Environ Eng-ASCE* **127**, 217-223.

Tang, J.W., Li, Y., Eames, I., Chan, P.K. and Ridgway, G.L. (2006) Factors involved in the aerosol transmission of infection and control of ventilation in healthcare premises. *J Hosp Infect* **64**, 100-114.

Theunissen, H.J., Lemmens-den Toom, N.A., Burggraaf, A., Stolz, E. and Michel, M.F. (1993) Influence of temperature and relative humidity on the survival of Chlamydia pneumoniae in aerosols. *Appl Environ Microb* **59**, 2589-2593.

Tsen, K.T., Shaw-Wei, D.T., Sankey, O.F. and Kiang, J.G. (2007) Selective inactivation of micro-organisms with near-infrared femtosecond laser pulses. *J Phys-Condens Mat* **19**, 472201.

Tseng, C. and Li, C. (2005) Collection efficiencies of aerosol samplers for virus-containing aerosols. *J Aerosol Sci* **36**, 593-607.

Tyrrell, D.A.J. (1967) The spread of viruses of the respiratory tract by the airborne route. *Symp Soc Gen Microbi* **17**, 286-306.

Vadivambal, R. and Jayas, D.S. (2010) Non-uniform temperature distribution during microwave heating of food materials-A review. *Food Bioprocess Tech* **3**, 161-171.

Vohra, A., Goswami, D.Y., Deshpande, D.A. and Block, S.S. (2005) Enhanced photocatalytic oxidation of indoor air. *Appl Catal B-Environ* **64**, 57-65.

Volkamer, R., Jimenez, J., San Martini, F., Dzepina, K., Zhang, Q., Salcedo, D., Molina, L., Worsnop, D. and Molina, M. (2006) Secondary organic aerosol formation from anthropogenic air pollution: Rapid and higher than expected. *Geophys Res Lett* **33**.

Wang, Z. (1999) Survival of bacteria on respirator filters. *Aerosol Sci Technol* **30**, 300–308.

Wang, Z., Reponen, T., Grinshpun, S., Górny, R. and Willeke, K. (2001) Effect of sampling time and air humidity on the bioefficiency of filter samplers for bioaerosol collection. *J Aerosol Sci* **32**, 661-674.

Ware, J.H., Spengler, J.D., Neas, L.M., Samet, J.M., G.R., W., Coultas, D., Ozkaynak, H. and Schwab, M. (1993) Respiratory and irritant health effects of ambient volatile organic compounds. The Kanawha County health study. *Am J Epidemiol* **137**, 1287-1301.

Wells, W.F. (1934) On air-borne infection. Study II. Droplet and droplet nuclei. *Am J Hyg* **20**, 611–618.

Willeke, K. and Qian, Y. (1998) Tuberculosis control through respirator wear: Performance of National Institute for Occupational Safety and health-regulated respirators. *Am J Infect Control* **26**, 139-142.

Williams, D.J., Franklin, J.G., Chapman, H.R. and Clegg, L.F.L. (1957) Methods of assessing the sporicidal efficiency of an ultrahigh-temperature milk sterilizing

plant. I. Experiments with suspensions of spores in water. *J Appl Bacteriol* **20**, 43-49.

Woo, M.H., Grippin, A., Anwar, D., Smith, T., Wu, C.Y. and Wander, J. (2012a) Effects of relative humidity and spraying medium on UV decontamination of filters loaded with viral aerosols. *Appl Environ Microb* **78**, 5781-5787.

Woo, M.H., Grippin, A., Wu, C. and Wander, J. (2012b) Microwave-irradiation-assisted HVAC filtration for inactivation of viral aerosols. *Aerosol Air Qual Res* **12**, 295-303.

Woo, M.H., Lee, J.H., Rho, S., Ulmer, K., Welch, J., Wu, C., Song, L. and Baney, R. (2011) Evaluation of the performance of dialdehyde cellulose filters against airborne and waterborne bacteria and viruses. *Ind Eng Chem Res* **50**, 11636-11643.

Workman, J. and Weyer, L. (2008) *Practical Guide to Interpretive Near-Infrared Spectroscopy*. Boca Raton, FL: Taylor and Francis Group, LLC.

Wu, Y. and Yao, M. (2010) Inactivation of bacteria and fungus aerosols using microwave irradiation. *J Aerosol Sci* **41**, 682-693.

Wu, Y. and Yao, M. (2011) Effects of microwave irradiation on concentration, diversity and gene mutation of culturable airborne microorganisms of inhalable sizes in different environments. *J Aerosol Sci* **42**, 800-810.

Xu, P., Peccia, J., Fabian, P., Martyny, J.W., Fennelly, K.P., Hernandez, M. and Miller, S.L. (2002) Efficacy of ultraviolet germicidal irradiation of upper-room air in inactivating airborne bacterial spores and mycobacteria in full-scale studies. *Atmos Environ* **37**, 405-419.

Yang, S.H., Huang, Y.C., Luo, C.H., Lin, Y.C., Huang, J.W., Chuang, C.P.J., Chen, C.J., Fang, W. and Chuang, C.Y. (2011) Inactivation efficiency of bioaerosols using carbon nanotube plasma. *Clean-Soil Air Water* **39**, 201-205.

Yao, M., Zhang, Q., Hand, D.W., Perram, D. and Taylor, R. (2009) Adsorption and regeneration on activated carbon fiber cloth for volatile organic compounds at indoor concentration levels. *J Air Waste Manage* **59**, 31-36.

Yu, I.T., Li, Y., Wong, T.W., Tam, W., Chan, A.T., Lee, J.H., Leung, D.Y. and Ho, T. (2004) Evidence of airborne transmission of the severe acute respiratory syndrome virus. *N Engl J Med* **350**, 1731-1739.

Yu, K., Lee, G.W., Lin, S. and Huang, C.P. (2008) Removal of bioaerosols by the combination of a photocatalytic filter and negative air ions. *J Aerosol Sci* **39**, 377-392.

Zhang, Q., Damit, B., Welch, J., Park, H., Wu, C.Y. and Sigmund, W. (2010a) Microwave assisted nanofibrous air filtration for disinfection of bioaerosols. *J Aerosol Sci* **41**, 880-888.

Zhang, Q., Welch, J., Park, H., Wu, C.Y., Sigmund, W. and Marijnissen, J.C.M. (2010b) Improvement in nanofiber filtration by multiple thin layers of nanofiber mats. *J Aerosol Sci* **41**, 230-236.

# BIOGRAPHICAL SKETCH

Brian Eduardo Damit was born in the summer of 1986 in Chicago with his twin brother Michael. After graduating high school in Illinois, Brian attended Florida State University and received a B.S. in meteorology in May 2008. Immediately after, he entered the PhD program in the Department of Environmental Engineering Sciences at the University of Florida. During his PhD study, Brian conducted research at Oak Ridge National Laboratory in Oak Ridge, Tennessee as well as at Peking University in Beijing, China. His hobbies and interests include fishing, playing the piano, traveling, jogging, eating, and watching baseball. Brian graduated with his PhD in August 2013.